A MICROFLOW CYTOMETRY BASED PLATFORM FOR BIOSENSING

QUANTIFICATION OF LOW-LEVEL CYANOBACTERIA USING A MICROFLOW CYTOMETRY PLATFORM FOR EARLY WARNING OF POTENTIAL CYANOBACTERIAL BLOOMS

BY

YUSHAN ZHANG, B.Eng & M.A.Sc.

A THESIS

SUBMITTED TO THE SCHOOL OF BIOMEDICAL ENGINEERING

AND THE SCHOOL OF GRADUATE STUDIES

OF MCMASTER UNIVERSITY

IN PARTIAL FULFILMENT OF THE REQUIREMENTS

FOR THE DEGREE OF

DOCTOR OF PHILOSOPHY

Doctor of Philosophy (2021) McMaster University

(School of Biomedical Engineering) Hamilton, Ontario, Canada

TITLE:	Quantification of Low-level Cyanobacteria Using a Microflow Cytometry Platform for Early Warning of Potential Cyanobacterial Blooms
AUTHOR:	Yushan Zhang Master of Applied Science
SUPERVISOR:	Prof. Chang-qing Xu
NUMBER OF PAGES:	xxi, 128

Lay Abstract

Harmful cyanobacterial blooms have been a rising risk to the public heath across the world in recent decades. Alert levels of cyanobacteria in water has also been established. In this case, a rapid on-side monitoring system for cyanobacteria is required. In this thesis, a microflow cytometer platform combined with a bacterial concentration and recovery system was built to quickly monitor the relatively low level of cyanobacteria for early warning alerts. A pre-enrichment system based on tangential flow filtration and back-flushing technique was applied to increase the concentration levels of microbial samples and a microfluidic device capable of collecting phycocyanin fluorescence was designed to count cyanobacterial cells. The limit of quantification for cyanobacterial concentration based on the microflow cytometry platform was as low as ~ 5 cells/mL. We can claim that the microflow cytometry platform can provide useful early warning alerts for the decision-makers to control the potential harmful cyanobacterial blooms at the very early stage and protect the aquatic animals and public health.

Abstract

Cyanobacteria, also known as blue-green algae for a long time, are the most ancient and problematic bloom-forming phylum on earth. An alert levels framework has been established by World Health Organization(WHO) to prevent the potential harmful cyanobacterial blooms. Normally, low cyanobacteria levels are found in surface water. 2000 cyanobacterial cells/mL and 100,000 cyanobacterial cells/mL are established for WHO Alert Level 1 and 2, respectively. However, eutrophication, climate change and other factors may promote the spread of cyanobacteria and increase the occurrence of harmful cyanobacterial blooms in water on a global scale. Hence, a rapid real time cyanobacterial monitoring system is required to protect public health from the cyanotoxins produced by toxic cyanobacterial species.

Current methods to control or prevent the development of harmful cyanobacterial blooms are either expensive, time consuming or not effective in the long term. The best method to control the blooms is to prevent the formation of the blooms at the very beginning. Although emerging advanced autofluorescence-based sensors, imaging flow cytometry applications, and remote sensing have been utilized for rapid real-time enumeration and classification of cyanobacteria, the need to accurately monitor low-level cyanobacterial species in water remains unsolved.

Microflow cytometry has been employed as a functional cell analysis technique in

past decades, and it can provide real-time, accurate results. The autofluorescence of cyanobacterial pigments can be used for determination and counting of cyanobacterial density in water. A pre-concentration system of an automated cyanobacterial concentration and recovery system (ACCRS) based on tangential flow filtration and back-flushing technique was applied to reduce the sample assay volume and increase the concentration of target cells for further cell capture and detection. In this project, a microflow cytometry platform with a microfluidic device and an automated pre-concentration system was established to monitor cyanobacteria and provide early warning alerts for potential harmful blooms.

In this work, quantification of low-level cyanobacterial samples (~ 5 cyanobacterial cells/mL) in water has been achieved by using a microflow cytometer together with a pre-concentration system (ACCRS). Meanwhile, this platform can also provide early warning alerts for potential harmful cyanobacterial blooms at least 15 days earlier before reaching WHO Alert Level 1. Results have shown that this platform can be applied for rapid determination of cyanobacteria and early warning alerts can be triggered for authorities to protect the public and the environment.

Acknowledgements

First and foremost, I would like to sincerely appreciate my supervisor, Dr. Chang-qing Xu, for his support and the longtime mentorship during my Ph.D. study. Thanks for giving me this excellent opportunity to pursue my study at McMaster University. I am also very grateful to his patience, kindness and his advices for me throughout my research. I was encouraged by his passion for science, and his open-minded attitude towards science and the outside world has really benefited me quite a lot.

I would also like to thank my co-supervisor during my master study, also my committee members, Dr. Qiyin Fang, Dr. Ravi Selvaganapathy, Dr. Leyla Soleymani, for providing me with invaluable help and feedbacks on my research. I am very happy and thankful for having them as my supervisory committee members during my study. In addition, I would like to thank the technicians from Centre for Emerging Device Technologies (CEDT), Doris V. Stevanovic and Shahram Tavakoli, for their training to use the equipments. I would also like to thank Tianyi Guo for teaching me and helping me merge into my study, and I also am very grateful to his support and kindness during my Ph.D. study. I'd like to thank the lab mates Dr. Qianli Ma, Dr. Bin Zhang, Jianxi Qu, Joshua Kneller, Tyler Kashak, Liam Flannigan, Rong Zha, Mahmoud Khalil Mahmoud, Fangfang Zhang, Linkun Cheng, and Ying Zhao. It is a great experience to work with theses excellent people and I learned a lot from them.

I would like to thank all the faculty members, staffs and students in the Department of Engineering Physics and School of Biomedical Engineering. I have experienced a lot with them and had a wonderful time studying here.

Many thanks to Wenzhi Tan, Bo Xiong, Qianxi He, Fengyan Wang, Dandan Wang, Gary Niu, Gloria Ding, Jinghua Qiu and many other friends for always supporting and helping me in the past few years. Special thanks to my close friend, Jie Yang, for her encouragement and telling me never to give up.

I want to share my happiness with my parents and my grandma. Thanks to their financial support, I can have a easier life and continue my education at McMaster University. Many thanks to my grandma who always supports me to study aboard and she is always proud of me. Their selfless love and care will be forever cherished.

Finally, I want to give my special thanks to all the front-line workers during the COVID-19 pandemic. Given to their selfish love and excellent work so that I can continue my research and finish my thesis.

Contents

List of Figures

List of Tables

Abbreviations

HCB	Harmful cyanobacterial bloom
ACCRS	Automated cyanobacterial concentration and recovery system
LOC	Lab-on-a-chip
MRP	South-to-North water diversion project
qPCR	quantitative polymerase chain reaction
ELISA	Enzyme-linked immunosorbent assays
HPLC	High-performance liquid chromatography
IFC	Imaging flow cytometry
MODIS	Moderate resolution imaging spectrophotometer
MERIS	Medium resolution imaging spectrometer
POC	Point-of-care
FL	Fluorescent light
FSC	Forward-scattered light

SSC	Side-scattered light
PMT	Photomultiplier tube
DAQ	Data acquisition card
DEP	Dielectrophoresis
MAP	Magnetophoresis
SSAW	Standing surface acoustic wave
IDT	Interdigital transducer
LED	Light-emitting diode
LCW	Liquid-core waveguide
HCW	Hybrid core waveguide
DI	Deionized
LA	Liquid-core/air cladding
SNR	Signal to noise ratio
PDMS	Poly(dimethylsiloxane)
FWHM	Full width at half-maximum
CV	Coefficient of variation
APD	Avalanche photodiodes
PIN	P-doped/Intrinsic/N-doped

CCD	Charge-coupled device
TiO_2	Titanium dioxide
PS	Polystyrene
PC	Polycarbonate
PMMA	Poly(methylmethacrylate)
COC	Cyclic olefin copolymer
HEK	Human embryonic kidney
LOD	Limit of detection
E.coli	*Escherichia coli*
TBS	Tryptic soy broth
PBS	Phosphate buffered saline
CFU	Colony forming unit
NaOH	Sodium hydroxide
RPM	Revolutions per minute
ABCRS	Automated bacterial concentration and recovery system
PCR	Polymerase chain reaction
LFA	Lateral flow assay
USEPA	United States Environmental Protection Agency

IMS	Immunomagnetic separation
SD	Standard deviation
RSD	Relative standard deviation
PLC	Programmable logic controller
CPCC	Canadian Phycological Culture Centre
IMHA	Immune-mediated hemolytic anemia
RBC	Red blood cell

Chapter 1

Introduction and Background

Floating cyanobacteria and algae are the main microorganisms that support the aquatic food webs in freshwater ecosystems, and they also are the main contributor to the harmful cyanobacterial or algal blooms. Within the numerous phyla that can form scums and blooms, cyanobacteria are considered as the most problematic and notorious bloom formers [1]. They can grow rapidly and proliferate cells that migrate between surface waters of adequate light and bottom waters with rich nutrients. Some bloom-forming genera of cyanobacteria (e.g., *Anabaena*) are capable of nitrogen fixation so that they can dominate the blooms in low nitrogen conditions [1]. Furthermore, cyanobacteria produce a variety of toxins called as cyanotoxins which are toxic to consumers ranked higher on the aquatic food chain. These harmful blooms also pose a threaten to human and animal health [2, 3]. In this chapter, the causes of the cyanobacterial/algal blooms are addressed. Due to the potential risks to human and animal health, the regulation of cyanobacteria in water bodies also are discussed. Current methods to manage and prevent the proliferation of harmful blooms are mentioned in this chapter. As the best method to control the blooms is to prevent it from forming, it is important to monitor the cell abundance in targeted waters. Subsequent investigation of state-of-art cyanobacterial monitoring methods and technologies are investigated in this chapter as well.

1.1 Harmful cyanobacterial blooms

1.1.1 What causes the blooms?

Cyanobacteria, also known as blue-green algae, are the most ancient (∼2.5 billion years) oxygenic photoautotrophs on Earth. Similar to algae, cyanobacteria can produce oxygen while absorb sunlight and take in carbon oxide. However, cyanobacteria are not algae and many genera are even not blue or green [4]. A major difference is that cyanobacteria are classified as prokaryotes, while algae are eukaryotes. In addition to the ubiquitous green pigment chlorophyll a, cyanobacteria contain unique photosynthetic pigments such as phycocyanin and allophycocyanin [5].

A large variety of algae and cyanobacteria are capable of forming blooms or scums. These phytoplankton utilize light as the energy source to perform photosynthesis process. Carbon dioxide is converted to oxygen and biomass increases. Normally, there is dynamic balance between the total phytoplankton biomass and the planktonic herbivores in aquatic ecosystems. Other than the phytoplankton consumers, the production rate of biomass also depends on certain physical, chemical factors. Vertical mixing is a common physical factor that has an impact on the growth of phytoplankton. In rich nutrients conditions and at proper temperature, the growth of the algae and cyanobacteria become more productive. Then the rapid proliferation of cyanobacterial/algal cells lead to visible discoloration of the water which is defined as a bloom [4]. The most common colors of the bloomed water are yellow, red, green, blue-green and brown. Increased loading of nitrogen and phosphorus into the water leads to eutrophication. As a result, the eutrophication of aquatic ecosystems accelerate the productive rates of phytoplankton.

The global dominance of cyanobacterial blooms can be exacerbated by increased nutrient inputs, higher nitrogen to phosphorus ratios, rising temperatures due to the climate changes, enhanced transport of cells by anthropogenic activities and overfishing that reduces the grazers [4, 6, 7]. Cyanobacterial harmful blooms has been reported since 1878, and they are the oldest and most problematic phytoplankton on the plant [6]. They have evolved to be more competitive in the aquatic ecosystems, especially under low nutrient conditions. Many genera are capable of fixing atmospheric nitrogen. Moreover, they are able to take up phosphorus for cellular growth when the extracellular phosphorus is rich, and store it in response to phosphorus deficiency [1, 7].

1.1.2 Cyanobacterial toxins and human health effects

Cyanobacteria-contaminated water has a negative impact on water quality and it can lead to significant environmental and economic problems. Global concerns about the effects of harmful cyanobacterial blooms on human health are increasing significantly in recent years. In 1878, domestic animals poisoned by toxic cyanobacteria was first published in the scientific literature [2]. Studies on the expansion of cyanobacterial blooms and the hazardous effects on human health have been conducting since 1980s. It is necessary to identify the cyanobacterial toxins for better management of the hazards to the public.

Cyanobacteria can produce toxins called cyanotoxins that mainly include hepatoxins, neurotoxins, dermatotoxins, and other bioactive compounds. According to the chemical structures, cyanotoxins can be divided into hepatotoxic cyclic peptides, cytotoxic and neurotoxic alkaloids, as well as lipopolysaccharides [1, 2, 3, 8, 9, 10].

Table 1.1 shows some general cyanobacterial toxins produced by various cyanobacterial genera. Microcystins, nodularins, cylindrospermopsins, anatoxin and saxitoxin are the most common and toxic cyanotoxins in water bodies.

Microcystins, nodularins and cylindrospermospins are primarily toxic to the liver. Anatoxin-a, anatoxin-a (s) and saxitoxins are strong neurotoxins. Other cyanobacterial compounds may cause allergic or irritant effects. *Microcystis aeruginosa* was the first species found to produce microcystins, and other microcystin-producing cyanobacterial species include *Anabaena, Anabaenopsis, Planktothrix, Aphanizomenon* et al [2, 9, 11]. Microcystin-producing cyanobacteria can dominate in many freshwater blooms, and microcystins are widely distributed in freshwaters. Animals poisoned by neurotoxic cyanobacteria were reported from North America, Europe and Australia [2].

Table 1.1: General cyanotoxins produced by cyanobacteria [1, 2]

Toxins	**Produced by**	**Target Organs**	**Type of toxicity**
Microcystins	*Microcystis, Anabaena, Aphanocapsa, Hapalosiphon, Nostoc, Oscillatoria(Planktothrix)*	Liver	Hepatotoxic cyclic peptides
Nodularins	*Nodularia*	Liver	Hepatotoxic cyclic peptides
Cylindrosper-mopsins	*Cylindrospermopsis, Aphanizomenon, Umezakia*	Liver	Cytotoxic alkaloids
Anatoxin-a	*Anabaena, Aphanizomenon, Oscillatoria (Planktothrix)*	Nerve synapse	Neurotoxic alkaloids
Anatoxin-a (s)	*Anabaena, Oscillatoria (Planktothrix)*	Nerve synapse	Neurotoxic alkaloids
Saxitoxins	*Anabaena, Aphanizomenon, Lyngbya, Cylindrospermopsis*	Nerve axons	Neurotoxic alkaloids

Continued on the next page

Table 1.1 (*Continued from previous page*)

Toxins	**Produced by**	**Target Organs**	**Type of toxicity**
Aplysiatoxins	*Lyngbya, Schizothrix, Oscillatoria (Planktothrix)* (marine)	Skin	Dermatotoxic alkaloids
Lipopolysaccharides (LPS)	All cyanobacteria	Exposed tissues	Irritant toxins

1.1.3 Prevention and control of harmful cyanobacterial blooms

The global expansion of HCBs can pose a high risk to the water suppliers, recreational water resources, human health, aquatic system and social economy [7]. Thus, it is of vital importance to prevent and control harmful cyanobacterial blooms in aquatic ecosystems. Nutrients loading, nitrogen to phosphorus ratio, water flushing, and temperatures are the most common factors that can affect the proliferation of cyanobacteria.

Physical, chemical, biological and environmental methods have been implemented to control and prevent HCBs [12]. The most straight forward solution is to reduce the nutrient loading in water environment. Reduction of N input and P input is an

effective means of preventing the growth and dominance of cyanobacteria. Nutrient-enriched water bodies are more likely to favor the dominance of cyanobacteria especially at high temperatures. Another key factor of nutrient management is the rations of N to P [4, 6, 7]. Point sources (e.g. wastewater treatment plant, industrial effluent) and non-point sources (e.g. land runoff) are the most common categories of nutrient inputs. Reduction of nutrients discharged from point sources are easier compared with controlling nutrient loading from non-point sources [7].

Physical manipulation of artificial mixing of different water bodies has been proved to be an effective method to prevent HCBs [4]. Hydrodynamic habitat conditions of the water bodies can be changed to suppress algae growth by water diversion projects. The Middle Route of the South-to-North Water Diversion Project (MRP) and Water Diversion Project from Yangtze River to Lake Taihu have shown that the nutrients and organic pollutants can be reduced significantly, the flow rates of the hydrological conditions can also be changed [13, 14]. Cyanobacterial and algal growth can be suppressed successfully by water diversion activities. Even though these water division activities have been successful, whereas they are costly. The Chinese State Council reported the construction cost for Niulanjiang Water Diversion Project was about 1.2 billion USD for a distance of 116 km in 2008 [15].

Chemical methods can effectively eradicate cyanobacterial blooms, whereas the effects can hardly provide long-term solutions. Algaecide, such as copper sulphate, has been approved to be an effective treatment method to the blooms [16]. Other chemical strategies include chlorine, potassium permanganate and ozone [16]. However, toxic effects of these chemicals can suppress the growth of other aquatic organisms as well. Another concern is that cyanotoxins and other intracellular metabolites can be

realized into water during the cell lysis caused by chemical treatments [4, 16]. Since algae and other eukaryotic phytoplankton are less sensitive to hydrogen peroxide compared with cyanobacteria, hydrogen peroxide can be considered as an effective and environmentally friendly algaecide. On the contrary, hydrogen peroxide can break down into water and oxygen. Therefore, it only temporarily suppresses the proliferation of cyanobacterial blooms [4].

Biological control strategy takes advantage of grazers or other natural enemies of cyanobacteria. Virus, pathogenic bacteria or fungi can be applied to prevent or collapse cyanobacterial biomass [4]. Reports have shown that cyanobacterial blooms can be suppressed by a large number of grazers [7, 4]. However, the effects and efficiency of grazers on cyanobacterial blooms still have Considerable debate [7].

The risk of harmful cyanobacterial blooms have increased in recent decades, and reports have shown that the proliferation of the blooms can be aggravated by eutrophication and climate change [6]. Some of these bloom-controlling methods have been effective and expensive, whereas others can only have little or temporary influence on the suppress of the blooms. The world-wide expansion of harmful cyanobacterial blooms requires extensive efforts to monitor the cyanobacterial biomass and cyanotoxins.

1.2 Current methods for rapid detection of cyanobacteria

Harmful cyanobacterial blooms have become a public nuisance all over the world. As discussed above, early warning monitoring and ongoing assessment of cyanobacterial blooms is necessary to ensure the safety of drinking and recreational water. Besides the traditional laboratory analysis of using a hemocytometer under the microscope, emerging technologies have been developed and promoted for quantification of cyanobacteria. Cyanobacterial monitoring methods can be divided into two broad categories: approaches that detecting extracted cyanobacterial compounds and methods without extraction [17]. Current methods can also be classified into three categories based on the monitoring methodologies: biological methods, biochemical and physicochemical methods, and other methods [18]. Biological methods include estimation of photosynthetic pigments, molecular techniques such as quantitative polymerase chain reaction (qPCR), microarray and microfluidic chip based methods. Enzyme-linked immunosorbent assays (ELISA), high-performance liquid chromatography (HPLC) are the most common biochemical methods that can be used for cyanobacterial monitoring. However, not all of these methods are capable of rapid detection of cyanobacteria. In this section, current approaches suitable for real time rapid cyanobacterial monitoring are addressed.

1.2.1 Autofluorescence-based biosensors

Most real-time monitoring technologies are based on the unique fluorescent pigments present in cyanobacterial cells [17]. Fluorescence of cyanobacterial probes can be

measured either in vivo [9, 19, 20, 21, 22] or in vitro (extracted pigments from the cells for measurements). In vivo fluorescence measurement with extraction of pigments provides the opportunity for rapid in situ cyanobacterial monitoring in water sources [19].

Phycocyanin is an unique cyanobacterial pigment that can be used to differentiate cyanobacteria from other phytoplankton. Phycocyanin has a major absorption band of 590-630 nm with a peak at 620 nm [17, 18, 19], and emits fluorescence with a maximum at 655 nm [17]. The amount of phycocyanin has a positive correlation with the cyanobacterial biomass [23, 24, 25, 26]. Multiple excitation lights are applied to selectively stimulate the photosynthetic pigments in algae and cyanobacteria to eliminate the algae interference on cyanobacterial measurement [27]. Chlorophyll a can be effectively excited by blue light (maximum absorption at 440 nm) and has a emission peak at 685 nm [17]. All cyanobacteria contain both phycocyanin and chlorophyll a, and the interference of eukaryotic algae chlorophyll needs to be corrected. Correction factors are developed to improve the accuracy of in vivo fluorescence probes for cyanobacterial detection [17, 28]. Other than chlorophyll a and turbidity, calibration range, colony size and algal growth phase can impact the performance of a phycocyanin probe [21].

McQuaid et al. studied the performance of in vivo phycocyanin fluorescence probes for rapid detection of microcystin-producing cyanobacteria [20] in drinking water. Fluorescence emitted from phycocyanin is converted into ratio fluorescent units (RFUs), and these probes need calibration before use. The quantification limit of the probe was 1 mm^3/L and was able to provide potential cyanobacterial blooms alerts for WHO's 2nd alert level (10 mm^3/L) [20]. Brient et al. reported that a

phycocyanin probe had a limit of quantification of 1,700 cyanobacterial cells/mL at its highest sensitivity [23].

Autofluorescence based biosensors have many advantages over other methods. These sensors can provide rapid real-time results and good estimations of total cyanobacterial biovolume. However, the accuracy of the read out of these sensors decreases when expressed as cell densities or concentrations [24]. Furthermore, specific species can not be identified by the fluorimetric probes. Another limitation of this method is the high threshold or detection limit. The readings are also affected by green algae, cell sizes and several other interferences.

1.2.2 Imaging flow cytometry

Novel imaging techniques together with fluid manipulation, and integrated fluorescence have been applied for the quantification of cyanobacterial cells [29]. Imaging flow cytometry (IFC) has been developed to quantitatively measure the cells or particles. IFC is a hybrid technique that takes advantage of flow cytometry and imaging features of cameras for the analysis of cyanobacteria and eukaryotic algae [30, 31]. Barteneva et al. addressed applications of IFC for determination of photosynthetic algae [32]. IFC has the ability to image cells of target at high resolution to improve the performance of flow cytometry.

As the rapid development of image features, traditional optical properties of the cell and morphological analysis are combined together to improve the accuracy of cyanobacterial cell identification. A digital imaging flow cytometer (FlowCAM) was presented by Park et al. to count *Microcystis* colonies with a novel model algorithm

to achieve there-dimensional cell counting [33]. Recently, machine learning was employed to FlowCam IFC by Mirasbekov et al. for identification and determination of *Microcystis* colonial morphospecies, and seasonal bloom of *Mirocystis* was investigated with high temporal and spatial resolution [34].

Imaging FlowCytobot (IFCB) is one of the application of the recent high-solution IFC technique for cyanobacterial monitoring [30, 35, 36, 37, 38]. IFCB was first deployed for coastal observatory to classify phytoplankton at genus or species level in 2006, and it has been developed rapidly in recent years. IFCB also combines the image capture and laser-based flow cytometry to sort and count cells. Image capture of targeted organisms was trigged by fluorescence signal at selected wavelengths, and cell-sorting was also activated using fluorescence as a trigger [31]. High frequency IFC was applied to identify filamentous cyanobacteria and studied the development of blooms in Baltic Sea by Kraft et al. [35].

IFC approach has been developed for more than 30 years, and the IFC applications are still expensive [32]. As the time for cells of interest to pass through the interrogation region or flow cell is typically on the millisecond or microsecond scale, the images are captured with limited amount of light [32]. Another limitation of IFC applications is the lower flow rate for image capture. The throughput of the IFC is lower than conventional flow cytometry.

1.2.3 Remote Sensing of cyanobacterial blooms

Remote sensing has been employed to monitor cyanobacterial blooms for large geographical areas with real-time data acquisition [39]. Surface pigment, spectral reflectance of water color, absorption, or temperature of water bodies have been utilized

for monitoring potential cyanobacterial blooms [40]. Landsat satellite, Moderate Resolution Imaging Spectrophotometer (MODIS) and Medium Resolution Imaging Spectrometer MERIS are main sensors to collect imagery for real-time monitoring of both temporal and spatial development of cyanobacteria in large regions [41]. Various algorithms have been developed based on different optical properties of cyanobacteria for remote sensing. The absorption characteristics of Chlorophyll a and the fluorescence properties of cyanobacterial pigments are widely utilized for remote sensing.

Matthews et al. improved algorithm to estimate Chlorophyll a in inland and near-coastal waters to perform routine monitoring of cyanobacteria [42]. In situ remote sensing reflectance characteristics were applied to identify mixed algal blooms by Dwivedi et al. [43], and Chlorophyll images collected by MODIS/SeaDAS were utilized. However, separation of cyanobacterial species from other eukaryotic green algae is very difficult with low Chlorophyll a level [18].

The presence of low-level cyanobacteria in water may not lead to water discoloration [18]. Moreover, dissolved organic matters and suspended solids in water bodies can also change the water color. Furthermore, remote sensing is expensive, and the high cost limits the use for routine monitoring.

1.2.4 Conclusions

Monitoring cyanobacteria, especially cyanobacterial samples with low abundance, in drinking and recreational water remains challenging due to the large variation of cyanobacterial biomass caused by the rapid change of environmental conditions. Climate changes, wind actions and other factors can favor the spread of scum-forming

cyanobacteria. Moreover, the dispersion of cyanobacterial biomass may change dramatically within hours to days especially at suitable conditions of higher temperature and enough nutrients.

Current in vivo fluorescence probes can provide rapidly monitor cyanobacterial samples with high numbers. However, fluorescence readout from Chl a present in eukaryotic algae and turbidity is the main limitation and needs to be corrected [19]. Meanwhile, large relative errors of these probes are observed for low density cyanobacterial samples under a wide calibration range [21].

IFC applications are originally developed for identification and classification of phytoplankton, and image features of target cells can be analyzed immediately after sample acquisition. Morphological characteristics of target cells are not always sufficient for classification of cyanobacteria to the species level [34].

Remote sensing has several unique advantages compared with other methods, e.g. large spatial scale, high-frequency observations, and high resolution images [39]. Current satellite date for remote sensing of cyanobacterial blooms is capable of providing the temporal and spatial distribution of cyanobacterial information in large water areas [39]. Accurately monitoring water bodies with low-level cyanobacterial using remote sensing remains a critical challenge.

1.3 Why early warning of cyanobacterial blooms is important?

1.3.1 Safety alert levels for cyanobacteria

To prevent the hazardous effects exposed to cyanobacteria and cyanotoxins, the World Health Organization (WHO) has established an alert levels framework for detection and management of a potential cyanobacterial bloom in water treatment plants. Although the framework has been established mostly from the perspective of operation of the drinking water supply, it can provide assessment and management action for raw water supply as well [2]. A threshold of cyanobacterial biomass 2,000 cells/mL is set for Alert Level 1 by WHO in 1999 [2], and that threshold indicates the concentration of microcystin accumulated in the water may be greater than the WHO guideline. Further assessment of the cyanobacterial biomass and monitoring of cyanotoxin concentration needs to be done as early as possible by the decision makers or health authorities at Alert Level 1. Cyanobacterial biomass of 100,000 cells/mL is determined for Alert Level 2 which indicates a toxic blooms or scums already formed [2], and the potential risks of cyanobacterial blooms to human health could therefore increase significantly. A few cyanobacterial colonies buoyant on the surface of water (Lake Dianchi, China) could be observed as the cyanobacterial biomass reached 15,000 cells/mL, indicating a slight bloom already occurred [44]. Ongoing monitor of cyanobacterial density in water takes on a heightened importance as the biomass may spread widely under suitable hydrological, meteorological, and nutritional conditions [44]. Early warning of potential cyanobacterial blooms is necessary to prevent the widespread of cyanobacterial bloom from escalating rapidly, exceeding Level 1 to

Level 2. At the meanwhile, risk levels of cyanobacterial biomass in drinking water can be split into three categories according to their adverse effects on human health. Cyanobacterial biomass less than 2,000 cells/mL can be considered as a low risk, and a high risk when it reaches 100,000 cells/mL. Moderate to high risks are within the range of 2,000 $\sim$ 100,000 cells/mL [2]. Continuous real-time monitoring of the status of cyanobacterial bloom is essential to ensure the safety of drinking water and recreational water.

Other than drinking water, recreational water can also be polluted with cyanobacteria and is very likely to contain cyanotoxins. A guideline level of cyanobacterial biomass in recreational water is also defined to protect public health from hazardous effects of cyanobacterial compounds other than cyanotoxins [3]. Compared to defined levels for drinking water, the guidance levels for recreational waters are much higher (as shown in Table 1.3). 20,000 cells/mL is determined as low probabilities to cause adverse health effects to human beings depending on the allergenic effects of cyanobacteria [2]. A moderate alert for recreational waters is at 100,000 cyanobacterial cells/mL, and high risk alerts can be observed as the formation of cyanobacterial blooms which indicates a thousand-fold concentration of moderate alert.

Cyanotoxins are the main hazardous concern in drinking water, while irritative or allergic symptoms caused by other cyanobacterial substances need to be considered in recreational waters. Health risks can be significantly increased when exposed to high concentration of cyanotoxins or cyanobacteria. Subject to the expansion of HCBs, it is important to perform regular monitoring of cyanobacteria in water, and provide information to the health authorities.

Table 1.3: Cyanobacterial safety alert levels [2, 3]

Critical Level	**Cyanobacterial Biomass (cells/mL)**	**Health Effects**	**Water Type**
WHO Alert Level 1	2000	low health risks	Drinking Water
WHO Alert Level 2	100,000	Elevated risk of adverse health outcomes	Drinking Water
Relatively low probability	20,000	Short-term adverse health outcomes	Recreational water
Moderate probability	100,000	Long-time illness, shoert term adverse health outcomes	Recreational water
High probabilitly	scum-forming	acute poisoning, long-term illness, and short-term adverse health outcomes	Recreational water

1.3.2 Early warning alerts for low-level cyanobacteria in water

Normally cyanobacteria present in low biomass in surface water bodies. However, cyanobacteria can proliferate and expand rapidly under suitable environmental conditions. Ressem et al. reported that the mean doubling time of several species was varying from 21 hours to 14.7 days [11]. Temperature was found as a significant factor influencing the growth rate of cyanobacteria. The doubling time of *Microcystis aeruginosa* was 6.79 days obtained at 20 °C , while the period decreased to 1.23 days at 32 °C [45]. During studied the growth rates of eight cyanobacteria species, and reported similar results [46]. The biomass of cyanobacteria doubled in 1.65 days in average at the optimum temperature (29.2 °C), while it only took 0.75 day to double the biomass at 20 °C [46]. The doubling time also depends on the cyanobacterial species, and it can vary from less than one day (20 hours) for *Synechocystis* sp. to a few days (6.25 days) for *H. hongdechloris* [47]. It can be seen that cyanobacterial blooms can establish in a few weeks up to a few months as the rapid growth rates in nutrient-rich water under warm temperatures, and the blooms can last for months [7].

Moreover, eutrophication and climate that may favor the growth of cyanobacteria and promote the expansion and intensification of HCBs. Global warming can intensify the dominance of some cyanobacterial species in freshwater [6]. Compared with other phytoplankton, cyanobacteria have some superior advantages over their competitors in the aquatic systems. Some cyanobacteria contain gas-vesicles (e.g. *Microcystis aeruginosa*) can float in the surface to capture more light. The dominance of cyanobacteria can be further promoted in warmer and more strongly stratified water

bodies [6, 46].

Conventional drinking water treatment processes have limited ability to effectively remove cyanotoxins [25]. On the contrary, the demand to reduce and remove the cyanobacterial biomass and cyanotoxins in water bodies are increasing dramatically. Regular monitoring of cyanobacterial blooms in drinking water, ground water and recreational water is quite important.

Figure 1.1 shows simplified current early warning alert levels framework for cyanobacterial biomass in water sources suggested by WHO [2]. Quantitative measurements of cyanobacterial cells need to be done regularly. If sample concentration is greater than 2000 cyanobacterial cells/mL, further assessments of toxins present in water and status of the cyanobacterial bloom are required. Meanwhile, strategic advice and consultation with relevant authorities are suggested. If measured value exceeds alert level 2 (100,0000 cyanobacterial cells/mL), the high biomass implies an established bloom. The risk of adverse health effects is significantly increased, and effective water treatment methods are needed.

Regular monitoring of low-level cyanobacterial is also necessary for an early warning of potential formation of cyanobacterial blooms. A vigilance level of cyanobacteria in low numbers is suggested. Monitoring of low biomass of cyanobacteria can stop a potential bloom at the early stage.

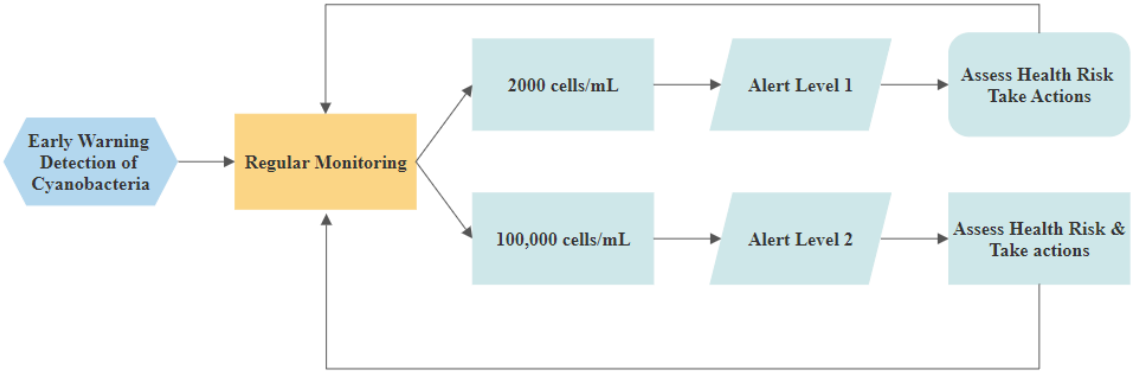

Figure 1.1: Early warning alert levels framework for cyanobacteria monitoring in water

1.3.3 The challenge of cyanobacterial detection

Microflow cytometer and emerging LOC devices have been deployed to evaluate the cell density of algae or other phytoplankton by the shape, cell size or the intrinsic pigment fluorescence. The determination and early warning alerts for potential harmful cyanobacterial have attracted more interest of scientists in recent years. However, some practical challenges remain there and need to be solved.

In general, three steps are involved in methods for rapid detection of cell/particle in water: pre-concentration, capture and detection of cell/particle of interest [48, 49]. The pre-concentration step fro sample preparation remains as a challenge in practical environmental monitoring due to the detection limit and the assay volume. First, microbial species (bacteria, viruses, protozoa) must not be detected in any 100 mL drinking water. For example, the standard of *E.coli* is zero per 100 mL for all water intended for drinking [10]. Similarly, dilute levels of microbial species are established

for recreational water standards [48]. A rough level range of 0 to 1000 CFU/100 mL are quite common for microbial standard in ground or recreational water [3]. As for early warning of potential cyanobacterial blooms, a low-level detection limit is required.

Second, 100 mL or larger samples are generally used for monitoring microbial species in drinking and recreational water. Many rapid detection technologies, especially emerging LOC devices are based on measuring assays on μL or mL scale. It takes very long time for these devices to process 100 mL or larger samples. For early warning level of cyanobacteria, at least 100 mL of water samples need to be processed in a relatively short period of time.

In this thesis, a cyanobacterial detection platform is proposed to solve some remaining problems and provide early warning alerts of potentially HCBs as shown in Figure 1.2. The water samples can be pumped to a pre-concentrator for sample preparation in which the cells of interest are captured, and unwanted suspended solids are removed. Then, the sample can be transferred to a proposed microflow cytometer for detection. The interaction of light and micro fluids can be applied for cell counting, and optical signals can be transduced into the measurable electrical voltages. A vigilance level of low-level (e.g. 5 cells/mL) can be set for the warning. If counted values are higher than the vigilance level, relevant authorities can be noticed to take proper actions to slow down and prevent the blooms. This platform can also be used for regular monitoring of water bodies.

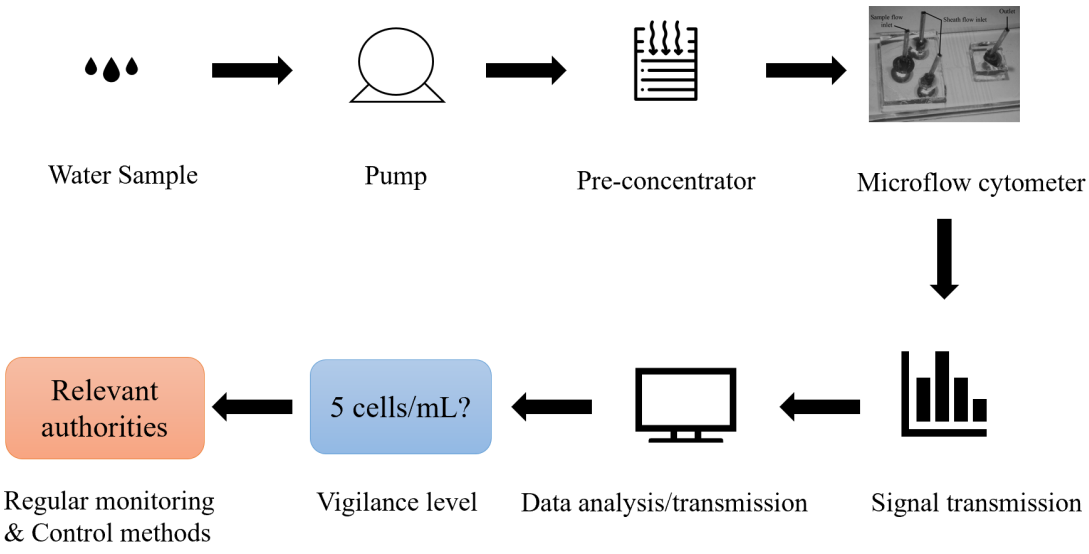

Figure 1.2: Proposed cyanobacterial detection platform for early warning alerts of potentially HCBs

1.4 Research motivations

Cyanobacterial blooms have been a risk all over the world for a few decades due to multiple reasons, such as,the climate change, population explosion, and rapid development of economy. Harmful cyanobacterial blooms pose a potential threat to human health and the environment, and various methods have been developed to attenuate the negative effects of the cyanobacterial scums. The best method to control the harmful cyanobacterial blooms is to prevent it before cyanobacterial cells actually bloom. After the formation of blooms, the cost of controlling the scum is expensive and the negative effects to the public health and the environmental are huge.

Cyanobacterial cells grow exponentially and the blooms can be formed in a few

days from a very low-level cell abundance, especially in summer at suitable temperature when enough nutrients are poured into the water bodies. It is necessary to monitor relatively low-level of cyanobacterial samples and make a early warning system for the decision makers to slow down the growth of cyanobacterial cells and prevent it from forming detrimental scums.

Although many techniques and methods have been developed for cyanobacterial detection in recent decades, these methods still have some drawbacks for pre-blooms of cyanobacteria. Conventional microscopic counting based cell culture, nucleic acid-based methods, immunoassays and advanced biosensors are the most common techniques for enumeration of particles/cells.

As most biosensors manipulate fluids on a micron or nano scale, it is still time-consuming or difficult for most of the biosensors or equipments to capture a few cells in a practical environmental water sample of a relatively large volume (e.g. 1 liter). A good pre-conditioning or pre-enrichment step can be added to enhance the monitoring of large-volume environmental samples with low-level microbial abundance.

1.5 Research Objectives

The overall objective of this research dissertation was to monitor cyanobacteria and provide early warning for possible blooms to the authorities, relevant sectors and organizations. The objectives can be summarized as follows, based on the proposed platform in Figure 1.2.

1. The built-up of a bacterial pre-concentration and recovery system (Chapter 2, 3 and 4).

To design and build up an automated bacterial filtration and recovery system to

reduce the original sample volume and increase the concentration of cells of interest. The aim of this sub-project was to provide a pre-conditioning step (A pre-concentrator proposed in Figure 1.2) for rapid cell/particle detection sensors, especially for practical environmental water samples.

2. The establishment of a microfluidic device based optofluidic microflow cytometer (Chapter 5 and 6).

Optofluidic devices which take advantage of both microfluidic devices and integrated on-chip optics have been utilized for enumeration and classification of particle/cell detection. Integrated on-chip waveguides, optical beam shaping, and built-in optical alignment are designed to provide high-sensitivity and highly integrated optical system. We aimed to design and establish a microfluidic device based optofluidic microflow cytometer for particle/cell characterization.

3. Data analysis of the microflow cytometer (Chapter 5).

The principle test and performance verification of the microflow cytometer platform needs to be validated by data analysis of polystyrene microspheres. In microfluidic devices, the setting of proper thresholds is vital important for accuracy of the results. We aimed to improve the accuracy of the microflow cytometer by optimization of current data analysis methods.

4. Exploring the proof of principle study at a device level (Chapter 5 and 6).

The optimized data analysis methods can be applied for validation of the principle for cyanobacterial detection at a device level. The rapid labeling-free detection of cyanobacteria is based on the microflow cytometer. Feasibility and principle tests of monitoring cyanobacteria needs to be done and figure out the limit of quantification for the microflow cytometry platform. It can provide safety alerts for harmful

cyanobacteria in water and prevent potential hazardous effects caused by cyanotoxins for WHO Alert Level 2. The aim of this work was to validate the capability of the microflow cytometer for cyanobacterial detection based on autofluorescence of cyanobacterial cells without labeling.

5. Reporting the proof of principle study at a system level (Chapter 7).

As addressed in Figure 1.2, a vigilance level for early warning alerts of potentially HCBs is suggested to the relevant sectors and organizations. Detection of cyanobacterial samples at low levels remains a challenge and needs to be solved. Figure 1.2 proposes a possible solution by using a pre-concentrator to capture and determination of target analyte. Combined with the bacterial filtration and recovery system and the microflow cytometry, it is able to decrease the limit of quantification and provide early warning alerts for potentially harmful cyanobacterial blooms. Therefore, the aim of this work was to investigate the proof of principle study at a system level, and to provide early warning alerts for potential HCBs by accurately monitoring cyanobacterial samples with low numbers.

1.6 Dissertation Overview

Harmful cyanobacterial blooms pose a risk to public health and it is necessary to set up a pre-warning alert system for the possible blooms. This thesis proposed a solve method to monitor cyanobacterial which can also provide early warning alerts of potential harmful blooms by cyanobacterial cell counts at low levels. A sandwich thesis consists of seven chapters is written by the author, including 4 published papers (Chapter 2, 3, 5 and 6) and one submitted manuscript (Chapter 7).

Chapter One studies the background of this project and describes the risks and

hazardous effects of harmful cyanobacterial blooms. State of art monitoring methods and the challenges of cyanobacteria detection are also addressed in Chapter One.

One of the biggest challenges of monitoring low-density of bacteria is the total cell abundance in the water sample. An automated bacterial concentration and recovery system has been designed and built up in Chapter Two as a pre-concentration step for sample preparation. Chapter Two also investigates the performance of the system for relatively-high concentration level of bacterial samples with experimental validation using *E. coli* samples. *E. coli* samples with the range of 10,000 $\sim$ 1000,000 CFU/mL were used in the concentration experiments for proof of principle studies.

Chapter Three further approves the performance of the system for bacterial samples with relatively-low abundance. Besides the systematic study that verifies the performance of the system, an extreme test of exist or non-exist is designed to determine the pre-enrichment limit of the recovery system. *E. coli* samples ranged from 0.005 CFU/mL to 10,000 CFU/mL was successfully concentrated and recovered using the subsystem. The first objective of a pre-concentrator proposed in Figure 1.2 has been completed.

Chapter Four optimizes the current concentration and recovery system for cyanobacterial use. *M. aeruginosa* samples with a wide range of cell densities were applied for the experiments to prove the performance of the automated cyanobacterial concentration and recovery system. Chapter four is based on previous work and completes the aim of the pre-enrichment process required for cyanobacterial detection.

Chapter Five is the literature review of particle/cell detection based on optofluidic microflow cytometers. In this chapter, optofluidic devices which manipulate the integrated optics and micro fluids for characterization of particle/cell are reviewed.

Conventional flow cytometry is a powerful tool for cell analysis and microflow cytometry is developing rapidly to meet the emerging needs for fast and low-cost detection of bacteria. Compared with other microfluidic devices, optofluidic devices include beam shaping, built-in optical alignment and other highly integrated on-chip optical features.

Meanwhile, a two-dimensional hydradynamic focusing microfluidic device is fabricated as the core device to monitor the cell/particle in the water flow. In Chapter Six, a microfluidic device based microflow cytometer platform for particle/cell detection has been built up. Based on the empirical experience and comparison with traditional microscopic counting methods, the data analysis method has been optimized through data filtering by transit time and amplitude thresholds. Results show that the false positive events are significantly reduced based on the optimized gating methods. The objectives to establish a microflow cytometer and the optimize data analysis have been achieved.

Rapid labeling free cyanobacteria detection and an early warning alert system are addressed in Chapter Seven. Cyanobacterial cells contain the special pigment that can emit fluorescent signals when excited by red lasers. The limit of quantification was determined as 15, 000 cells/mL without any pre-filtration process, which can provide cyanobacterial early warning alert for WHO Alert Level 2 (20,000 cells/mL). It can also provide cyanotoxins alert from recreational waters to the public health. An automated cyanobacterial concentration and recovery system (ACCRS) was built-up based on the previous system by optimizing parameters and it was designed and developed for cyanobacterial experiments. Combined with ACCRS, the detection limit of the water samples can be further reduced to 5 cells/mL which is 400 fold less

than the WHO Alert Level 1. The microflow cytometer platform can provide early warning alerts for potential cyanobacterial blooms and it also extends the application of microfluidic devices for measuring practical environmental samples. The proposed methods are validated at device and system level for cyanobacterial detection, and the objective 4 and 5 have been accomplished.

The Conclusions chapter makes a summary of the overall work in this thesis and addresses some perspectives on future work. Although the specific fluorescence signals emitted by the cyanobacterial cells were collected and analyzed in this work, the data can only determine the cyanobacterial concentration in the samples. As forward-scattered light intensity is proportional to the cell size and side-scattered light intensity is affected by the cell granularity, the collected data can be used for analyzing cell morphology. Meanwhile, the high-speed cameras are developing rapidly in recent decades. Images of cells of interest and the fluorescence of the cells can be combined together to provide more information on the cyanobacterial species. Also, on-line algal/cyanobacterial tracking system and data base can be a good idea for the prevention and control of potential harmful blooms.

References

[1] H. W. Paerl, R. S. Fulton, P. H. Moisander, and J. Dyble. Harmful freshwater algal blooms, with an emphasis on cyanobacteria. *The Scientific World*, 1:76–113, 2001.

[2] Jamie Bartram, Wayne W Carmichael, Ingrid Chorus, Gary Jones, and Olav M. Skulberg. *Toxic Cyanobacteria in Water: a guide to their public health consequences, monitoring and management*. CRC Press, Londan and New York, 1999.

[3] WHO. *Guidelines for safe recreational water environments*, volume 1. World Health Organization, 2013.

[4] Jef Huisman, Geoffrey A. Codd, Hans W. Paerl, Bas W. Ibelings, Jolanda M.H. Verspagen, and Petra M. Visser. Cyanobacterial blooms. *Nature Reviews Microbiology*, 16(8):471–483, 2018.

[5] Govindjee. Adventures with cyanobacteria: a personal perspective. *Frontiers in Plant Science*, 2(July):28, 2011.

[6] J. M. O'Neil, T. W. Davis, M. A. Burford, and C. J. Gobler. The rise of harmful

cyanobacteria blooms: The potential roles of eutrophication and climate change. *Harmful Algae*, 14:313–334, 2012.

[7] Hans W Paerl and Timothy G Otten. Harmful Cyanobacterial Blooms : Causes , Consequences , and Controls. *Microb Ecol*, 65:995–1010, 2013.

[8] Judy a Westrick, David C Szlag, Benjamin J Southwell, and James Sinclair. A review of cyanobacteria and cyanotoxins removal/inactivation in drinking water treatment. *Analytical and bioanalytical chemistry*, 397(5):1705–14, 2010.

[9] A. Barra Caracciolo, L. Dejana, C. Fajardo, P. Grenni, M. Martin, G. Mengs, S. Sánchez-Fortún, T. Lettieri, M. L. Saccà, and L. K. Medlin. A new fluorescent oligonucleotide probe for in-situ identification of Microcystis aeruginosa in freshwater. *Microchemical Journal*, 148(May):503–513, 2019.

[10] World Health Organization. *Guidelines for drinking-water quality*, volume 1. World Health Organization, 2011.

[11] Clark Svrcek and Daniel W Smith. Cyanobacteria toxins and the current state of knowledge on water treatment options: a review. *Journal of Environmental Engineering and Science*, 3(3):155–185, 2004.

[12] Mingzhi Qu, Stephen Anderson, Pin Lyu, Y. Malang, Jizhou Lai, Jianye Liu, Bin Jiang, Feng Xie, Hugh H.T. Liu, Daniel D. Lefebvre, and Yuxiang S. Wang. Effective aerial monitoring of cyanobacterial harmful algal blooms is dependent on understanding cellular migration. *Harmful Algae*, 87(March 2018):101620, 2019.

[13] Jiangyu Dai, Shiqiang Wu, Xiufeng Wu, Wanyun Xue, Qianqian Yang, Senlin Zhu, Fangfang Wang, and Dan Chen. Effects of water diversion from Yangtze River to Lake Taihu on the phytoplankton habitat of the Wangyu River Channel. *Water*, 10(6), 2018.

[14] Jie Zhu, Xiaohui Lei, Jin Quan, and Xia Yue. Algae Growth Distribution and Key Prevention and Control Positions for the Middle Route of the. *water*, 11(1851):1–18, 2019.

[15] Yong Liu, Yilin Wang, Hu Sheng, Feifei Dong, Rui Zou, Lei Zhao, Huaicheng Guo, Xiang Zhu, and Bin He. Science of the Total Environment Quantitative evaluation of lake eutrophication responses under alternative water diversion scenarios : A water quality modeling based statistical analysis approach. *Science of the Total Environment*, 468-469:219–227, 2014.

[16] Jiajia Fan, Peter Hobson, Lionel Ho, Robert Daly, and Justin Brookes. The effects of various control and water treatment processes on the membrane integrity and toxin fate of cyanobacteria. *Journal of Hazardous Materials*, 264:313–322, 2014.

[17] Arash Zamyadi, Florence Choo, Gayle Newcombe, Richard Stuetz, and Rita K. Henderson. A review of monitoring technologies for real-time management of cyanobacteria: Recent advances and future direction. *TrAC - Trends in Analytical Chemistry*, 85:83–96, 2016.

[18] Ankita Srivastava, Shweta Singh, Chi Yong Ahn, Hee Mock Oh, and Ravi Kumar Asthana. Monitoring approaches for a toxic cyanobacterial bloom. *Environmental Science and Technology*, 47(16):8999–9013, 2013.

[19] Arash Zamyadi, Natasha McQuaid, Sarah Dorner, David F. Bird, Mike Burch, Peter Baker, Peter Hobson, and Michèle Prévost. Cyanobacterial detection using in vivo fluorescence probes: Managing interferences for improved decision-making. *Journal - American Water Works Association*, 104(8):466–479, 2012.

[20] N. McQuaid, A. Zamyadi, M. Prévost, and F. Bird. Use of in vivo phycocyanin fluorescence to monitor potential microcystinproducing cyanobacterial biovolume in a drinking water source. *Journal of environmental monitoring : JEM*, 13:455–463, 2011.

[21] De Wei Chang, Peter Hobson, Michael Burch, and Tsair Fuh Lin. Measurement of cyanobacteria using in-vivo fluoroscopy - Effect of cyanobacterial species, pigments, and colonies. *Water Research*, 46(16):5037–5048, 2012.

[22] Christian Bastien, Richard Cardin, Éloïse Veilleux, Christian Deblois, Annabelle Warren, and Isabelle Laurion. Performance evaluation of phycocyanin probes for the monitoring of cyanobacteria. *Journal of Environmental Monitoring*, 13(1):110–118, 2011.

[23] Luc Brient, Marion Lengronne, Emilie Bertrand, Delphine Rolland, Arnaud Sipel, Delphine Steinmann, Isabelle Baudin, Michèle Legeas, Bertrand Le Rouzic, and Myriam Bormans. A phycocyanin probe as a tool for monitoring cyanobacteria in freshwater bodies. *Journal of Environmental Monitoring*, 10(2):248–255, 2008.

[24] Edoardo Bertone, Michele A. Burford, and David P. Hamilton. Fluorescence probes for real-time remote cyanobacteria monitoring: A review of challenges and opportunities. *Water Research*, 141:152–162, 2018.

[25] Katarzyna Izydorczyk, Malgorzata Tarczynska, Tomasz Jurczak, Jaroslaw Mrowczynski, and Maciej Zalewski. Measurement of phycocyanin fluorescence as an online early warning system for cyanobacteria in reservoir intake water. *Environmental Toxicology*, 20(4):425–430, 2005.

[26] Chi Yong Ahn, Seung Hyun Joung, Sook Kyoung Yoon, and Hee Mock Oh. Alternative alert system for cyanobacterial bloom, using phycocyanin as a level determinant. *Journal of Microbiology*, 45(2):98–104, 2007.

[27] Young Ho Shin, Jonathan Z. Barnett, M. Teresa Gutierrez-Wing, Kelly A. Rusch, and Jin Woo Choi. A hand-held fluorescent sensor platform for selectively estimating green algae and cyanobacteria biomass. *Sensors and Actuators, B: Chemical*, 262:938–946, 2018.

[28] F. Choo, A. Zamyadi, R. M. Stuetz, G. Newcombe, K. Newton, and R. K. Henderson. Enhanced real-time cyanobacterial fluorescence monitoring through chlorophyll-a interference compensation corrections. *Water Research*, 148:86–96, 2019.

[29] Chao Jin, Maria M.F. Mesquita, Jason L. Deglint, Monica B. Emelko, and Alexander Wong. Quantification of cyanobacterial cells via a novel imaging-driven technique with an integrated fluorescence signature. *Scientific Reports*, 8(1):1–12, 2018.

[30] Veronika Dashkova, Dmitry Malashenkov, Nicole Poulton, Ivan Vorobjev, and Natasha S Barteneva. Imaging flow cytometry for phytoplankton analysis. *Methods*, 112:188–200, 2017.

[31] Bennett S Lambert, Robert J Olson, and Heidi M Sosik. A fluorescence-activated cell sorting subsystem for the imaging flowcytobot. *Limnology and Oceanography: Methods*, 15(1):94–102, 2017.

[32] Natasha S Barteneva, Ivan A Vorobjev Editors, and John M Walker. *Imaging Flow Cytometry IN Series Editor*. New York: Springer, 2016.

[33] Jungsu Park, Yongje Kim, Minjae Kim, and Woo Hyoung Lee. A novel method for cell counting of microcystis colonies in water resources using a digital imaging flow cytometer and microscope. *Environmental Engineering Research*, 24(3):397–403, 2019.

[34] Yersultan Mirasbekov, Adina Zhumakhanova, Almira Zhantuyakova, Kuanysh Sarkytbayev, Dmitry V Malashenkov, Assel Baishulakova, and Natasha S Barteneva. Semi automated classification of colonial Microcystis by FlowCAM imaging flow cytometry in mesocosm experiment reveals high heterogeneity during seasonal bloom. *Scientific Reports*, 11(1):1–14, 2021.

[35] Kaisa Kraft, Jukka Seppälä, Heidi Hällfors, Sanna Suikkanen, Pasi Ylöstalo, Sílvia Anglès, Sami Kielosto, Harri Kuosa, Lauri Laakso, Martti Honkanen, Sirpa Lehtinen, Johanna Oja, and Timo Tamminen. First Application of IFCB High-Frequency Imaging-in-Flow Cytometry to Investigate Bloom-Forming Filamentous Cyanobacteria in the Baltic Sea. *Frontiers in Marine Science*, 8(March), 2021.

[36] Robert J Olson, Alexi Shalapyonok, Daniel J Kalb, Steven W Graves, and Heidi M Sosik. Imaging FlowCytobot modified for high throughput by in-line

acoustic focusing of sample particles. *Limnology and Oceanography: Methods*, 15(10):867–874, 2017.

[37] Robert J. Olson and Heidi M. Sosik. A submersible imaging-in-flow instrument to analyze nano-and microplankton: Imaging FlowCytobot. *Limnology and Oceanography: Methods*, 5(6):195–203, 2007.

[38] Heidi M. Sosik and Robert J. Olson. Automated taxonomic classification of phytoplankton sampled with imaging-in-flow cytometry. *Limnology and Oceanography: Methods*, 5(6):204–216, 2007.

[39] Kun Shi, Yunlin Zhang, Boqiang Qin, and Botian Zhou. Remote sensing of cyanobacterial blooms in inland waters: present knowledge and future challenges. *Science Bulletin*, 64(20):1540–1556, 2019.

[40] Kevin G Sellner, Gregory J. Doucette, and Gary J Kirkpatrick. Harmful algal blooms: Causes, impacts and detection. *Journal of Industrial Microbiology and Biotechnology*, 30(7):383–406, 2003.

[41] Jennifer P. Cannizzaro, Brian B. Barnes, Chuanmin Hu, Alina A. Corcoran, Katherine A. Hubbard, Eric Muhlbach, William C. Sharp, Larry E. Brand, and Christopher R. Kelble. Remote detection of cyanobacteria blooms in an optically shallow subtropical lagoonal estuary using MODIS data. *Remote Sensing of Environment*, 231(November 2018):111227, 2019.

[42] Mark William Matthews and Daniel Odermatt. Improved algorithm for routine monitoring of cyanobacteria and eutrophication in inland and near-coastal waters. 2015.

[43] R. Dwivedi, M. Rafeeq, B. R. Smitha, K. B. Padmakumar, Lathika Cicily Thomas, V. N. Sanjeevan, Prince Prakash, and Mini Raman. Species identification of mixed algal bloom in the Northern Arabian Sea using remote sensing techniques. *Environmental Monitoring and Assessment*, 187(2), 2015.

[44] Li Wei Sun, Wen Jing Jiang, Jun Yi Zhang, Wen Qian Wang, Yang Du, Hiroaki Sato, Masanobu Kawachi, and Ran Yu. Identification and detection sensitivity of Microcystis aeruginosa from mixed and field samples using MALDI-TOF MS. *Environmental Monitoring and Assessment*, 190(12), 2018.

[45] A J Van Der Westhuizen and J N Eloff. Effect of temperature and light on the toxicity and growth of the blue-green alga Microcystis aeruginosa (UV-006). *Planta*, 163:55–59, 1985.

[46] Miquel Lürling, Fassil Eshetu, Elisabeth J. Faassen, Sarian Kosten, and Vera L.M. Huszar. Comparison of cyanobacterial and green algal growth rates at different temperatures. *Freshwater Biology*, 58(3):552–559, 2013.

[47] Yaqiong Li, Yuankui Lin, Patrick C Loughlin, and Min Chen. Optimization and effects of different culture conditions on growth of Halomicronema hongdechloris - A filamentous cyanobacterium containing chlorophyll f. *Frontiers in Plant Science*, 5(FEB):1–12, 2014.

[48] Rachel T Noble and Stephen B Weisberg. A review of technologies for rapid detection of bacteria in recreational waters. *J Water Health*, 3(4):381–392, 2005.

[49] Yushan Zhang, Chang qing Xu, Tianyi Guo, and Lingcheng Hong. An automated

bacterial concentration and recovery system for pre-enrichment required in rapid Escherichia coli detection. *Scientific Reports*, 8(1):1–8, 2018.

Chapter 2

Optimization of An Enhanced Ceramic Micro-filter for Concentrating Escherichia coli in Water

The objective of this chapter was to built up a pre-concentrator for automated bacterial concentration and recovery. The proof of principle was first validated by microspheres of varying sizes, and the minimum size of the microspheres tested in the experiments was 1 μm in diameter. *E. coli* cells have similar dimensions: 1.0 - 2.0 μm long and 0.25 - 1.0 μm in diameter. Furthermore, *E. coli* is often considered as a representative microorganism in water quality. Therefore, *E. coli* was applied as cells of interest to validate the performance of the system to concentrate and recover bacteria.

In this chapter, an automated bacterial concentration and recovery system was built up to concentrate the cells of interest in the water samples. As a pre-conditioning step for the following detection process, the system was able to recover more than 90% of the *E.coli* cells from 1 liter sample to a final retentate of 5 $\sim$ 10 mL. The results have shown that the system provides a pre-treatment method to lower the limit of detection of biosensors and reduce the volume of the original sample to a mL scale that works for most of the biosensors.

Designing and conducting the experiments, data analysis and manuscript writing were conducted by the author of this thesis. The author of this thesis was also the main contributor and first author of this publication.

Zhang, Yushan, Tianyi Guo, Changqing Xu, and Lingcheng Hong. "Optimization of an enhanced ceramic micro-filter for concentrating E. coli in water." In Imaging, Manipulation, and Analysis of Biomolecules, Cells, and Tissues XV, vol. 10068, p. 100681B. International Society for Optics and Photonics, 2017.

Optimization of An Enhanced Ceramic Micro-filter for Concentrating Escherichia coli in Water

Yushan Zhang[a], Tianyi Guo[bc], Changqing Xu[a] and Lincheng Hong[d]

[a]McMaster University, 1280 Main Street West, Hamilton, Canada
[b]Forsee Instruments Ltd, 175 Longwood Road South, Suite 305, Hamilton, Canada
[c]Institute of Microelectronics, Chinese Academy of Science, Beijing, China
[d]Jiangsu Delin Environmental Protection Technology Ltd, 88 Runqi Road, Nanjing, China

ABSTRACT

Recently lower limit of detection (LOD) is necessary for rapid bacteria detection and analysis applications in clinical practices and daily life. A critical pre-conditioning step for these applications is bacterial concentration, especially for low level of pathogens. Sample volume can be largely reduced with an efficient pre-concentration process. Some approaches such as hollow-fiber ultrafiltration and electrokinetic technique have been applied to bacterial concentration. Since none of these methods can provide a concentrating method with a stable recovery efficiency, bacterial concentration still remains challenging Ceramic micro-filter can be used to concentrate the bacteria but the cross flow system keeps the bacteria in suspension. Similar harvesting bacteria using ultrafiltration showed an average recovery efficiency of 43% [1] and other studies achieved recovery rates greater than 50% [2]. In this study, an enhanced ceramic micro-filter with 0.14 µm pore size was proposed and demonstrated to optimize the concentration of *E.coli*. A high recovery rate (mean value >90%) and a high volumetric concentration ratio (>100) were achieved. Known quantities (10^4 to 10^6 CFU/ml) of *E.coli* cells were spiked to different amounts of phosphate buffered saline (0.1 to 1 L), and then concentrated to a final retentate of 5 ml to 10 ml. An average recovery efficiency of 95.3% with a standard deviation of 5.6% was achieved when the volumetric concentration ratio was 10. No significant recovery rate loss was indicated when the volumetric concentration ratio reached up to 100. The effects of multiple parameters on *E.coli* recovery rate were also studied. The obtained results indicated that the optimized ceramic micro-filtration system can successfully concentrate E.coli cells in water with an average recovery rate of 90.8%.

Keywords: *E.coli* concentration, ceramic micro-filter, LOC devices

1 INTRODUCTION

Drinking water safety has been a world public health concern during the past decades, and the detection of waterborne diseases is still challenging. Due to the varieties of bacteria,

Further author information: (Send correspondence to Changqing Xu)
Changqing Xu: E-mail: cqxu@mcmaster.ca, Telephone: 1 905 525 9140 x 24314

protozoa and virus, it is impossible to detect every species of the microorganisms in water. In this case, *Escherichia coli (E.coli)* is used as one of the indicators to microbiological quality of drinking water. Meanwhile, the detection of *E.coli* and other foodborne pathogens is also required in food industries [3]. *E.coli* needs to be aseptically removed from vegetables, fresh meats and poultry to liquids for enrichment and determination [4]. The *E.coli* concentration levels of these water samples are very low. For example, the acceptable concentration of *E.coli* in milk is less than 10 CFU/g [5]. A traditional method to solve the extreme low concentration problem is cultural enrichment which makes analysis time reach up to 24h to 48 h [5]. Although some rapid detection methods successfully shorten the analysis time such as DNA extraction [5] and enzyme immunoassay [3], these approaches can only achieve the best performance when the level of target bacteria is around 10^3 to 10^4 CFU/ml [3].

Recently lab-on-a-chip devices such as microfluidic biochips [6] and microfabricated flow cytometer [7] provide a rapid and robust method to simultaneously monitor the bacteria in water. For example, Wang et al. made a microfluidic device to monitor *E.coli* samples of 10^4 and 10^7 cells/ml [8] in a few minutes. However, the common detection limit of a microflow cytometer for *E.coli* is 10^3 CFU/ml [7], and this value may vary from 10 to 10^8 CFU/ml in different microfluidic devices [9]. If the *E.coli* is isolated and concentrated from the water sample instead of enrichment culture, the lab-on-a-chip devices and other rapid detection biosensors can be largely expand their uses in many other areas [3].

Centrifugation and filtration are typical methods for harvesting and concentrating bacteria [3]. Usually chemicals are needed for centrifugation, subsequent clarification and purification process can cause some bacteria loss [10]. Compared to centrifugation, tangential flow microfiltration and ultrafiltration make sure that the sample flow recirculated on the surface of a micro or ultra filter membrane until the desired volumetric concentration factor is achieved. The continuous recirculated flow can largely reduce the accumulation on the membrane and increase the recovery rate.

In this study, tangential flow microflitration with a 0.14 um pore size ceramic membrane is used to harvest *E.coli* from water samples. The purpose of this study was to optimize a ceramic membrane based tangential flow microfiltration to efficiently harvest and concentration *E.coli* from water samples. Furthermore, the effects of multiple parameters on *E.coli* recovery rate was discussed in details. Finally, this study confirmed preconcentraion of bacteria samples was a good method to bring the signals within the detection limits of some microfluidic devices and extend their use in clinical practices and daily life.

2 MATERIALS AND METHODS

2.1 Sample Preparation

Escherichia coli K-12 MG1655 was cultured overnight in a shaking incubator at 37°C. Tryptic soy broth (TBS) was used as nutrients for *E.coli* cells growth. The *E.coli* cells were centrifuged and then resuspended in phosphate buffered saline (PBS) right before filtration. A 10X liquid concentration solution of PBS was diluted to 1X by deionized (DI) water. Resuspended *E.coli* cells were first enumerated by a microscope and further diluted to lower concentration levels that vary from 10^4 to 10^6 colony forming units (CFU)/ml. Diluted *E.coli* PBS solution can be used as water samples to test the performance of the enhanced ceramic micro-filter system.

2.2 Micro-Filter Setup

A ceramic membrane (Sterlitech Corp., U.S.A.) with a pore size of 0.14 µm was applied to this tangential flow filtration system. The ceramic filter needed to be washed by 0.5 mol/L sodium hydroxide (NaOH) at a temperature of 85°C for 30 minutes and 5 ml/L nitric acid (HNO_3) at a temperature of 50°C for 15 minutes, respectively. Use DI water to rinse the ceramic membrane to maintain a neutral pH value after cleaning with alkaline and acid. The ceramic membrane is set inside a stainless steel cylinder with special channels that guide fluid from the inlet to outlets. An inlet in the center of top surface was used to connect the water sample tank via a peristaltic pump, and an outlet on the top surface recirculated sample water to the water tank. Another outlet was located in the center of the bottom surface, delivering the permeate flow to the filtrate tank.

2.3 Enhanced Concentration System Setup

As shown in Figure 1, the principle of the concentration system is based on tangential flow filtration. Compared to traditional dead end filtration, there is one extra outlet on the surface of the stainless steel cylinder. Original water flow was pumped into the filter setup by a peristaltic pump, flowing along the special channel inside the filter setup to return to the water sample tank. At the same time, water molecules and particles with smaller diameters than the pore size of the ceramic membrane will penetrate the filter and were pumped to the filtrate tank. Generally, backflushing was performed at the end of the concentration process by adding extra water or PBS to wash the filter, while forward flushing and backflushing shifted at a special frequency in this study. For example, in one experiments water sample ran to the filter for 30 seconds, then the flow was reversed by changing the rotation direction of the peristaltic pumps. Backwash solution ran from the filtrate tank to the filter to force the *E.coli* cells back into the circulating fluid for a few seconds. The dependence between *E.coli* cells recovery rate and various backflushing conditions was addressed later. Two peristaltic pumps were used to pump the water from water sample tank to the filter and from the filter to the filtrate tank, respectively. The permeate flow rate was controlled at around 1.8-2.5 L/h in this study, depending on the pressure provided by two pumps and the frequency of backflushing.

2.4 Concentraion Factors

The recovery rate is a main factor to determine the performance of the concentration system, and was defined by the following equation [11]:

$$\text{Recovery Rate} = \frac{\text{Total number of } \textit{E.coli} \text{ in the retentate}}{\text{Total number of } \textit{E.coli} \text{ in water sample}} \times 100\%$$

The volumetric concentration ratio (C) is used to testify the performance of the concentration system, defined as the ratio of the initial volume of the water sample to the final volume of the retentate as followed equation:

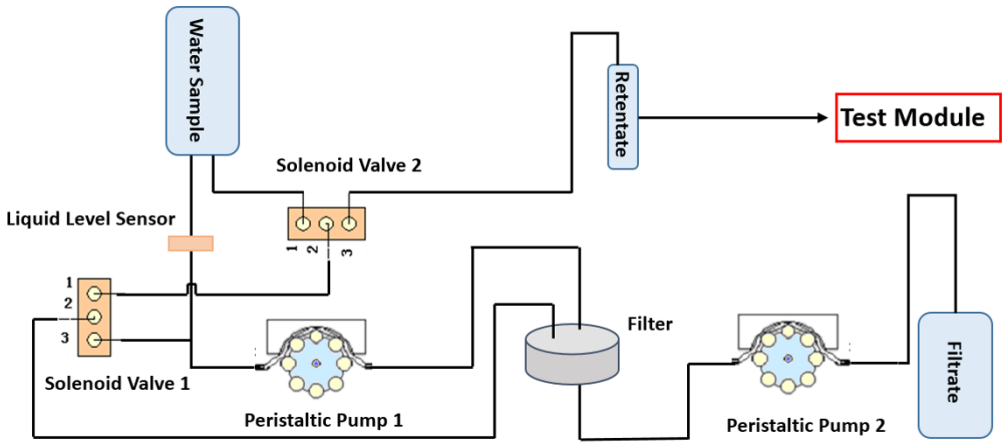

Figure 1. A schematic diagram of the proposed concentration system.

$$\text{Volumetric Concentration Ratio (C)} = \frac{\text{Initial volume of the water sample}}{\text{Final volume of the retentate}}$$

3 RESULTS AND DISCUSSION

3.1 Effect of Backflushing Ratio on *E.coli* Recovery Rate

Peristaltic pump 2 (Fig.1) was mainly used to backflush the flow from the filtrate tank back to the filter and wash the ceramic membrane backwards to reduce the bacteria accumulation on the surface of the ceramic membrane and bring *E.coli* back to the flow. 5000 revolutions per minute (rpm) of peristaltic pump 2 was set for backfluching in contrast to 1500 rpm for forward flow. Instead of backflushing the bacteria at the end of filtration process to recover the bacteria [12], sample flow runs in a forward and backward direction at a certain frequency until the desired concentration ratio is achieved in this study.

The time period set for backflushing was 1 second, and the time period set for forward flow varied from 10 s to 60 s. As shown in Fig.2, the average recovery rate of concentrating initial 500 ml water sample to a final 5 ml retentate declined from 92.84% to 71.62% when the time interval increased from 10 s to 60 s. The *E.coli* concentration range of the initial water samples was 2.58 to 4.33 10^5 CFU/ml. The values of average recovery rate were stable when the forward to backward time ratio were 10:1, 20:1, and 30:1, as well as 40:1, then decreased sharply from above 90 % to 84.16 % at 50:1, finally dropped to 71.62 % at the ratio of 60:1. These results indicated that backflushing was necessary for harvesting bacteria by tangential flow filtration. Shifting the flow direction frequently reduced the fouling and bacteria accumulation and washed the bacteria back into the flow all the time. Meanwhile, the shear force in tangential flow kept the bacteria running to achieve an average recovery

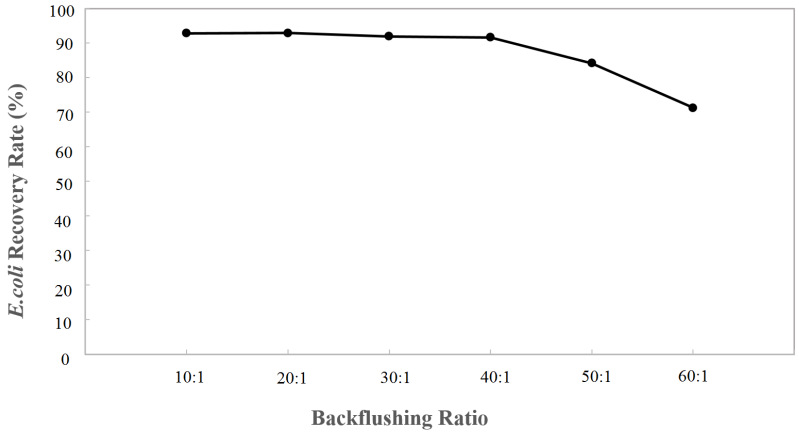

Figure 2. Effect of backflushing ratio on *E.coli* recovery rate.

rate of 92.84 %. Compared to using extra 100 ml water for backflushing [12], the final concentration volume was only 5 ml or 10 ml in this study with a stable recovery rate.

3.2 Final Concentration Volume

The desired final retentate volume was about 5 ml to 10 ml by controlling the position of the liquid sensor located in the filtrate cylinder. No additional backflushing liquid was needed after filtration, thus the final concentraion volume was the same as the retentate volume. Most literature achieved a final retentate of 100 - 150 ml [13] plus additional 100 ml or 150 ml for backflushing [1, 12]. Polaczky et al. [13] used ultrafiltration technique to rapidly concentrate microbe from 100 L tap water samples and achieved a 200 to 250 ml retentate along with additional 150 ml backflush liquid. Although the throughput was high, the volumetric concentration factor was 250 times. If the final volumes were reduced to 5 ml, the volumetric concentration factor could be 50 times larger than before and it could be 20,000. Table 1 showed the effect of final concentration volume on *E.coli* recovery rate. A final volume of 5 ml and 10 ml was achieved respectively by adjusting the configuration of the liquid sensor (Fig.1). An average recovery rate value of 95.27% with a standard deviation of 5.56% was tested when final concentration volume was 10 ml. A slightly lower recovery rate of 91.96% with a standard deviation of 5.64% was observed when the final concentration volume was reduced to 5 ml. Less final concentration volume can cause a little more bacteria loss when the filtration process is very close to the end. In this study, the final concentration volume was designed as 5 ml to get a higher volumetric concentration factor for more studies.

3.3 Effect of Initial E.coli Concentration Level on Recovery Rate

To testify the performance of the enhanced ceramic micro-filter for concentrating *E.coli*, the effect of initial bacteria concentration on recovery rate was also studied. The initial *E.coli* concentration varied from 2.48×10^4 to 9.35×10^5 CFU/ml, achieving a mean recovery rate of 90.32% (SD $\pm$6.94%). Higher concentration samples were more likely to cause

Table 1. The effect of final concentration volume on *E.coli* recovery rate

C	Sample Volume (ml)	Final Concentration Volume (ml)	Recovery Rate (%) ± SD
10	100	10	95.27 ± 5.56
20	100	5	91.96 ± 5.64

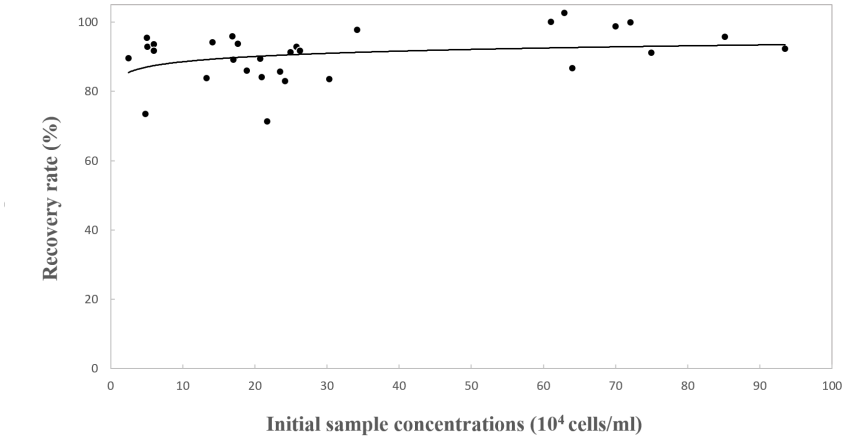

Figure 3. Effect of initial sample concentration on *E.coli* recovery rate

bacteria fouling on the ceramic membrane. However, as the initial *E.coli* concentration increased, no significant difference in recovery rate was observed. This indicated that the backflushing process along with the tangential flow filtration technique can successfully reduced the bacteria accumulation.

3.4 Effect of Volumetric Concentration Ratio on Recovery Rate

E.coli recovery efficiencies with variable volumetric concentration ratios were also compared in our research. An average recovery efficiency of 95.3% with a standard deviation of 5.6% was achieved when the volumetric concentration ratio was 10. The recovery rate decreased to 89.3% (SD =11.5%) as the volumetric concentration radio increased to 75. An initial 500 ml water sample achieved an average recovery rate of 93.36 (SD = 1.57%) when concentrated to 5 ml. The recovery rate remained stable as the volumetric concentration ratio varied. The enhanced concentration system showed good performance to both a high concentration water samples and high volume water samples.

4 CONCLUSIONS

The enhanced ceramic micro-filter has been proposed and demonstrated for concentrating E.coli in water. It has shown an average recovery rate as high as 90.32% with a final

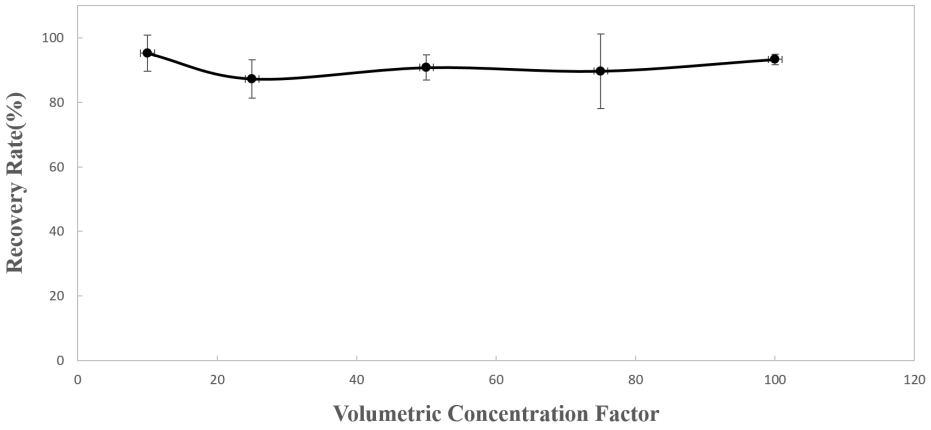

Figure 4. Effect of volumetric concentration ratio on *E.coli* recovery rate

concentration volume as low as 5 ml, implying a highly increased volumetric concentration ratio. Combined with backflushing and tangential flow microfiltration technique, the enhanced concentration system achieved a better performance than the hollow fiber ultrafiltration. In this studies, the effect of multiple parameters on the bacteria recovery have been investigated. Compared to backflush the filter at the end of the filtration process, the shifted backflushing during the whole process can lower the accumulation of the bacteria and reduce the bacteria loss. A 5 ml final concentration volume has been achieved for subsequent analysis, and the recovery rate has reached up to 95.3%. The effect of volumetric concentration ration on *E.coli* recovery rate indicated the stabilization of the enhanced system. No significant recovery rate loss has been found when the volume of water sample increased. This enhanced ceramic based tangential flow microfiltration system can be used as a preconcentration process for microfluidic devices and many other biotechnical devices.

ACKNOWLEDGMENTS

This research is partially supported by an ORF grant (grant no. RE-WR-10) and an NSERC Discovery grant (grant no. RGPIN/262023-2013).

References

[1] R. C. Kuhn and K. H. Oshima, "Hollow-fiber ultrafiltration of Cryptosporidium parvum oocysts from a wide variety of 10-L surface water samples," *Can. J. Microbiol.* **48**(6), pp. 542–549, 2002.

[2] P. Liu, V. R. Hill, D. Hahn, T. B. Johnson, Y. Pan, N. Jothikumar, and C. L. Moe, "Hollow- fi ber ultra fi ltration for simultaneous recovery of viruses , bacteria and parasites from reclaimed water," *J. Microbiol. Methods* **88**(1), pp. 155–161, 2012.

[3] K. A. Stevens and L.-A. Jaykus, "Bacterial separation and concentration from complex sample matrices: a review.," *Crit. Rev. Microbiol.* **30**(1), pp. 7–24, 2004.

[4] M. P. Doyle and J. L. Schoeni, "Isolation of Escherichia coli 0157 : H7 from Retail Fresh Meats and Poultry," *Appl. Environ. Microbiol.* **53**(10), pp. 2394–2396, 1987.

[5] A. Mortari and L. Lorenzelli, "Recent sensing technologies for pathogen detection in milk: A review," *Biosens. Bioelectron.* **60**, pp. 8–21, 2014.

[6] J. Mairhofer, K. Roppert, and P. Ertl, "Microfluidic systems for pathogen sensing: A review," *Sensors (Basel)* **9**(6), pp. 4804–4823, 2009.

[7] J. S. Kim, G. P. Anderson, J. S. Erickson, J. P. Golden, M. Nasir, and F. S. Ligler, "Multiplexed detection of bacteria and toxins using a microflow cytometer," *Anal. Chem.* **81**(13), pp. 5426–5432, 2009.

[8] Z. Wang, T. Han, T.-J. Jeon, S. Park, and S. M. Kim, "Rapid detection and quantification of bacteria using an integrated micro/nanofluidic device," *Sens Actuators B Chem* **178**, pp. 683–688, 2013.

[9] A. M. Foudeh, T. F. Didar, T. Veres, and M. Tabrizian, "Microfluidic designs and techniques using lab-on-a-chip devices for pathogen detection for point-of-care diagnostics.," *Lab Chip* **12**(18), pp. 3249–66, 2012.

[10] M. R. Bilad, D. Vandamme, I. Foubert, K. Muylaert, and I. F. J. Vankelecom, "Bioresource Technology Harvesting microalgal biomass using submerged microfiltration membranes," *Bioresour. Technol.* **111**, pp. 343–352, 2012.

[11] H. A. Morales-Morales, G. Vidal, J. Olszewski, C. M. Rock, D. Dasgupta, K. H. Oshima, and G. B. Smith, "Optimization of a reusable hollow-fiber ultrafilter for simultaneous concentration of enteric bacteria, protozoa, and viruses from water," *Applied and Environmental Microbiology* **69**(7), pp. 4098–4102, 2003.

[12] J. S. Kim, G. P. Anderson, J. S. Erickson, J. P. Golden, M. Nasir, and F. S. Ligler, "Mutiplexed Detection of Bacteria and Toxins Using a Microflow Cytometer," *Appl. Environ. Microbiol.* **35**(2), pp. 4098–4102, 2009.

[13] A. L. Polaczyk, J. Narayanan, T. L. Cromeans, D. Hahn, J. M. Roberts, J. E. Amburgey, and V. R. Hill, "Ultrafiltration-based techniques for rapid and simultaneous concentration of multiple microbe classes from 100-L tap water samples," *J. Microbiol. Methods* **73**(2), pp. 92–99, 2008.

Chapter 3

An Automated Bacterial Concentration and Recovery System for Pre-enrichment Required in Rapid Detection of Escherichia coli

In previous chapter, the principle and the performance of the ABCRS has been approved and verified for bacterial samples of high concentration levels. However, we aimed at monitoring low-level cyanobacterial samples for early warning alerts. In order to achieve this goal, the capability of the pre-concentration system still needs to be improved for concentration and recovery of bacterial samples with lower levels.

The pre-enrichment is one of the biggest challenges in monitoring bacterial samples of low concentration level. *E. coli* samples with a wide concentration range (0.005 - 10,000 CFU/mL) was used in the validation experiments. *E. coli* was chosen as the targeted bacteria due to its dimension and the role as an indicator of microbial water quality. More importantly, low numbers of *E. coli* (even a few cells in 1 liter water sample) can be determined using USEPA Method 1603. *E. coli* colonies can turn deep purple on modified mTEC agar by USEPA Method 1603, which can improve the sensitivity and accuracy of the results. Therefore, the limit of the pre-concentration system can also be determined accurately. In this chapter, the automated bacterial concentration and recovery system was used to increase bacterial concentration and reduce the assay volume of the *E. coli* samples with low numbers.

This chapter is reproduced from a published paper and the author of this thesis is the first author and main contributor.

Yushan Zhang, Chang-qing Xu, Tianyi Guo, and Lingcheng Hong. "An automated bacterial concentration and recovery system for pre-enrichment required in rapid Escherichia coli detection." Scientific Reports 8, no. 1 (2018): 1-8.

SCIENTIFIC REPORTS

OPEN

An automated bacterial concentration and recovery system for pre-enrichment required in rapid *Escherichia coli* detection

Received: 5 April 2018
Accepted: 9 November 2018
Published online: 13 December 2018

Yushan Zhang[1], Chang-qing Xu[1], Tianyi Guo[2] & Lingcheng Hong[3]

One of the biggest challenges in rapid low concentration bacterial detection is the pre-concentration or pre-enrichment, which aims to increase bacteria concentration and reduce sample volume for easy bacterial detection. In practical bacterial detection, large-volume water samples with a pathogenic bacterial concentration of less than 1 CFU/mL have to be tested rapidly. The reported biosensors either have insufficient detection limit or have limited capability of handling a sufficiently large water sample. Therefore, a high-performance automated pre-enrichment process is strongly demanded in rapid practical bacterial detection. In this paper, a practical high performance automated bacterial concentration and recovery system (ABCRS) based on the combination of a ceramic membrane and tangential flow filtration technique was presented with short processing time (less than one hour), low pre-enrichment limit ($\leq$0.005 CFU/mL), high concentration ratio ($\geq$ 500), high recovery efficiency (~ 90%), and small final retentate volume ($\leq$ 5 mL).

Rapid detection of pathogenic bacteria has attracted a lot of attention as it has enormous impact on public health. It is estimated that more than 2.2 million deaths per day are caused by the water contaminated with infectious diseases around the world[1], and about 9.4 million illnesses and 1351 deaths every year in the United States are due to foodborne pathogen contaminated food[2]. In the drinking water and food industry, rapid bacterial detection methods that are capable of monitoring the pathogenic bacteria at low concentrations (e.g. <1 CFU/mL for *E. coli*) are vitally demanded to reduce risks to public health. Generally speaking, a rapid pathogenic bacteria detection system consists of five modules: pre-enrichment, capture, detection, signal transmission and data analysis[3]. The total processing time should include the length of time each necessary step takes, from the pre-enrichment step to the read-out of the results. For practical applications, the system must meet the following requirements: low detection limit ($\leq$1 CFU/mL), fast processing ($\leq$1 hour), and high specificity/portability/stability, as well as fully automatic [4–7].

The current bacterial detection methods include cell culture, nucleic acid-based sensing, immunoassays and biosensors[8]. The standard microbiological culture method requires a few days to obtain the results, implying that this method is not appropriate for rapid bacteria detection. Furthermore, the total number of the cultured bacteria can be underestimated as some specific bacteria can enter a viable but non-culturable state in environment[9,10]. Polymerase chain reaction (PCR)-based assays are the most common nucleic acid-based techniques used in laboratory for rapid bacterial detection. Real time PCR-based assays have a detection limit of 10 to 100 CFU/mL for *E. coli* detection[11,12]. However, PCR usually needs at least 6 ~ 48 hours enrichment for low concentration bacterial detection[12–16]. In addition, expensive equipment and highly-trained personnel are required for the PCR-based assays. Rapid immunoassays, such as, enzyme-linked immunosorbent assays (ELISA) are also labor-intensive and the detection limit of ELISA is usually high (10^4 ~ 10^6 CFU/mL)[11]. This relatively high detection limit still needs to be lowered to monitor the pathogenic bacteria at low concentration in drinking water. Other than ELISA, lateral flow assay (LFAs) can be operated by non-specialized personnel[17,18], and this method reduces the assay times from hours to minutes[19–21]. The detection limit of the LFAs is also limited by the bacterial concentration in initial water sample. Sample enrichment process is needed in many LFAs to improve the specificity and sensitivity[17,21].

[1]Faculty of Engineering, McMaster University, Hamilton, Canada. [2]Forsee Instruments Ltd., Hamilton, Canada. [3]Jiangsu Delin Environmental Protection Technology Co., Ltd., Jiangsu, China. Correspondence and requests for materials should be addressed to C.-q.X. (email: cqxu@mcmaster.ca)

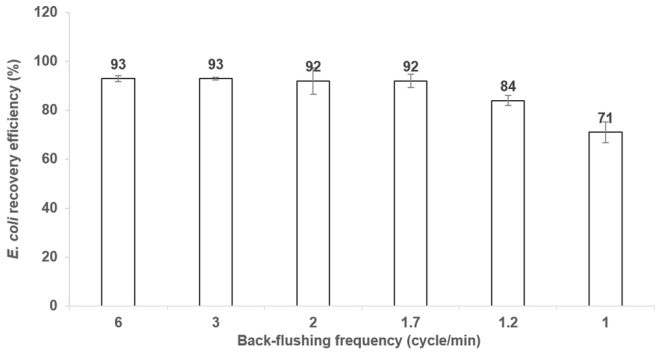

Figure 1. Measured *E. coli* recovery efficiencies of the ABCRS at various back-flushing frequencies.

Recently, various detection techniques based on biosensors have been developed to reduce the assay time and to improve the sensitivity for rapid monitoring of the pathogenic bacteria. A label-free immune-based biosensor with a detection limit of 2 CFU/mL has been reported for detection of *E. coli*[22]. However, the flow rate used in the immunosensor detection was 56 µL/min. In other words, the sensors can only test a sample with an assay volume on nanoscale or microscale (i.e. µL ~ mL)[22]. Considering the fact that large volumes of initial water samples (100 mL ~ 1000 L) are required for the tests in food industries and environmental monitoring[23], the total assay volume of these single-cell detection biosensors can handle is too small for practical rapid detection. Moreover, the bacterial indicators in recreational water should be less than 100 CFU/100 mL suggested by the United States Environmental Protection Agency (USEPA)[3]. Therefore, the assay volume in bacterial detection should be at least 1 mL so that at least 1 cell is included in the tested assay. As can be seen, a high-performance pre-treatment process is necessary to reduce the initial water sample from a relatively large volume to a small final assay volume (e.g. ~ mL) for single-cell detection biosensors in practical applications.

For the biosensors or lab-on-a-chip devices with a moderate detection limit (e.g. 10 ~ 10^4 CFU/mL), the pre-enrichment process is also important since the target bacterial concentration in the assay needs to be increa sed[3,8,13,23–25]. As discussed below, in combination with a high-performance pre-enrichment process, biosensors with a moderate detection limit can be used to detect bacteria of low initial concentrations (e.g. $\leq$1 CFU/mL).

The reported pre-enrichment methods for rapid pathogen detection include microbial culture, centrifugation, immunomagnetic separation (IMS) and bacterial concentration. Bacterial concentration is the most appropriate method to concentrate the large amount of initial water sample to a few milliliters in a short time period. The use of hollow-fiber, NanoCeram filter, and porous anodic alumina membrane, as well as some other filters to recover multiple microorganisms from large amounts of water samples have been reported[26–31]. Hollow-fiber with tangential-flow ultrafiltration technique has been applied to concentrate and recover *E. coli* by Liu *et al.*, resulting in a final volume of about 440 mL[32]. Usually, final volumes around 250 ~ 500 mL can be achieved by the hollow-fiber[32–41]. Thus, a secondary treatment as centrifugation has been reported to increase the concentration ratio and further reduce the final volume[38]. Furthermore, the reported recovery efficiency of pathogen is in a range of 42% ~ 96% depending on different filtration techniques[32–41]. Therefore, the reported methods still need to be improved to satisfy the requirements for rapid low concentration bacterial detection.

In this paper, an automated bacterial concentration and recovery system (ABCRS) as a high-performance pre-enrichment step is presented for rapid low concentration bacterial detection ($\leq$1 CFU/mL). As the microbial indicator of water quality, *E. coli* was used to evaluate the performance of the ABCRS. The results show that the ABCRS can concentrate large amount of water sample (e.g. 1 ~ 2 liters) to a few milliliters (e.g. 4 ~ 5 mL) with an average recovery efficiency above 92% in less than one hour. The recovery efficiency of the ABCRS is studied in terms of the back-flushing technique, final retentate volume and volume concentration factor.

Results and Discussions

Effects of back-flushing on the ABCRS. As a key factor, recovery efficiency was used to evaluate the capability of the ABCRS to harvest the bacteria from an original large-volume water sample. Fig. 1 shows the measured effects of forward time and back-flushing frequency on the recovery efficiency. 100 mL solutions of known quantities of 10^5 ~ 10^6 *E. coli* cells were spiked to the sample reservoir and these samples were concentrated to about 5 mL by the ABCRS. The ABCRS with back-flushing frequency of 6 cycles/min recovered 93% of *E. coli* cells and the recovery efficiency remained stable as the back-flushing frequency dropped down to 3 cycles/min. A slight decrease in *E. coli* recovery efficiency was found when the back-flushing frequency decreased to 2 cycles/min. A significant decrease was noted at 1.2 cycles/min, resulting in an average *E. coli* recovery efficiency of 84% (as shown in Fig. 1). In contrast, a steep recovery efficiency decline was paralleled by a further drop in back-flushing frequency. The recovery efficiency was only 71% at a back-flushing frequency of 1 cycle/min. As a result, the back-flushing frequency was set at 2 cycles/min for subsequent experiments to achieve stable recovery efficiency and higher permeate flow rate. It is worth noting that the effect of back-flushing on increasing the recovery efficiency has also been reported[27,32,42]. In the previous studies, back-flushing was performed at the very end of the concentration process by adding extra solution (50 mL or more) to the retentate reservoir to wash the target micro-organisms off from the filters or membranes[33,43–45]. The total final volume was100 mL or more in these filtration techniques[37,43,44], and this assay volume is much larger than that can be handled by most microfluidic based sensors. In this study, the back-flushing was used at the end of each forward flow in the filtration cycle, and

Initial volume (mL)	Final volume (mL)	Recovery efficiency (%)	± SD (%)	± RSD (%)
100	10	95	5.6	5.9
250	10	87	6.0	6.9
500	10	91	3.9	4.3
750	10	90	11.5	12.7
100	5	94	4.1	4.4
500	5	94	1.6	1.7
1000	5	90	4.4	4.9

Table 1. *E. coli* recovery efficiencies of the ABCRS at various final retention volumes.

Concentration Ratio	Initial volume (mL)	Final volume (mL)	Recovery efficiency (%)	± SD (%)	± RSD (%)
50	200	4	87	0.5	0.6
100	400	4	107	9.9	9.3
250	1000	4	99	10.9	11
500	2000	4	86	8.3	9.7

Table 2. *E. coli* recovery efficiencies of the ABCRS at various volume concentration factors.

this back-flushing method without elution-solution reduced the final volume collected at the retentate reservoir. The reduced final volume of milliliter-scale can be processed by microfluidic sensors[46].

In the reduced final volume, the bacteria were blocked and captured by the ceramic membrane, and these bacteria cells needed to be transferred to the reservoir. The current study confirmed that back-flushing was effective for bacterial recovery and proved that a higher back-flushing frequency was more effective than a lower back-flushing frequency (Fig. 1). The reason for the increased recovery efficiency was that the back-flushing flow provided a reverse force from the bottom to the top of the ceramic membrane to wash the bacteria cells off from the membrane to the liquid flow. As a result, more bacteria cells were then transferred to the retentate reservoir. The optimized back-flushing methods in this study significantly reduced the final retentate volume to a milliliter scale and a stable recovery efficiency of higher than 92% was achieved simultaneously.

Final retentate volume of the ABCRS. Subsequent experiments were carried out to determine if the final volume can be minimized to obtain a higher concentration factor while maintaining stable and high recovery efficiency. As described above, precise final volume can be obtained by the PLC and the liquid level sensor. At first, the final volume was set at 10 mL, and the concentration factor increased with the increase of initial sample volume. As shown in Table 1, the measured recovery efficiency of a 10 mL retentate was 95%, 87%, 91%, and 90%, corresponding to the concentration factor of 10, 25, 50 and 75, respectively. As the final volume reduced to 5 mL from 100, 500, and 1000 mL initial samples with $10^5 \sim 10^6$ *E. coli* cells, the measured recovery efficiency was 94%, 94% and 90%, respectively. No significant difference of recovery efficiency was observed as the change of initial sample volume or final retentate volume. Obviously, the ABCRS can recover *E. coli* from different amounts of water samples to a small amount of water. In this case, the initial volume and final assay volume can be altered by the ABCRS to meet the volumetric requirements in practical bacterial detection for biosensors. In particular, the results also indicated that 1000 mL water sample with a concentration of 1 CFU/mL can be concentrated in less than one hour and then monitored by a biosensor with a detection limit of 200 CFU/mL. This pre-enrichment step provided by the ABCRS can largely extend the application of biosensors in drinking water quality monitoring.

Volume concentration factor of the ABCRS. In the pre-enrichment process, a higher volume concentration factor implies a lower detection limit for the rapid pathogen sensing system. Table 2 shows the dependence of the measured recovery efficiency of the ABCRS on the volume concentration factor. 2.1×10^7 to 2.4×10^7 *E. coli* cells were seeded to 200 mL, 400 mL, 1000 mL and 2000 mL of phosphate buffered saline (PBS), corresponding to the concentration factor of 50, 100, 250 and 500, respectively. An average recovery efficiency of 87% was calculated when concentrating initial sample of 200 mL to a final volume of 4 mL. The recovery efficiency was 107% as the concentration ratio was 100, and this percent greater than 100% was due to a relative standard deviation (RSD) of 9.3%. The recovery efficiency ranged from 87% to 107%, indicating that more than 87% cells in the sample reservoir were recovered and the performance of the ABCRS under high concentration ratio was verified.

As mentioned above, a large volume of water sample with extremely low bacterial concentration has to be analyzed rapidly in water monitoring. The result in Table 2 indicates that the ABCRS has the capability to concentrate relatively large volumes of bacterial samples (e.g. 2000 mL) to small assay volumes (e.g. 4 mL) with recovery efficiencies above 86%. These results further imply that an initial water sample of 1000 mL with a bacterial concentration of 1 CFU/mL can be detected within one hour based on the fact that it only takes a few minutes to test a 1 ~ 4 mL water sample for a biosensor with a moderate detection limit (e.g. 100 CFU/mL[47]). We therefore

ABCRS (cells)	Method 1603 (avg. cells)	Initial concentration (CFU/mL)	Permeate (cells)	Recovery efficiency (%)
54	57	0.11	0	95
41	45	0.09	0	91
18	20	0.04	0	90
56	64	0.13	0	88
22	28	0.06	0	79
43	60	0.12	0	72
28	47	0.09	0	60
Average recovery efficiency (%)				82
±Standard deviation (%)				13
±Relative standard deviation (%)				15

Table 3. Recovery efficiencies of extremely low *E. coli* concentration using the ABCRS (20 ~ 80 *E. coli* cells).

Method 1603 (avg. cells)	ABCRS (cells)	Permeate (cells)	Initial concentration (CFU/mL)	Recovery efficiency (%)
3	2	0	0.005	67
5	4	0	0.010	80
8	5	0	0.016	63
10	10	0	0.020	100
11	8	0	0.022	73
11	9	0	0.023	82
17	11	0	0.033	65
18	9	0	0.036	50
Average recovery efficiency (%)				73
±Standard deviation (%)				15
±Relative standard deviation (%)				20

Table 4. Recovery efficiencies of extremely low *E. coli* concentrations using the ABCRS (<20 *E. coli* cells).

assume that a detectable initial bacterial concentration of 0.004 ~ 0.04 CFU/mL can be expected if the ABCRS is connected to a sensitive biosensor with a lower detection limit of 1 ~ 10 CFU/mL[22,48].

The ABCRS pre-enrichment of extremely low *E. coli* concentration. To test the performance limit of the ABCRS, pre-enrichment experiments were carried out for water samples of extremely low *E. coli* concentrations. 500 mL PBS containing 20 ~ 80 *E. coli* cells were concentrated to 10 mL, and the recovered cells were cultured and counted by the USEPA Method 1603 (Table 3). Even though the initial concentration levels were about 0.1 CFU/mL, an average recovery efficiency of 82% was achieved for these low-seed *E. coli* samples.

Less than 20 *E. coli* cells were introduced to 500 mL PBS and then concentrated by the ABCRS. Due to the extremely-low concentration, the real numbers of *E. coli* cells were about 3 ~ 18 measured by the USEPA Method 1603 (Table 4). As shown in Table 4, the recovery efficiency varied between 50% and 100% with an average value of 73%. In the absence/presence pathogen detection, 2 out of 3 *E. coli* cells were successfully captured by the ABCRS with an initial bacterial concentration of 0.005 CFU/mL. Therefore, the minimum concentration limit of the ABCRS was 0.005 CFU/mL.

As mentioned above, a large volume of water sample with *E. coli* O157:H7, as few as 10 cells may have to be handled and detected in practical water quality monitoring[49]. Biosensors that can detect 10 *E. coli* O157:H7 cells in 1000 mL water have not been reported. By using the pre-enrichment process enabled by the ABCRS, 5 bacteria cells in 1 liter can be captured and recovered in a few milliliters for further detection by a highly-sensitive biosensor.

Conclusions

Substantial amounts of initial water samples with low bacterial concentration need to be monitored in practical bacterial detection. Conventional bacterial culture and other time-consuming pre-enrichment methods are still necessary to increase the bacterial concentration for detection and the overall assay time is strongly affected. As for sensitive single-cell detection biosensors, the assay volumes still need to be improved to handle substantial amounts of water samples[4,24,27,50]. With the aim of developing a fast and reliable pre-enrichment process for the existing biosensors and other devices to rapidly detect water samples of extremely low bacterial concentrations in practical situations, a high performance automated bacterial concentration and recovery system based on a ceramic membrane has been proposed.

The recovery efficiency of the ABCRS has been studied in terms of back flushing frequency, final retentate volume, volume concentration factor, and extremely low *E. coli* concentration Therefore, the ABCRS can satisfy

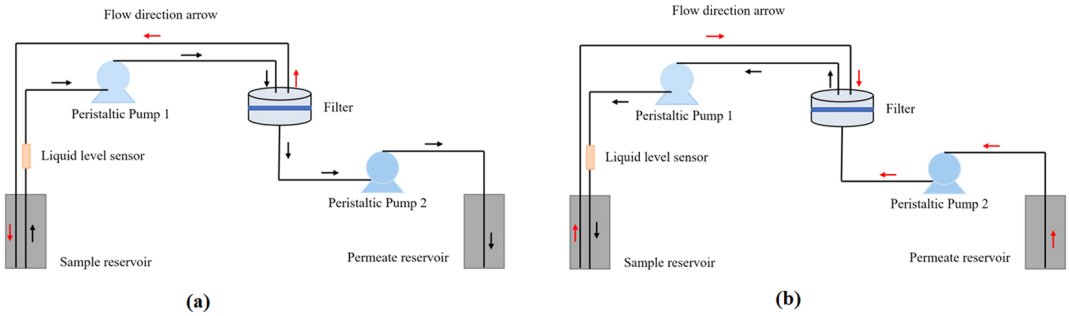

Figure 2. Schematic diagrams of an automated bacterial concentration and recovery system (ABCRS) with the tangential flow filtration technique used in the pre-enrichment process for (**a**) forward, and (**b**) backward flow procedure.

all the requirements for practical rapid pathogen detection, i.e. fast (<1 h), small retentate final volume (<5 mL), high recovery efficiency (>92%), and large concentration factor (from >2000 mL to <5 mL). It has been found that the proposed ABCRS has capability to harvest 20 ~ 80 *E. coli* cells and less than 20 *E. coli* cells in a water sample volume of 500 mL with an average recovery efficiency 82%, and 73%, respectively. It is considered that, in combination with biosensors, the ABCRS will find profound applications in rapid pathogen detection for drinking water.

Materials and Methods

Sample preparation. *Automated bacterial concentration and recovery system (ABCRS).* Figure 2 shows the schematic diagrams of the ABCRS with the tangential flow filtration technique used in the experiments for (a) forward, and (b) backward flow procedure. Fluid was pumped from a sample reservoir to a filter through a pump (peristaltic pump 1), running along the specially designed circular channels, and crossing a ceramic membrane surface inside the filter. The retentate flowed back to the sample reservoir and the permeate flow ran out to the permeate reservoir via another pump (peristaltic pump 2). The ABCRS was based on the tangential flow filtration technique which can efficiently recover the bacteria from water samples. The system consisted of two peristaltic pumps, a ceramic membrane holder, and two reservoirs for water sample and filtrate, as well as a liquid level sensor. PTFE (polytetrafluoroethylene) tubing with inner diameter of 1.6 mm and outer diameter of 3.2 mm was used to connect the ports in the flow system. Polyethylene bottles were used as the sample and retentate reservoirs. All these components were controlled by a programmable logic controller (PLC). The rotation direction and speed of the pumps, and the final volume can be controlled precisely by the PLC.

Concentration and recovery process. As shown in Fig. 2, the concentration process included two steps: the forward flow to filtrate the water sample (Fig. 2(a)), and the backward flow to reduce the bacterial accumulation on the ceramic membrane (Fig. 2(b)). A complete concentration and recovery cycle contained one forward flow process and one backward flow process. In the forward flow process, peristaltic pump 1 was mainly used to pump the water samples from the sample reservoir to the cylindrical filter holder, then peristaltic pump 2 guided the filtrate to the permeate reservoir. A recirculating flow ran back to the sample reservoir along the specially designed circular channels under a high pressure provided by the pumps. In the backward flow process, the reversal rotational direction of pump 2 provided a high-pressure permeate flow running back to wash the ceramic membrane. The concentration and recovery process can be stopped immediately when the designed final volume is achieved, and then the collected retentate can be transferred to the next step for detection.

Microorganism seeding. *E. coli* K-12 MG 1655 was cultured in tryptic soy broth at 37 °C for one night before the experiments. The cultured *E. coli* was centrifuged and re-suspended in PBS, then enumerated under microscope (Nikon Eclipse E200, Japan) before use. Re-suspended *E. coli* cells were diluted to different concentration levels for the following concentrating process.

Microfilter set-up. A ceramic membrane (Sterlitech Corp., USA) was used in all experiments. Membrane diameter was 47 mm and the pore size was 0.14 µm. The ceramic membrane was kept in a stainless-steel cylindrical holder with a specially designed circulating channel (Fig. 2). 70% ethanol was injected to the flow system for sterilization after each run, then the system was rinsed with DI water serval times before next use. The membrane can be reused after cleaning with alkaline solution (sodium hydroxide) and acid solution (nitric acid) respectively.

Manual E. coli cells determination. Microscope counting with a hemocytometer (Bright-Line Hemacytometer, Hausser Scientific, USA) was used to determine the *E. coli* cells in the final volume obtained after concentration process for the concentration ranging between 10^5 and 10^6 CFU/mL. For low-seed *E. coli* samples, contrast groups containing the same amounts of *E. coli* were monitored by the USEPA Method 1603 directly. The experimental groups containing the same numbers of *E. coli* were first spiked to either 500 mL or 1000 mL PBS to run through the ABCRS, and then the *E. coli* cells recovered in the final retentate were measured by the USEPA Method 1603.

The pre-enrichment of the ABCRS. The above described ABCRS was studied and optimized based on four important parameters: back-flushing condition, volume concentration factor, final volume and recovery efficiency.

Back-flushing. A backwashing procedure (the alternative working of the forward and backward flows) was set at the end of each forward flow process, instead of at the very end of the filtration process. The duration of the back-flow process was fixed at 1 second (s), while the duration of forward flow process was set at different values in subsequent experiments. By alternating the rotation direction of the peristaltic pumps, the forward flow proce-dure and backward flow procedure worked alternatively at a specific frequency controlled by the PLC. The timer of backward flow procedure was set at 1 s and the timer of forward flow procedure was set at 10 s, 20 s, 30 s, 40 s, 50 s and 60 s in the experiments, which corresponded to a backwashing frequency of 6, 3, 2, 1.7, 1.2 and 1 cycle(s)/min, respectively. *E. coli* samples of 100 mL with known concentration levels ranging from $2 \times 10^4 \sim 2 \times 10^5$ CFU/mL were concentrated to about 5 mL at various back-flushing frequencies to study the effect of the backwashing on *E. coli* recovery efficiency.

Final volume. A liquid level sensor (Fig. 2) located on a tube between the sample reservoir and peristaltic pump 1 was used to control the final retentate volume. During the concentration process, the tube was filled with water and the sensor started to monitor the liquid level. Once air bubbles were observed, the liquid level sensor sent a signal to the PLC to stop the process. By adjusting the position of sensor and the diameter of the tube, a specified retentate volume (final volume) was achieved. In this research, final volumes were set at 10 mL, 5 mL and 4 mL, respectively, to satisfy the typical assay volume requirement for the subsequent process of bacterial detection.

Volume concentration factor. The volume concentration factor (C) was defined as the ratio of the initial volume of the water sample to the final retentate volume. In the experiments, *E. coli* samples with an initial volume of 500 mL, 1000 mL and 2000 mL were concentrated to a final volume of 10 mL and 5 mL to test the sensitivity and reliability of the ABCRS.

E. coli absence/presence detection. To evaluate the performance of the ABCRS for *E. coli* absence/presence detec-tion, original *E. coli* samples were diluted to 5 ~ 150 CFU/mL according to the standard dilution process sug-gested in the USEPA Method 1603. In absence/presence experiments, 5 ~ 150 *E. coli* cells were seeded in 500 mL PBS to run through the ABCRS and then the recovered *E. coli* cells in the retentate were measured by the USEPA Method 1603. In the contrast groups, the 5 ~ 150 *E. coli* cells were counted by the USEPA Method 1603 directly.

Calculation and data analysis. The recovery efficiency of each test was calculated as the ratio of the total number of *E. coli* in the final retentate to the total number of *E. coli* in the initial water sample. The volumetric concentration ratio (C) of individual test was calculated by the ratio of initial sample volume to the final reten-tate volume. All the experiments of back-flushing, final volume, and volume concentration factor sections were repeated for more than five times. The average recovery efficiency and standard deviation of these repeated tests were used to evaluate the performance of the ABCRS. For *E. coli* absence/presence detection, the range of the total *E. coli* cells were controlled to 20 ~ 80 cells and less than 20 cells in 500 mL PBS. Each test was done once due to the extreme-low number of the bacteria cells.

References

1. Efstratiou, A., Ongerth, J. E. & Karanis, P. Waterborne transmission of protozoan parasites: Review of worldwide outbreaks - An update 2011–2016. *Water Res* **114**, 14–22 (2017).
2. Scallan, E., Hoekstra, R. M., Mahon, B. E., Jones, T. F. & Griffin, P. M. An assessment of the human health impact of seven leading foodborne pathogens in the United States using disability adjusted life years. *Epidemiol Infect* **143**, 2795–2804 (2015).
3. Noble, R. T. & Weisberg, S. B. A review of technologies for rapid detection of bacteria in recreational waters. *J Water Health* **3**, 381–392 (2005).
4. Mortari, A. & Lorenzelli, L. Recent sensing technologies for pathogen detection in milk: A review. *Biosensors and Bioelectronics* **60**, 8–21 (2014).
5. Cho, I. H., Bhandari, P., Patel, P. & Irudayaraj, J. Membrane filter-assisted surface enhanced Raman spectroscopy for the rapid detection of *E. coli* O157: H7 in ground beef. *Biosensors and Bioelectronics* **64**, 171–176 (2014).
6. Ettenauer, J., Zuser, K., Kellner, K., Posnicek, T. & Brandl, M. Development of an automated biosensor for rapid detection and quantification of *E. coli* in water. *Procedia Engineering* **120**, 376–379 (2015).
7. Suaifan, G. A. R. Y., Alhogail, S. & Zourob, M. Paper-based magnetic nanoparticle-peptide probe for rapid and quantitative colorimetric detection of Escherichia coli O157:H7. *Biosensors and Bioelectronics* **92**, 702–708 (2017).
8. Ahmed, A., Rushworth, J. V., Hirst, N. A. & Millner, P. A. Biosensors for whole-cell bacterial detection. *Clin. Microbiol. Rev.* **27**, 631–646 (2014).
9. Xu, H. S. *et al*. Survival and viability of nonculturable Escherichia coli and Vibrio cholerae in the estuarine and marine environment. *Microb. Ecol.* **8**, 313–23 (1982).
10. Ramamurthy, T., Ghosh, A., Pazhani, G. P. & Shinoda, S. Current Perspectives on Viable but Non-Culturable (VBNC) Pathogenic Bacteria. *Front Public Health* **2**, 1–9 (2014).
11. Roda, A., Mirasoli, M., Roda, B., Bonvicini, F. & Colliva, C. Recent developments in rapid multiplexed bioanalytical methods for foodborne pathogenic bacteria detection. *Microchim Acta* **178**, 7–28 (2012).
12. Bono, J. L. *et al*. Evaluation of a Real-Time PCR Kit for Detecting Escherichia coli O157 in Bovine Fecal Samples. *Appl. Environ. Microbiol.* **70**, 1855–1857 (2004).
13. Alocilja, E. C. & Radke, S. M. Market analysis of biosensors for food safety. *Biosens. Bioelectron.* **18**, 841–846 (2003).
14. Elizaquível, P., Sánchez, G. & Aznar, R. Quantitative detection of viable foodborne *E. coli* O157: H7, Listeria monocytogenes and Salmonella in fresh-cut vegetables combining propidium monoazide and real-time PCR. *Food Control* **25**, 704–708 (2012).
15. Jothikumar, N. & Griffiths, M. W. Rapid Detection of Escherichia coli O157: H7 with Multiplex Real-Time PCR Assays. *Appl. Environ. Microbiol.* **68**, 3169–3171 (2002).
16. Ju, W., Moyne, A.-L., Marco, M. L. & Marco, M. L. RNA-Based Detection Does not Accurately Enumerate Living Escherichia coli O157: H7 Cells on Plants. *Front Microbiol.* **7**, 1–9 (2016).

17. Bahadır, E. B. & Sezgintürk, M. K. Lateral flow assays: Principles, designs and labels. *TrAC - Trends in Analytical Chemistry* **82**, 286–306 (2016).
18. Zhao, X., Lin, C.-W., Wang, J. & Oh, D. H. Advances in Rapid Detection Methods for Foodborne Pathogens. *Journal of Microbiology and Biotechnology* **24**, 297–312 (2014).
19. Cui, X. *et al*. A remarkable sensitivity enhancement in a gold nanoparticle-based lateral flow immunoassay for the detection of Escherichia coli O157:H7. *RSC Adv.* **5**, 45092–45097 (2015).
20. Xie, Q. Y. *et al*. Advantages of fluorescent microspheres compared with colloidal gold as a label in immunochromatographic lateral flow assays. *Biosensors and Bioelectronics* **54**, 262–265 (2014).
21. Wu, W. *et al*. A sensitive lateral flow biosensor for Escherichia coli O157: H7 detection based on aptamer mediated strand displacement amplification. *Analytica Chimica Acta* **861**, 62–68 (2015).
22. Dos Santos, M. B. *et al*. Highly sensitive detection of pathogen Escherichia coli O157: H7 by electrochemical impedance spectroscopy. *Biosens. Bioelectron.* **45**, 174–180 (2013).
23. Bridle, H., Miller, B. & Desmulliez, M. P. Y. Application of microfluidics in waterborne pathogen monitoring: A review. *Water Research* **55**, 256–271 (2014).
24. Wang, Z., Han, T., Jeon, T.-J., Park, S. & Kim, S. M. Rapid detection and quantification of bacteria using an integrated micro/nanofluidic device. *Sensor Actuat B Chem* **178**, 683–688 (2013).
25. Velusamy, V., Arshak, K., Korostynska, O., Oliwa, K. & Adley, C. An overview of foodborne pathogen detection: In the perspective of biosensors. *Biotechnol. Adv.* **28**, 232–254 (2010).
26. Stevens, K. A. & Jaykus, L.-A. Bacterial separation and concentration from complex sample matrices: a review. *Crit Rev Microbiol* **30**, 7–24 (2004).
27. Ikner, L. A., Gerba, C. P. & Bright, K. R. Concentration and Recovery of Viruses from Water: A Comprehensive Review. *Food Environ Virol.* **4**, 41–67 (2012).
28. Albinana-Gimenez, N. *et al*. Comparison of methods for concentrating human adenoviruses, polyomavirus JC and noroviruses in source waters and drinking water using quantitative PCR. *J. Virol. Methods* **158**, 104–109 (2009).
29. Yakub, G. P. & Stadterman-Knauer, K. L. Evaluation of immunomagnetic separation for recovery of Crytosporidium parvum and Giardia duodenalis from high-iron matrices. *Appl. Environ. Microbiol.* **66**, 3628–3631 (2000).
30. Lambertini, E. *et al*. Concentration of enteroviruses, adenoviruses, and noroviruses from drinking water by use of glass wool filters. *Appl. Environ. Microbiol.* **74**, 2990–2996 (2008).
31. Kuhn, R. C., Rock, C. M. & Oshima, K. H. Effects of pH and Magnetic Material on Immunomagnetic Separation of Cryptosporidium Oocysts from Concentrated Water Samples Effects of pH and Magnetic Material on Immunomagnetic Separation of Cryptosporidium Oocysts from Concentrated Water Samples. *Appl. Environ. Microbiol.* **68**, 2066–2070 (2002).
32. Liu, P. *et al*. Hollow-fiber ultrafiltration for simultaneous recovery of viruses, bacteria and parasites from reclaimed water. *J Microbiol Methods.* **88**, 155–161 (2012).
33. Hill, V. R. *et al*. Development of a rapid method for simultaneous recovery of diverse microbes in drinking water by ultrafiltration with sodium polyphosphate and surfactants. *Appl. Environ. Microbiol.* **71**, 6878–6884 (2005).
34. Hill, V. R., Mull, B., Jothikumar, N., Ferdinand, K. & Vinjé, J. Detection of GI and GII Noroviruses in Ground Water Using Ultrafiltration and TaqMan Real-time RT-PCR. *Food Environ Virol.* **2**, 218–224 (2010).
35. Hill, V. R. *et al*. Comparison of hollow-fiber ultrafiltration to the USEPA VIRADEL technique and USEPA method 1623. *J. Environ. Qual.* **38**, 822–825 (2009).
36. Karim, M. R., Rhodes, E. R., Brinkman, N., Wymer, L. & Fout, G. S. New electropositive filter for concentrating enteroviruses and noroviruses from large volumes of water. *Appl. Environ. Microbiol.* **75**, 2393–2399 (2009).
37. Kuhn, R. C. & Oshima, K. H. Hollow-fiber ultrafiltration of Cryptosporidium parvum oocysts from a wide variety of 10-L surface water samples. *Can. J. Microbiol.* **48**, 542–549 (2002).
38. Mull, B. & Hill, V. R. Recovery and detection of Escherichia coli O157:H7 in surface water, using ultrafiltration and real-time PCR. *Appl. Environ. Microbiol.* **75**, 3593–3597 (2009).
39. Olszewski, J., Winona, L. & Oshima, K. H. Comparison of 2 ultrafiltration systems for the concentration of seeded viruses from environmental waters. *Can. J. Microbiol.* **51**, 295–303 (2005).
40. Winona, L., Ommani, A., Olszewski, J. Nuzzo, J. & Oshima, K. Efficient and predictable recovery of viruses from water by small scale ultrafiltration systems. *Canadian journal of microbiology* **47**, (2001).
41. Simmons, O. D., Sobsey, M. D., Francy, C. D., Schaefer, F. W. & Francy, D. S. Concentration and Detection of Cryptosporidium Oocysts in Surface Water Samples by Method 1622 Using Ultrafiltration and Capsule Filtration Concentration and Detection of Cryptosporidium Oocysts in Surface Water Samples by Method 1622 Using Ultrafiltratio. *Appl. Environ. Microbiol.* **67**, 1123–1127 (2001).
42. Leskinen, S. D. *et al*. Automated dead-end ultrafiltration of large volume water samples to enable detection of low-level targets and reduce sample variability. *J. Appl. Microbiol.* **113**, 351–360 (2012).
43. Polaczyk, A. L. *et al*. Ultrafiltration-based techniques for rapid and simultaneous concentration of multiple microbe classes from 100-L tap water samples. *J Microbiol Methods.* **73**, 92–99 (2008).
44. Morales-Morales, H. A. *et al*. Optimization of a reusable hollow-fiber ultrafilter for simultaneous concentration of enteric bacteria, protozoa, and viruses from water. *Appl. Environ. Microbiol.* **69**, 4098–4102 (2003).
45. Kuhn, R. C. & Oshima, K. H. Evaluation and optimization of a reusable hollow fiber ultrafilter as a first step in concentrating Cryptosporidium parvum oocysts from water. *Water Res* **35**, 2779–2783 (2001).
46. Guo, T. *et al*. Counting of Escherichia coli by a microflow cytometer based on a photonic-microfluidic integrated device. *Electrophoresis* **36**, 298–304 (2015).
47. David, S. *et al*. Assessment of pathogenic bacteria using periodic actuation. *Lab Chip* **13**, 3192 (2013).
48. Choi, J. R. *et al*. An integrated paper-based sample-to-answer biosensor for nucleic acid testing at the point of care. *Lab Chip* **16**, 611–621 (2016).
49. Wang, Y., Ye, Z., Si, C. & Ying, Y. Subtractive inhibition assay for the detection of *E. coli* O157:H7 using surface plasmon resonance. *Sensors* **11**, 2728–2739 (2011).
50. Nge, P. N., Rogers, C. I. & Woolley, A. T. Advances in microfluidic materials, functions, integration, and applications. *Chem. Rev.* **113**, 2550–2583 (2013).

Acknowledgements

The authors would like to thank Joshua Kneller for his careful proof reading of the manuscript, and the Ontario Research Fund – Research Excellence (ORF-RE) and NSERC Discovery grant for the support of the project.

Author Contributions

T.G. and L.H. designed the system and made the automatic control system. C.Q.X. proposed the study and improved the experimental plan. Y.Z. and T.G. performed the study and optimized the design. Y.Z. and C.Q.X wrote the paper.

Additional Information

Competing Interests: The authors declare no competing interests.

Publisher's note: Springer Nature remains neutral with regard to jurisdictional claims in published maps and institutional affiliations.

Chapter 4

An Automated Cyanobacterial Concentration and Recovery System for Sample Pre-enrichment Required in Rapid Detection of Cyanobacteria

The bacterial concentration and recovery system has been continuously developed and refined to accomplish the aim of sample pre-enrichment process required in the rapid detection of low levels of cyanobacteria. Pre-enrichment or pre-concentration, analyte capture and detection are the general processes for rapid detection of bacteria. Pre-enrichment remains challenging for environmental sample monitoring due to the fact that normally cyanobacteria present in low numbers in water. On the contrary, cyanobacteria can grow rapidly and form blooms with harmful effects under suitable conditions. The growth rate of cyanobacteria depends on significantly on temperature, and it may take a few days up to a few weeks to form the visible blooms. More importantly, harmful cyanobacterial blooms can not be fully stopped. Currently, various methods have been investigated to slow down and control the spread of theses blooms. The best approach to stop the blooms is to prevent the forming of potential blooms, which indicates that extremely low numbers of cyanobacterial samples in large volumes (e.g. 1 Liter) need to be accurately measured. Pre-enrichment process was applied here to reduce the assay volume of these environmental samples to a 1 mL scale. Cells of interest also need to be captured and recovered to the reduced retentate for the increase of sample concentration level.

In this chapter, a new automated cyanobacterial concentration and recovery system was established based on experience accumulated in previous *E. coli* experimental studies. The performance of the system was further improved and optimized for the concentration and recovery of cyanobacterial cells. The work of this chapter shows the results of the pre-enrichment, and indicates that the aim of a bacterial pre-concentration and recovery system listed in research objectives (Figure 1.2) has

been completed. Meanwhile, this chapter connects the previous bacterial concentration work with the subsequent study of cyanobacterial detection using a microflow cytometer. The pre-enrichment process was a partial solution proposed in Figure 1.1 to the overall project of quantification of low-level cyanobacteria present in environmental samples for early warning of potential cyanobacterial blooms.

4.1 Introduction

In previous chapters, *E. coli* cells were used to testify the principle of the approached applied in the system. The empirical experiment results of *E. coli* cells with a wide range of cell densities proved the feasibility of the proposed methods. *E. coli* cells were chosen for validation of the system for four reasons. First, *E. coli* is considered as the best biological indicator of contamination and health risk in both drinking water and recreational water. The size of *E. coli* cells is the second reason. *E. coli* cells are about 2 μm long and less than 1 μm, which is much greater than the pore size (0.14 μm) of the ceramic membrane. The other two reasons relate to the cell culture and detection methods. *E. coli* samples were concentrated and detected at extremely low cell densities (0.005 CFU/mL) to validate the performance of the system. USEPA Method 1603 can be used for accurate determination of *E. coli* samples with extremely low population densities. The *E. coli* colonies grow on the modified membrane-thermotolerant agar can turn deep purple. Meanwhile, the culture condition is not complicated, and it is not time consuming for *E. coli* cells to form colonies for cell counting.

The empirical data obtained from the *E. coli* experimental studies validated the feasibility of the proposed pre-enrichment methods. Based on the theoretical calculation and empirical experience, an average recovery efficiencies above 90% with the pre-enrichment limit as low as 0.005 CFU/mL has been achieved. The final retentate volume was concentrated to 10 mL and then further lowered to $4 \sim 5$ mL leading to a higher concentration ratio. Since we aimed at extremely low cyanobacterial detection, the ideal final retentate volume goal was set on a 1 mL scale.

The work of this chapter was the optimization of the pre-enrichment system for

cyanobacterial use. Final retentate volume which also considered as the assay volume for the subsequent analyte capture and detection process, was one of the main parameters that needs to be optimized. The optimized parameters of the pre-enrichment system were specially developed for cyanobacterial species.

4.2 Materials and Methods

Microcystis aeruginosa, as a common bloom-forming cyanobacterial species, was cultured as the cyanobacterial sample for the concentration and recovery experiments. *M. aeruginosa* was purchased from Canadian Phycological Culture Centre. The diameters of the cells were in the range of $4 \sim 9$ μm. *M. aeruginosa* cells were cultured in liquid flasks with 3N-BBM medium. *M. aeruginosa* samples were diluted and spiked into phosphate buffered saline right before use.

The diluted samples were spiked into the optimized concentration and recovery system to a designed retentate volume of 1 mL. A serial dilution of *M. aeruginosa* in a range of $4 \sim$ 4,200,000 cells/mL were preprepared right before the experiments. The total numbers of cells retained in the retentate after the concentration process was counted using a hemocytometer under a microscope. The extreme low concentration samples were counted using a microflow cytometer in Chapter 7. Meanwhile, more details about the optimization of ACCRS system were described in Chapter 7.

4.3 Results and Discussion

Table 4.1 shows the results of pre-enrichment of *M.aeruginosa* samples. Samples with a large range of *M. aeruginosa* concentrations were concentrated, and the final retentate assay volume of the system for cyanobacterial samples has been reduced from 10 mL to 1.1 mL$\sim$ 1.5 mL. The final assay volume was set at 1 mL initially. In practice, there was a small variation of 0.1 mL $\sim$ 0.5 mL caused by the peristaltic pump, resulting of a final volume of 1.1 mL $\sim$ 1.5 mL. The samples were concentrated from 1 liter, then the cell densities were increased by 909-fold and 667-fold, respectively.

As can be seen in Table 4.1, an average recovery efficiency of 93.29% $\pm$ 3.63% has been achieved. No significant difference was found on the recovery efficiency among the groups with different final retentate volumes. The ACCRS shows good performance for the concentration and recovery of cyanobacteria.

Table 4.1: Cyanobacteria pre-enrichment results obtained by the ACCRS

Initial Cyanobacterial Biomass (cells/mL)	**Concentration Ratio**	**Final retentate volume (mL)**	**Recovery efficiency(%)**
4,200,000	909	1.1	96 $\pm$ 6
420,000	909	1.1	97 $\pm$ 5
40,000	909	1.1	89 $\pm$ 4
4,000	909	1.1	92 $\pm$ 5
400	909	1.1	98 $\pm$ 6

40	909	1.1	90 ± 2
5	667	1.5	91 ± 7

4.4 Conclusions

The work of this chapter aims at the optimization and verification of the cyanobacterial concentration and recovery system. *M. aeruginosa* samples were applied for the feasibility study, and the experimental results with an average recovery efficiency greater than 92% indicated that the goals of the pre-enrichment process can be accomplished by the ACCRS.

The principle tests were done with *E.coli*, and further systematic studies were conducted to show the effects of key parameters on the recovery efficiency. Meanwhile, the wide range of cell densities were tested, and indicated the reliability, repeatability of the automated bacterial concentration and recovery system.

The ACCRS can work as a pre-enrichment process for the further rapid detection of cyanobacteria. The assay volume can be significantly reduced from greater than 1 liter to $\sim$ 1 mL, which can be analyzed by emerging biosensors. Meanwhile, the detection limit required for the biosensors can be largely reduced. More importantly, the ACCRS can retain the cells of target in a small volume and make the capture process easier for the biosensors.

Chapter 5

Optofluidic Device Based Microflow Cytometers for Particle/Cell Detection: A Review

In previous chapters, the pre-enrichment of cyanobacterial detection was completed and addressed. The next step was to find a rapid, accurate, reliable and low-cost detection approach for cyanobacterial detection. In this chapter, a review paper was written to state the current state of art for particle/cell counting using emerging microfluidic devices.

In this work, we aimed to seek a rapid and real-time method for particle/cell counting. Microflow cytometer has been a useful and powerful tool for cell/particle detection, and recent optofluidic microflow cytometers have highly integrated optics on-chip with higher sensitivity. A literature study of optofluidic devices based microflow cytometers for particle/cell detection was investigated in this review paper. The interaction between fluid and micro-optical components in recent microfluidic devices for particle/cell detection was also addressed in this review paper. In this chapter, the optofluidic devices refers to optical systems that synthesized with fluids on a micro or nano device. Beam shaping, built-in optical alignment and waveguides can be designed and employed on the microfluidic chip to improve the performance in fluorescence and scattering detection. This review paper provides the basic principles and useful functions to inspire the design and fabrication of the proposed microflow cytometer.

This chapter is reproduced from a journal article and the author of this thesis is the first author and the main contributor of the reprinted paper.

Zhang, Yushan, Benjamin R. Watts, Tianyi Guo, Zhiyi Zhang, Changqing Xu, and Qiyin Fang. "Optofluidic device based microflow cytometers for particle/cell detection: a review." Micromachines 7, no. 4 (2016): 70. DOI: `https://doi.org/10.3390/mi7040070`

micromachines

MDPI

Review

Optofluidic Device Based Microflow Cytometers for Particle/Cell Detection: A Review

Yushan Zhang [1], Benjamin R. Watts [2], Tianyi Guo [1], Zhiyi Zhang [3], Changqing Xu [4,*] and Qiyin Fang [4]

1 School of Biomedical Engineering, McMaster University, 1280 Main Street West, Hamilton, ON L8S 4L8, Canada; zhang749@mcmaster.ca (Y.Z.); guot2@mcmaster.ca (T.G.)
2 ArtIC Photonics, 260 Terence Matthews Cres, Ottawa, ON K2M 2C7, Canada; benjamin.r.watts@gmail.com
3 Information and Communication Technologies, National Research Council of Canada, 1200 Montreal Road, Ottawa, ON K1A 0R6, Canada; zhiyi.zhang@nrc-cnrc.gc.ca
4 Department of Engineering Physics, McMaster University, 1280 Main Street West, Hamilton, ON L8S 4L8, Canada; qiyin.fang@mcmaster.ca
* Correspondence: cqxu@mcmaster.ca; Tel.: +1-905-525-9140 (ext. 24314)

Academic Editors: Shih-Kang Fan and Nam-Trung Nguyen
Received: 1 March 2016; Accepted: 12 April 2016; Published: 15 April 2016

Abstract: Optofluidic devices combining micro-optical and microfluidic components bring a host of new advantages to conventional microfluidic devices. Aspects, such as optical beam shaping, can be integrated on-chip and provide high-sensitivity and built-in optical alignment. Optofluidic microflow cytometers have been demonstrated in applications, such as point-of-care diagnostics, cellular immunophenotyping, rare cell analysis, genomics and analytical chemistry. Flow control, light guiding and collecting, data collection and data analysis are the four main techniques attributed to the performance of the optofluidic microflow cytometer. Each of the four areas is discussed in detail to show the basic principles and recent developments. 3D microfabrication techniques are discussed in their use to make these novel microfluidic devices, and the integration of the whole system takes advantage of the miniaturization of each sub-system. The combination of these different techniques is a spur to the development of microflow cytometers, and results show the performance of many types of microflow cytometers developed recently.

Keywords: optofluidic device; microfluidics; microflow cytometer; microfabrication

1. Introduction

Since the original attempt in 1934 when researchers first successfully counted particles and cells in a small tube [1], flow cytometry has developed into a powerful technique for cell analysis, sorting and counting. Recently, flow cytometry has been applied in many fields, such as point-of-care (POC) diagnostics, cellular immunophenotyping, rare cell analysis and genomics [2]. The commercialization of conventional flow cytometers has been very successful: the market of modern microflow cytometers is expected to reach $3.6–5.7 billion by 2018 at a compound annual growth rate of 18%–29% [3]. Compared to a bulky conventional flow cytometer, microchip-based flow cytometers (referred to as microflow cytometers in this paper) are simple to use, time efficient, consume low amounts of expensive reagents and have overall lower associated costs (capital, operation, training, *etc*). With the rapidly developing demands of POC applications, the growing demands of *in situ* and *in vitro* diagnostics in the biomedical field and the need to improve rapid analysis and synthesis in the chemical field, microflow cytometers are poised to facilitate great advancement in these and other fields and allow applications that will change many aspects of everyday life in the near future.

The term "optofluidics" was first mentioned in 2003 and was coined to reference new devices that integrated the fields of optics and microfluidics [4]. Microfluidics is the technology that

manipulates fluids on the nL–fL scale on a microchip platform, whereas optofluidics manipulates both fluids and optics simultaneously in a seamlessly integrated platform. A microchip-based device that is based on the technology of microfluidics is called a microfluidic device, while an optofluidic device is a device based on optofluidics, requiring both fluidic and optical capabilities. A microflow cytometer is a highly integrated system that utilizes a microchip-based device for the fluidic handling and manipulation in a flow cytometry application. An optofluidic microflow cytometer utilizes an optofluidic device to apply flow cytometry using a single device to integrate both the fluidic and optical sub-systems onto a single device. Classification of the terminology and the function of the device is shown in Table 1.

In an optofluidic microflow cytometer, the optical components are integrated into a microfluidic system and *vice versa* [5]. Integration allows the benefits of including new optical features on the device, such as built-in optical alignment, beam shaping, high optical sensitivity and tenability-each seamlessly integrated in one platform with fluidics. Previous review papers have already summarized the fundamentals and applications of optofluidic technology [4–6]. In this paper, we will discuss the basic principles and components of an optofluidic device-based microflow cytometer in detail, as well as review the performance of a few microflow cytometers developed recently and compare the performance of the devices.

Table 1. Terminology.

Terminology	Main Device Used	Description
Microflow cytometer	Microfluidic device	Integrated optics are not necessary
Optofluidic microflow cytometer	Optofluidic device	Integrated optics are necessary

1.1. The Principles of Flow Cytometry

Flow cytometry is a powerful analysis technology for the characterization of cells or particles. Multiple parameters, *i.e.*, size, shape, cell granularity and cell viability, can be detected simultaneously at rates of up to 50,000 particles per second [1]. The original intention of flow cytometry was to measure particles or cells one-by-one as they passed through a laser beam in a single file stream flowing through a glass tube [7]. Scattered light at both small and large angles, as well as fluorescence light (FL) emitted from fluorescent labels are detected and analyzed for every single cell or particle. Light scattered at a small angle from the input beam axis is referred to as forward scattered light (FSC), whereas large angles of scattered light are called side scattered light (SSC). The intensity of FSC is generally determined by the size of the cell, while the granularity of the particle or cell determines the intensity of SSC. Through the analysis of the two data parameters, the cells or particles can be identified, counted and sorted downstream. The performance of a flow cytometer is dependent on one of the four main techniques integral to flow cytometry: particle focusing, beam shaping, signal detection and data analysis.

In flow cytometry, particle focusing is applied to ensure the cells of interest pass through the optical interrogation point one by one, reducing the possibility of a double detection. The interrogation region is the intersection between the excitation light beam and the solid angle accepting scattered light or fluorescence from the detection optics. The sample fluid containing cells or particles is surrounded by a sheath fluid which confines the particles to a narrow stream in the center of the channel, roughly one cell or particle in diameter.

Conventional flow cytometers focus and shape the excitation beam by using a free-space lens system. Ideally, the beam would be aligned with focused sample stream, and the beam width would be no less than the width of sample stream to ensure the entire particle or cell can be illuminated. In addition, the portion of the light beam outside the sample stream is minimized to keep the background illumination, thus the noise on the detection channels, as low as possible.

A pulse is produced when a particle or cell passes through the laser beam. The pulse shape and amplitude relates to the interaction between the incident beam and the particle or cell, including the incident light intensity, particle size, geometry and granularity, as well as the fluorescence efficiency. The pulse duration depends on the beam width and linear velocity of the particle along the channel. Therefore, light beam intensity with a super-Gaussian distribution along the flow direction is preferred to generate pulses close to a square waveform.

When particles pass through the laser beam, SSC, FSC and fluorescence light signals are detected by a number of detectors. A modern flow cytometer can detect as many as 17 independent channels featuring a combination of several FL wavelengths, FSC and several different angles of SSC simultaneously by using a series of dichroic mirrors [1]. Thus, multi-parameters can be monitored by analyzing those light signals. In some circumstances, in conjunction with or in place of an optical interrogation method, impedance-based cell or a particle sorting, counting and differentiating method can also be applied in flow cytometry [8,9]. Cells or particles pass through a small area enclosed by two electrodes, where electrophysiological impedance variation can be detected for every single cell or particle.

1.2. Microflow Cytometer

Although conventional flow cytometers have gained profound success in cell sorting and analysis, they are bulky, demand large amounts of expensive reagents with complicated processing steps, are complicated in manipulation and require high maintenance costs. Typically, a flow cytometer will be located in a single facility where many hundreds of users will need access to it. These limitations restrict their uses in POC diagnostics, *in situ* pathogen monitoring and other application where portability, handling small volume samples, low operation costs and ease of operation are essential.

Owing to the recent development of lab-on-chip (LOC) technology, microfabrication and micromachining techniques, the miniaturization of a flow cytometer can be achieved. The microfabrication of a flow cytometer with 3D microstructures can be accomplished by 3D microfabrication techniques utilizing UV lithography [10]. Microfluidic mixing [11], microfluidic cell sorting and the miniaturization of pumps and valves [12] provide a basic foundation for miniaturizing the fluidic handling to develop a microchip-based flow cytometer. Researchers have been able to take advantage of these advanced microfabrication technologies to miniaturize a flow cytometer to a microscale or even a nanoscale platform. Controlling fluids in a microchannel allows microchip-based flow cytometer to be applied in POC diagnostics and lab-on-a-chip devices offers unique advantages [13], such as reducing the volumes of reagents, shortening the turnaround time between inspection and results and lowering the associated costs [14].

To date, the throughput of microflow cytometers can reach up to 50,000 cells/s [1], allowing microflow cytometers to have many applications: Titmarsh *et al.* [15] discussed how microfluidic technology spurred on the development of stem cell-derived therapies. Hashemi *et al.* [16] successfully distinguished different populations of phytoplankton with high sensitivity by measuring light scatter and fluorescence properties by a microflow cytometer. More demonstrations on diagnostic and point-of-care applications have been addressed in recent review papers [14,17].

A novel optofluidic device-based microflow cytometer emerged recently. Optical components and novel liquid lenses are used in microfluidic devices. Liquid-core/liquid-cladding waveguides and liquid core/air-cladding lens systems with larger refractive index contrast lead to less propagation losses and resulted in better optical confinement [18]. Additionally, an integrated on-chip lens system or grooved on-chip fibers further reduce the size of the microflow cytometer. Built-in waveguides also are free of optical alignment, making operation much easier. Recently, Liang *et al.* took advantage of evanescent waves present at the liquid-liquid interface of immiscible flows to count the nanoparticles on an optofluidic microchip [19].

2. Major Components of an Optofluidic Microflow Cytometer

Typically, the creation of an optofluidic device-based microflow cytometer includes four principle design areas: (1) the flow control; (2) the optical design; (3) the microfabrication of functional layers; (4) the integration of the entire system. The flow control includes how to bring flow into a device and to ensure cells or particles are being focused in the interrogation region, which is usually achieved by 2D or 3D hydrodynamic focusing methods. The optical system provides light for interaction and collects light signals for analysis. The microfabrication of fluid control and optical components provide a microscale or nanoscale platform for cell analysis. System integration includes the miniaturization of the device and provides user-friendly control environment and easy-to-use data analysis software.

Figure 1 shows a system setup of a typical optofluidic microflow cytometer [20]. Cells are delivered to the interrogation region in a sample fluid surrounded by two sheath fluids. Cells traverse the light in the interrogation region that has been focused by the on-chip lens system and produces its characteristic optical signature containing SSC, FSC and FL signals. In this iteration of the device, the collection arm is not integrated on the device like the excitation optics, and thus, the signals are collected via a free space objective and directed to a spectral and spatial filter where they are finally detected and amplified by a photomultiplier tube (PMT). In this device, the bulky and expensive free space optical lens system for excitation in a conventional flow cytometer was replaced by cost-effective, space-saving and free optical alignment on-chip lens system.

The challenge and difficulty of miniaturizing the flow cytometer is how to make the performance of a microflow cytometer comparable to the conventional benchtop flow cytometer. In this chapter, optofluidic microflow cytometers with different features classified in Table 2 will be discussed. All of the aspects in Table 2 contribute to the performance of an optofluidic microflow cytometer and will be discussed in detail in later sections.

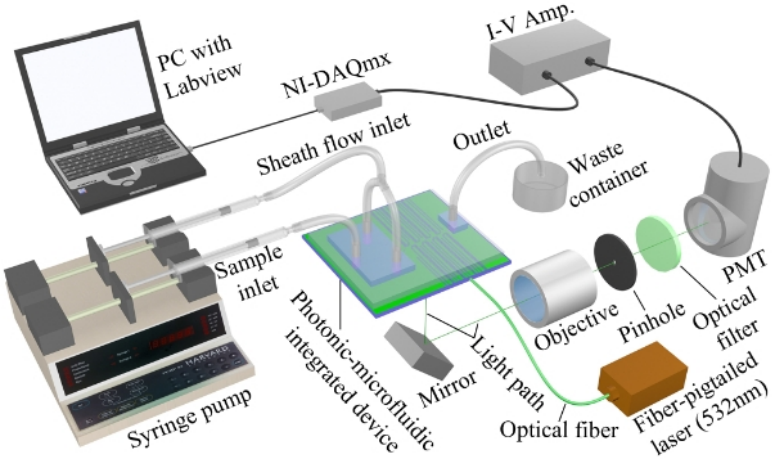

Figure 1. System setup of an optofluidic device (also referred to as photonic-microfluidic integrated device)-based microflow cytometer. Laser light is focused through on-chip lenses, and side scattered light (SSC) and fluorescence light (FL) signals are detected via free-space lens system. Light signals are amplified by a photomultiplier tube (PMT), then data are analyzed by a data acquisition card (DAQ). Reproduced from [20] with kind permission from Wiley.

Table 2. Techniques related to the performance of an optofluidic microflow cytometer.

Flow Control	Light Guide	Light Collection	Collected Signal
2D hydrodynamic focusing	Free-space/on-chip	Free-space/on-chip	Fluorescence collection (FL)
3D hydrodynamic focusing	Free-space/on-chip	Free-space/on-chip	Side scattered light (SSC)
Other methods	Free-space	Free-space	Forward scattered light (FSC)

2.1. Flow Control

In microfluidics, the sheath fluids and sample fluid can be considered as Newtonian fluids, which are continuous, laminar and incompressible. In microflow cytometers, passive flow driven by capillary force or gravity or active pumps driven by an external power source are used to provide continuous flow through the devices [21,22]. Since the cross-section of the channel on the scale of a few 10s of micrometers and the sidewalls are smooth, the flow in the microchannels can be classified as a Stokes flow with a Reynolds number less than one, meaning that the flow in the channel is in the laminar regime. Small dimensions of the microchannel may raise the risk of clogging by big particles or cells, clumps of cells or even extraneous debris. Details about basic concepts, fabrication strategies and advanced applications of hydrodynamic focusing in microflow cytometers can be found in a review by Ainla *et al.* [23].

2.1.1. 2D Hydrodynamic Flow Focusing

The hydrodynamic focusing technique used in both benchtop and microflow cytometers is one of the most successful and ubiquitous flow focusing techniques. The sample fluid is sandwiched between a sheath fluid in both sides, and since the Reynolds number is low and the fluids are in the laminar regime, there will be no turbulent mixing of the fluids. Figure 2a shows a typical structure used to achieve 2D hydrodynamic focusing in a microflow cytometer [24]. Similar structures that narrow the sample fluid between two sheath fluids have been widely used in microflow cytometry [16,25–29]. The width of the focused sample stream is related to the ratio of sample to sheath flow rate and effectively allows the user to tailor the sample stream width to the application's requirements [30]. The sample stream's width must be large enough to accommodate the largest particles in the sample population, yet not too large as to allow particles to flow side-by-side in the sample stream. It must be noted that the vertical channel height defines the height of sample fluid in 2D hydrodynamic scheme, and thus, careful consideration must be taken as to the channel height and the characteristic size of the cells or particles under inspection.

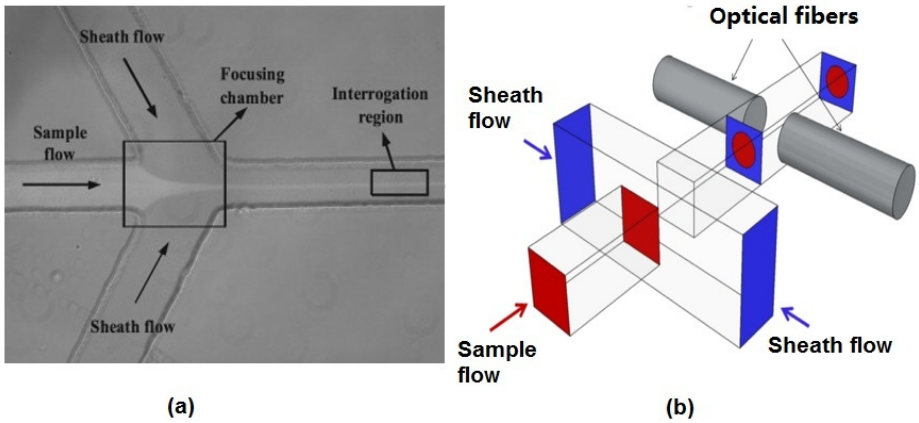

Figure 2. Reported hydrodynamic focusing methods in a microflow cytometer. (**a**) A typical structure of 2D hydrodynamic focusing. Reproduced from [24]. (**b**) A straight forward 3D hydrodynamic focusing structure. Reprinted from [31] with kind permission from OSA Publishing.

2.1.2. 3D Hydrodynamic Flow Focusing

3D hydrodynamic focusing confines the sample fluid to the center of the microchannel in both vertical and horizontal directions, an improvement on the inability of 2D hydrodynamic focusing to focus fluid in the channel's vertical dimension. The straightforward way to achieve 3D hydrodynamic focusing is to use deeper orthogonal sheath fluids, as shown in Figure 2b [31]. Two lateral fluids get in

above and below the sample fluid in addition to lateral directions and push the sample fluid from both vertical and horizontal directions in a microchannel with a larger dimension than that of the sample channel. Since deeper channels are difficult to fabricate, requiring three fabrication and two alignment steps, 2D hydrodynamic focusing and its one fabrication step is preferred. However, a strategy of using 2D hydrodynamic focusing twice has been applied to achieve 3D hydrodynamic focusing. By using a planar structure, two sheath fluids A and B can be used to focus the sample fluid vertically, and the sample fluid was focused horizontally by another sheath fluid, C [32]. Experimental results and numerical simulation results show that the sample stream is focused to a small region in the center of the microchannel.

With 3D microfabrication technology, more complex structures are fabricated to focus the particles in two dimensions, such as oblique cylinders or grooves [10]. Sundararajan *et al.* used the "membrane sandwich" method, which contained two sheath fluids from lateral directions and another two on top and at the bottom stacked on the inlet point to create a 3D hydrodynamic focusing microchip [33]. Hairer *et al*. focused the sample fluid by using three sheath fluids in a non-coaxial sheath flow device [34]. V-shaped or chevron-shaped grooves were fabricated in microchannels to focus the sample fluid in both lateral and vertical directions [35,36]. Similar V-shaped slants were also applied in 3D mixing [37]. More recently, Nawaz *et al.* achieved 3D hydrodynamic focusing by using microfluidic drifting with different curvature angles [38].

2.1.3. Other Methods

Besides hydrodynamic focusing, acoustics [39–43], dielectrophoresis (DEP) force [44–47], electrokinetics and magnetophoresis (MAP) [48–50] can be used alternatively to focus particles and cells in a microflow cytometer. Acoustic-based focusing methods do not need sheath fluids for 3D focusing. The standing surface acoustic waves (SSAW) field generated by two parallel interdigital transducers (IDTs) applies lateral and vertical acoustic radiation force to the particles or cells, as shown in Figure 3a. Particles or cells are focused in the center of the microchannels where the pressure node is located. Recently, Chen *et al.* created an SSAW-based 3D focusing microflow cytometer [41], as shown in Figure 3b.

Dielectrophoresis (DEP) is another approach to achieve 3D focusing in microchannels without sheath fluids. In DEP, a non-uniform oscillating electric field creates a dipole on the cells or particles that will experience a negative or positive force depending on the dipole's phase with the applied AC field and the strength of the electric field at each end of the dipole. By changing the frequency of the field, it is possible to tune the strength of the force on the particles or even to switch the direction of the DEP force. The DEP force can adjust particle's or cell's equilibrium position-normally at the center of the channel in the vertical position by utilizing a pair of parallel microelectrodes on the top and bottom surface of the microchannel. Usually, particles or cells experience a negative force as a positive DEP force pulls the particles or cells towards the surface of the electrode where the greatest field gradient occurs that could destroy the cells [51]. The DEP force depends on the size and electrical properties of the particles or cells, the electrical properties of the sample fluids and the electric field. Large particles or cell move slower than smaller particles or cells, and the focusing pattern of each cell or particle is different. Many microchip-based flow cytometers now use more than one technique to confine sample flow. Lin *et al*. [52] combined the 2D hydrodynamic focusing and DEP method to obtain 3D focusing: two electrodes exerted a DEP force from the vertical direction on the particles and cells, which had already been focused laterally hydrodynamically by two sheath fluids. More recently, Zhang *et al.* presented a novel DEP-inertial microflow cytometer, which combined the DEP force and inertial force to achieve vertical-focusing [46]. The MAP theory is similar to DEP force, except that the electric field is replaced by the magnetic field. In addition, particles or cells need to be attached to a magnetic bead so that they can move to the interrogation point exactly.

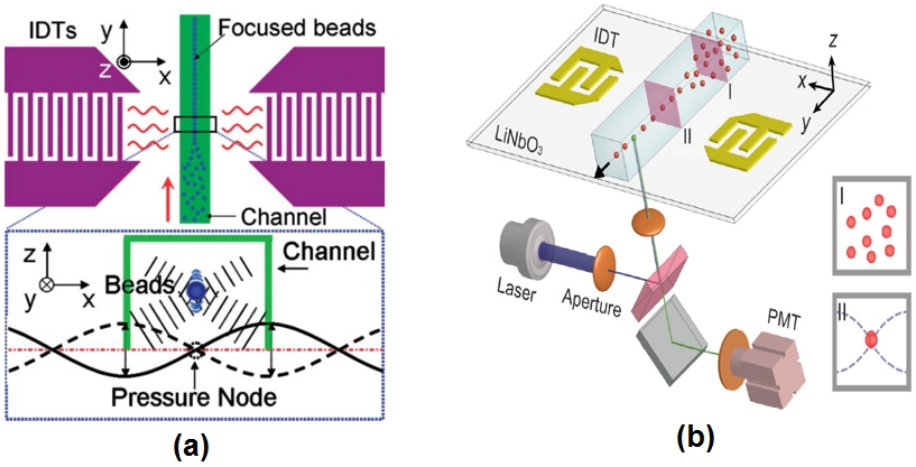

Figure 3. (**a**) A schematic diagram of standing surface acoustic waves (SSAW) focusing. The pressure node located at the center of the microchannel was generated by the SSAW field created by two parallel interdigital transducers (IDTs). When particles or cells enter the SSAW field, the acoustic radiation force (vertically and horizontally) moves the particles to the pressure node. Reprinted from [39] with kind permission from Royal Society of Chemistry. (**b**) A schematic diagram of a SSAW-based microflow cytometer. Reprinted from [41] with kind permission from Royal Society of Chemistry.

2.2. Light Guide and Collection

Particles or cells focused in the center of the microfluidic channel are interrogated by a light beam. In a conventional flow cytometer, a light beam is guided to the capillary tube for excitation, while the various light signals are collected by an objective lens and subsequently split and detected in free-space by bulky optical lenses, dichroic mirrors and other components. A first step towards an optofluidic microflow cytometer involved moving the excitation optics to the chip. Integrating lenses onto the chip eliminates the need for free-space optical alignment while reducing the size of the microflow cytometer device and making the device more portable and durable. Free-space light collection was very similar to the conventional flow cytometer, as shown in Figure 1 [20]. This section will focus on the simulation and design of integrated on-chip optical systems for optical excitation in an optofluidic microchip-based flow cytometer.

2.2.1. Excitation Sources and Optical Fibers

As shown in Figure 1, a laser beam is coupled into a fiber, and the fiber subsequently couples light to an integrated waveguides on the chip to precisely deliver the light to the channel to excite the FL of the particles or cells and generate the scatter signals [20]. In some research papers, light-emitting diodes (LEDs) and laser diodes are used as a source, and either could be used; however, light from an LED is noncoherent light with a wide bandwidth, but has a low cost, while the light from a laser diode is coherent light with a narrow bandwidth and has a higher cost. The correct source can be selected based on the application.

Optical fibers (both single-mode fibers and multi-mode fibers) can be coupled with lasers to provide decent beam shaping at the interrogation region; however, the beam diverges as it leaves the guiding medium. Optofluidic devices coupled with single-mode fibers have been well-reviewed by Blue *et al.* [53]. A device with an integrated on-chip lens system couples light from an optical fiber to an on-chip waveguide to deliver the light to the lens system and focuses and shapes the light in the interrogation region [54,55]. Instead of integrated waveguides on the chip, microgrooves fabricated in the functional layer can help embed optical fibers into the microchip eliminating the need to align fibers to the chip. These inserted fibers can be used for the collection of light signals, as

well. Inserted fibers ensure a complete optically-guided approach, from source to detector [2,26,56]. Matteucci *et al.* [56] fabricated grooves for the insertion of optical fibers to achieve precise alignment of optical power (as shown in Figure 4a).

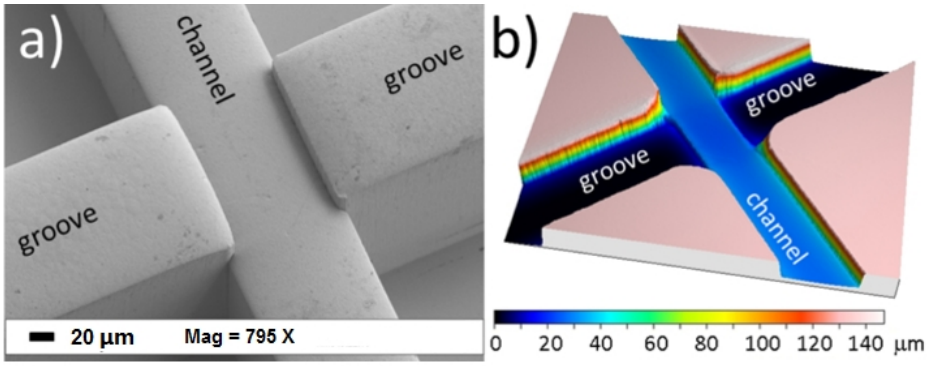

Figure 4. (**a**) SEM microgram of microgrooves for optical fibers. (**b**) confocal microscope profilometry of the microchip that shows the depths of microchannel and microgrooves. Reproduced from [56] from *Micromachines* published by MDPI.

2.2.2. Waveguides

Optofluidic waveguides, such as solid-core/liquid-cladding waveguides (SCLC), liquid-core waveguides (LCW) [57,58] and hybrid core waveguides (HCW) [59,60], have been reported. Guiding of the light is ensured if the refractive index of the core material is higher than that of the cladding. In an optofluidic microflow cytometer, deionized (DI) water, water-based liquids and organic-based liquids are typically used for cladding materials, while glasses, polymers and semiconductors are typical materials used for the core. Choi *et al.* [61] used DI water as a core fluid and 2,2,2-trifluoroethanol as cladding fluid to form a waveguide. Liquid-core/air-cladding (LA) waveguides have been integrated into an optofluidic device by Lim *et al.* [62]. Shi *et al.* [60] demonstrated a hybrid waveguide consisting of a liquid-liquid waveguide and a liquid-solid waveguide to achieve real-time self-imaging in a microchannel. Compared to 2D liquid-liquid waveguide, the 3D liquid-liquid waveguide is surrounded by cladding fluid in both directions, and the confinement of light is better [63]. Yang *et al.* demonstrated bending and manipulating light via optofluidic waveguides with their unique optical properties [64].

Optically transparent photoresists, such as SU-8, are widely used to fabricate on-chip waveguides integrated simultaneously with the microfluidic channel during the fabrication process [54]. SU-8 can function as the core while voids provide air to function as cladding material. As the refractive index of SU-8 (about 1.59) is higher than that of the air, strong optical confinement is observed, lowering the background noise [65]. Figure 5a shows a typical air cladding SU-8 core waveguide fabricated by Watts *et al.* [65]. Light is guided through the long straight waveguide to the lens system, shaping in the microchannel and then collected by multiple waveguides at angles at 5°, 30° and 75° to the input laser beam axis. FSC, FL and SSC are collected from each of the angled waveguides (respectively), where the angled on-chip waveguides help to avoid noise due to a couple of stray light signals from the input laser diode. To further improve the signal to noise ratio (SNR), an angled input waveguide along with an angled lens system were used to reduce the noise by allowing a full 90° angle between the input and SSC, as shown in Figure 5b. A low background noise is created for SSC, which has the same wavelength as that of the excitation beam. Waveguides made by optically transparent polymers, such as poly(dimethylsiloxane) (PDMS), can also be integrated onto the device. In addition to polymers and photoresists, researchers have shown that other materials can also function as waveguides. For example, Emile *et al.* [66] used 1D soap films as waveguides to guide light coming from a laser diode.

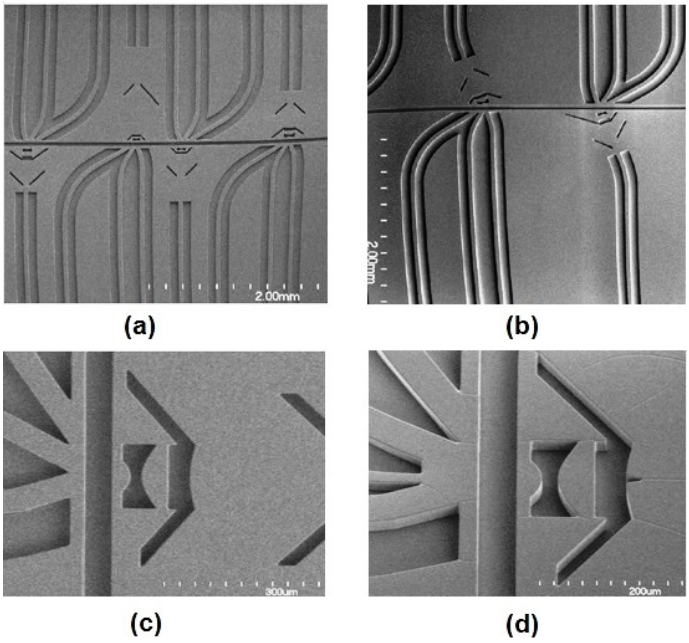

Figure 5. (**a**) SEM images of four microflow cytometers with different optical systems. Long straight waveguides direct lights to the lens system; waveguides at different angles are used to collect signals. (**b**) Images of angled input waveguides and the lens system to reduce background noise for SSC and FSC detection. (**c**) SEM images of on-chip air lens system without notches. (**d**) SEM images of on-chip air lens system with notches. Reproduced from Watts [65] with permission.

2.2.3. On-Chip Lens System

Due to the large numerical aperture of the on-chip waveguide inherit in the materials' large index contrast, the beam coming out of the waveguide will diverge and expand as it traverses the distance from the waveguide facet to the interrogation region. In other words, the light that propagates to the interrogation region will have a large spot size and poor uniformity. For an optofluidic microflow cytometer, on-chip lens systems can be integrated in the microchip to replace bulky and expensive optical components used in free-space solutions. Beam shaping is used to focus the laser beam via a 2D lens system embedded on the microchip between the waveguide and the microchannel, increasing the uniformity of the light for interrogation (Figure 5). Watts *et al.* [54,55,65,67–70] reshaped the beam from the excitation laser to an optimized geometry in the interrogation region to enhance detection. Beam shaping process specifically reshaped the input laser spot geometry to a designed spot geometry where the center portion of the laser beam was altered to obtain a much smaller and uniform beam. For example, by adjusting design parameters of each surface in the lens system, a beam size of 1.5 μm and 3.6 μm, defined by the full width at half-maximum (FWHM), was formed at the focusing point in the microchannel [65]. The initial beam waist was around 50 μm, which was almost 33 times larger than the reshaped beam waist, and the added benefit of a significant corresponding increase in the beam intensity is also achieved. Simulations using commercial ZEMAX software (2005) shown in Figure 6a demonstrate the process of the shaping the beam from the input to output. Light emitted from the laser passes through the SU-8 waveguide, propagates along the SU-8/air lenses, and forms beam waists of 3.6 μm and 10 μm in the two examples shown. Fluorescent images of the beam with and without shaping (Figure 6b,c, respectively) show that the waveguide without integrated lenses have no control over the beam geometry. It is worth noting that the measured coefficient of variation (CV) of fluorescent beads was strongly dependent on the beam geometry and bead sizes: 2.5-μm fluorescent beads had the best CV of 8.5% for a 3.6-μm beam waist [65].

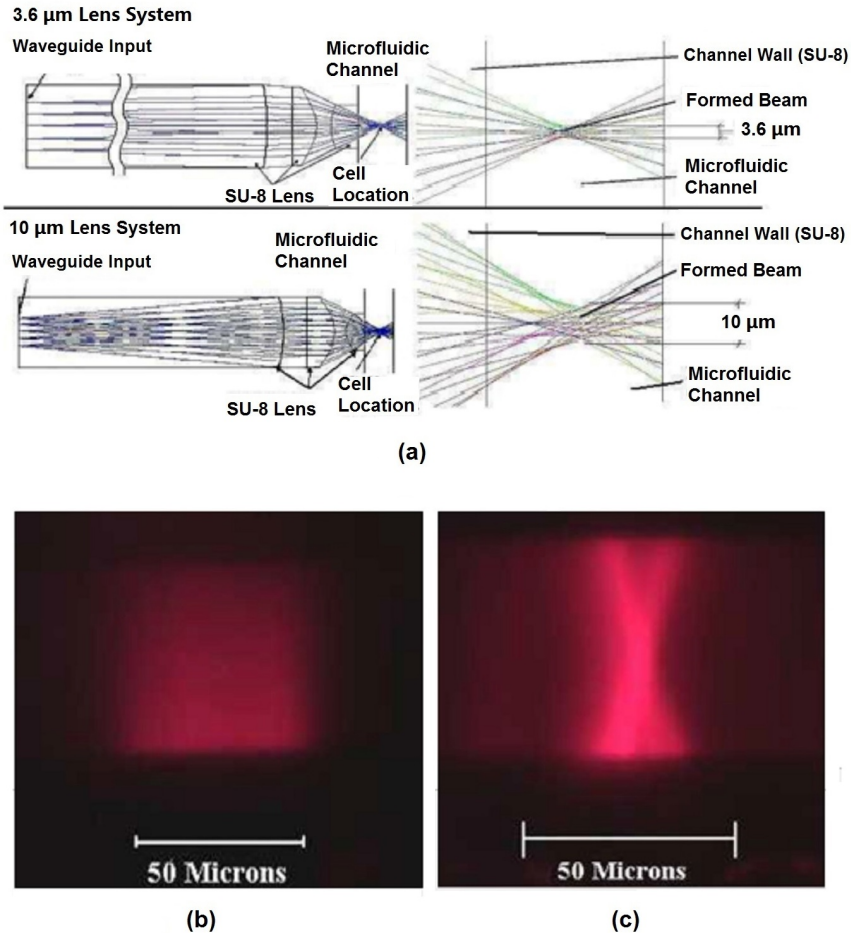

Figure 6. Beam shaping simulation results and fluorescent images of formed beam shape. (**a**) ZEMAX simulation results of 3.6-µm and 10-µm on-chip beam shaping lens systems. (**b**) Fluorescent image of the input excitation beam input directly from a waveguide without any lens. (**c**) Fluorescent image of formed beam shape after passing through a 10-µm beam shaping lens system. Reprinted from [67] with permission from OSA Publishing.

In conventional flow cytometry, a thin obscuration bar located before the detector, onto which the input beam is focused, is used to block the laser beam from reaching the detector directly. This technique is done because the laser beam propagates along the same axis that the FSC and obscures the FSC signal. In an optofluidic device, a notch was applied in the first surface of the lens system, functioning as an obscuration bar, as seen in Figure 7 [65]. The notched lens system forms a dark spot on the facet of a collection waveguide without influence on the beam geometry in the interrogation region. This notched design enhanced the SNR and improved the reliability of on-chip detection for FSC: results show that a false positive rate as low as 0.4% can be achieved [70].

In some optofluidic microflow cytometers, researchers combined the advantages of both liquid and light. Tang *et al.* [18] created a reconfigurable liquid-core/liquid-cladding lens (L^2 lens) formed by three laminar flows. Very similar to the air lens system, two streams of a lower refractive index function as the cladding, and a stream of a higher refractive index functions as the core. The focal length of the lens can be changed in real time by changing the relative flow rates of the three streams without mechanical moving parts. At the same time, the liquid lenses provide an optically-smooth interface for light manipulation. Those novel optofluidic components provide new opportunities for on-chip flow cytometers and cross the boundary of multiple disciplines.

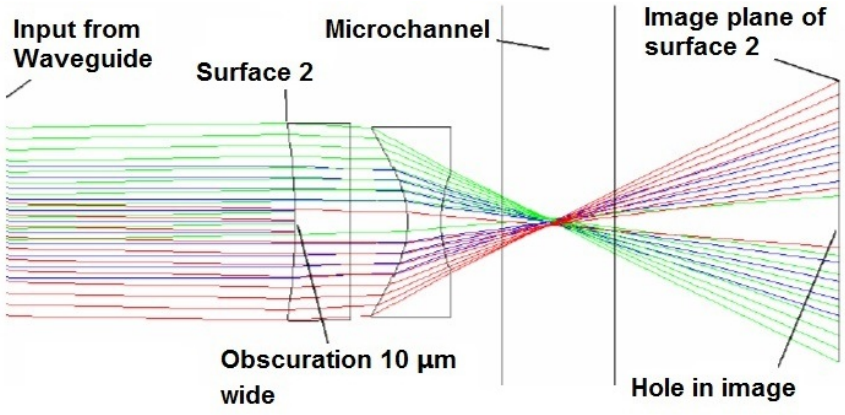

Figure 7. ZEMAX simulations for a 3-µm lens system that inserts a notch for forward scattered light detection. Note how the notch is re-imaged on the waveguide behind the channel. Reprinted from [65] with permission.

To minimize losses in the system, it is important to match the size of the on-chip waveguide and coupling fiber. The roughness of the waveguide, lens surfaces and channel wall can also cause propagation losses in the device. The SEM image in Figure 8 shows that the sidewall and facets are very smooth. The excellent quality of the waveguide facet, channel wall and lens surfaces allow low amounts of escaping light due to scattering from imperfection in the photolithographically-formed side walls. To further improve the sensitivity of the device, higher input laser power can be provided to enhance the SSC or FL signal of the particles or cells. The effect of roughness of the on-chip lens system can be ignored due to the high signal-to-noise ratio.

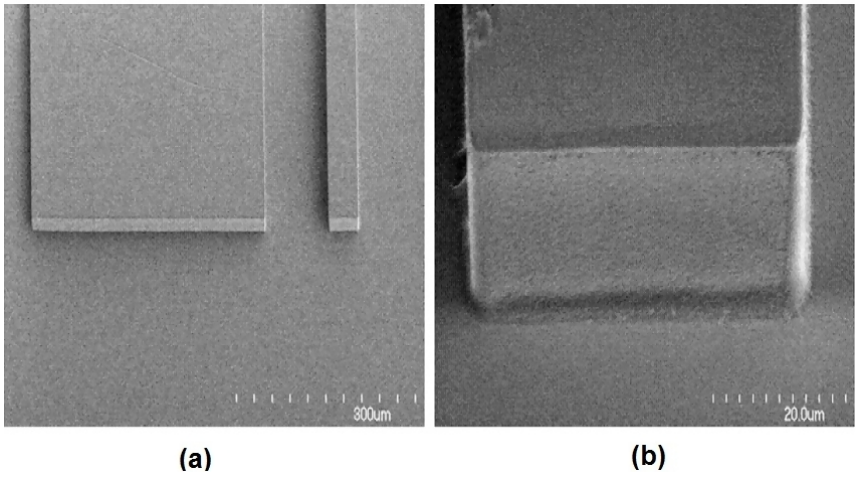

Figure 8. (**a**) SEM image of a waveguide facet. (**b**) A close-up SEM image of a waveguide facet showing the smooth optical coupling face. Reprinted from [65] with permission.

2.3. Data Collection

Scattered light and fluorescent light produced by the interaction between the light beam and particles or cells are detected by the optical detectors connected to a computer. The most common optical detectors are photomultiplier tubes (PMTs), avalanche photodiodes (APDs), P-doped/Intrinsic/N-doped (PIN) photodiodes [21,26], charge-coupled device (CCD) cameras and CMOS arrays [71–73]. PMTs have been widely used in commercial flow cytometers due to the high sensitivity and reliability, especially when dichroic mirrors are used to split the beam for multi-color

fluorescence detection. PMTs and other photodiodes can convert incident light to an electrical current and multiply it by as much as 10^8 times. Recently, compact PMTs have been made available on the commercial market, which can be used to replace the old large PMTs and to reduce the overall size of the detection system. Compared to PMTs, APDs are sensitive to temperature, and PIN photodiodes have a much simpler structure. PIN photodiodes can replace PMTs and APDs to reduce the cost when the light signal is strong. PIN photodiodes with lock-in amplification can be utilized for the single cell or particle fluorescence detection [26]. Kettlitz *et al.* avoid expensive PMTs and substitute them with a PIN photodiode, achieving a maximum particle detection frequency of 600 particles/s [74].

Compared to photodiode detectors, CCD camera and CMOS imaging can provide instant images, but the speed of the fluid is limited [51]. Hoera *et al*. utilized a CCD camera for fluorescence imaging of temperature and reaction process in a microfluidic chip reactor [75]. Yang *et al.* conducted an experiment at a flow rate of 10 µL/h to allow CCD cameras to capture the accurate images for real-time cell separation in a microflow cytometer [72]. To further improve the sensitivity of the detector and reduce the cost of the microflow cytometer, Eyer *et al.* [73], added titanium dioxide (TiO_2) particles into PDMS to increase the light signal intensity from the interaction between particles and light source, improving the sensitivity of CCD cameras indirectly.

2.4. Data Analysis

As shown in Figure 2, light signals collected by optical detectors are further amplified by a current-to-voltage amplifier, and then, the voltage signals are digitized by a data acquisition card. LabView programs can be utilized to record the data for further analysis [20]. Data analysis is usually performed using customized MATLAB codes [20,76].

When a cell or a particle passes through the interrogation region, a burst of light will generate an electrical pulse in the analysis system. The pulse duration relates to flow rate, the beam waist and the size of cell or particle. FSC intensity is proportional to the size of the cell or particle, and SSC intensity depends on the granularity. Each pulse is characterized by FSC, SSC, single-color or multi-color FL and pulse duration. The average intensity and pulse duration are typically calculated. To remove some background noise or internal PMT noise, a threshold is set. Figure 9a shows the data analysis results of a of mixture beads and cells flowing in an optofluidic microflow cytometer [20]. One dashed threshold is set to distinguish 2- and 4-µm beads; another dotted threshold is set to separate beads and *Escherichia coli* cells.

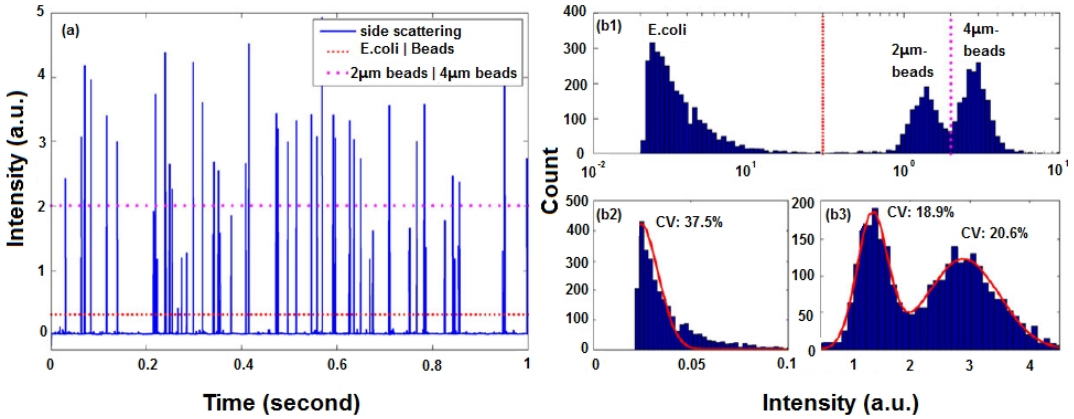

Figure 9. Data analysis results of a mixture of beads and cells flowing in an optofluidic microflow cytometer. (**a**) One second raw data of SSC signal intensity from a test with a mixture of *E. coli* cells and beads of 2 µm and 4 µm in diameter. (**b1**) Statistical histograms of events by total beads and *E. coli* cells with intensity on a logarithmic scale. (**b2**) Statistical histograms of events produced by *E. coli* cells on a linear scale and its Gaussian fitting. (**b3**) Statistical histograms of events by beads with intensity on a linear scale and Gaussian fittings. Reprinted from [20] with permission from Wiley.

In flow cytometry, simultaneous detection of multiple parameters is the source of its analytical power. By analyzing and comparing the scattered light signals and fluorescent light signals of a single-cell or single-particle against the total population, it is possible to see the similarities and differences for further counting and identification. Figure 9b shows histograms of events with intensity on a logarithmic scale and a linear scale. Cells and beads of different diameters show various distribution features, which can be fitted by Gaussian curves with different coefficients of variation (CV). For a microflow cytometer with multi-color fluorescence channels, a multi-parameter plot can be used to do further analysis.

3. Fabrication and Integration

3.1. Materials

Traditionally, silicon and glass substrates are the most common materials used in microflow cytometers. Recently, inorganic materials, like ceramics, and polymers, like PDMS, and even paper [77] have been used to construct microfluidic devices. Silicon and glass technologies, as well as polymer technology have been reviewed in many papers [12,77,78].

Wet or dry etching methods are applied to create microstructures on a silicon or glass substrate, but organic long-chain polymers are attracting more and more attention with the growing interest in fabricating multilayered structures. Polymers are less expensive and convenient for mass production. More importantly, most polymers are optically transparent to visible wavelengths of light and adaptable through chemical modification for bonding to glass or silicon substrates. Polymers can be divided into elastomers and thermoplastics. PDMS, as one of the elastomers, was first used as a substrate in the late 1990s. Since then, PDMS has established itself as the most commonly-used elastomer in microfluidics. Chemical modification of PDMS has allowed the diversification of its application in microfluidics. PDMS structures can be cured on molds at room temperature for microchannels or other microstructures, and PDMS can provide good sealing properties after chemical modification. Zhang *et al.* [79] sealed SU-8 microfluidic channels using PDMS after the N_2 plasma treatment. Amino groups generated by N_2 plasma on the PDMS surface reacted with the residual epoxy groups on the SU-8 surface. The bond was long-term resistant to water, and the structure could withstand a high degree of stress. Polystyrene (PS), polycarbonate (PC), poly(methyl methacrylate) (PMMA) and cyclic olefin copolymer (COC) are other thermoplastic polymers that are used in microfluidics.

As stated earlier, SU-8 is a commonly-used epoxy-based negative photoresist that can be utilized to form the functional layer (waveguides or lenses) when processed on a substrate [24,67,80]. High aspect ratio structures can be obtained in SU-8 by lithography. Researchers now are seeking methods to integrate PDMS and SU-8 together to take advantage of both materials. Ren *et al.* [80] bonded SU-8 and PDMS using the aminosilane-mediated bonding method in a microfluidic device for neuroscience research. Paper is a promising new material with low cost and easy fabrication process. Furthermore, paper is available everywhere and relatively environmentally-friendly. Liu and Crook [77] fabricated a 3D paper microfluidic devices simply by hand folding. Colorimetric and fluorescence detection of glucose and protein were achieved.

3.2. Device Integration

A multilayered PDMS/SU-8 devices is commonly used in an optofluidic microflow cytometer. Standard techniques, like wet and dry etching on glass or silicon substrates, have been replaced by soft lithography, photolithography and different bonding techniques in recent decades. Figure 10 shows the individual layers for the integration of the device, and the detailed process can be seen in Figure 11. The PDMS layer is fabricated by PDMS molding and functioned as a upper layer to seal the fluidics and to form an upper optical cladding layer. The SU-8 layer is patterned on a silicon or glass substrate by exposure to UV light through photomasks. Due to the high aspect ratio, the waveguides

and optical components can be integrated on the SU-8 layer. To assemble the device, the PDMS layer is bonded to the SU-8 layer after a plasma treatment [67,80]. The PDMS cover provides a complete seal, and extra glass pads are bonded on the top surface of PDMS. The sandwiched device is rigid enough and can withstand a high pressure. Custom optical and fluidic components can be integrated on a small chip to achieve specialized and efficient function.

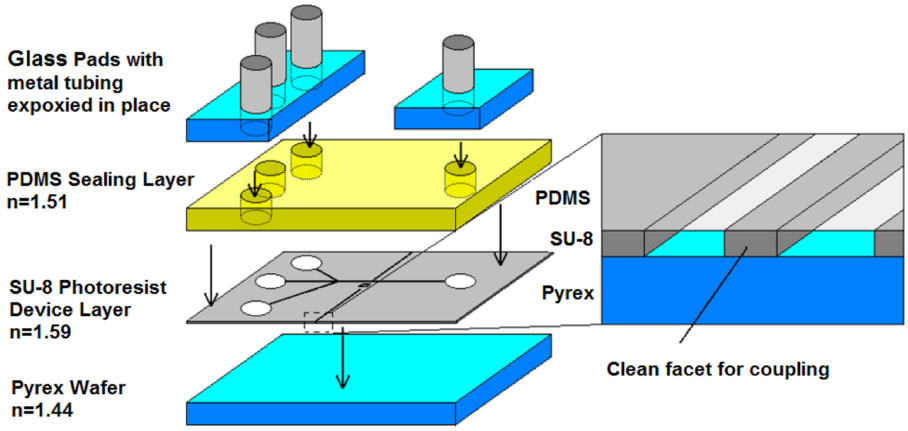

Figure 10. A schematic diagram showing the integration of a multilayered PDMS/SU-8 device. SU-8 is the functional layer; PDMS covers and seals the device; and glass pads allow solid fluidic interconnects. Reproduced from [65] with permission.

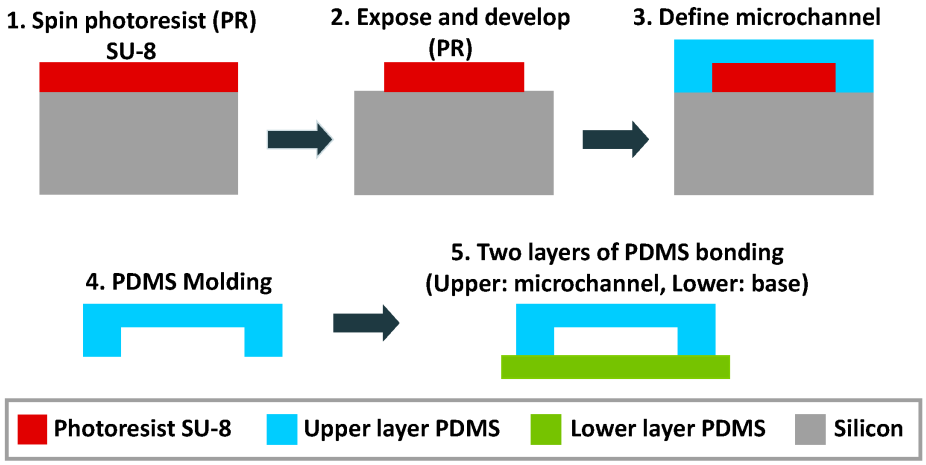

Figure 11. Standard fabrication procedure of a PDMS/SU-8 device. Reprinted from [81] from *Micromachines* published by MDPI.

4. Performance of Optofluidic Microflow Cytometers

Optofluidic microflow cytometers aim to provide a compact and automated method capable of high-throughput screening, low reagent consumption, high sensitivity and high selectivity for small particles or cells detection. Current researchers are moving forward step by step to achieve those goals and narrowing the performance difference between the conventional benchtop and optofluidic microflow cytometers.

The sensitivity of the optofluidic microflow cytometer is improved by the on-chip lens system. The fluorescence sensitivity of flow cytometers depends on the background noise, effective intensity of light signal and the detection efficiency. SNR is the ability to resolve a pulse from the noise.

The minimum SNR ratio for a reliable detection is three, while the SNR value of fluorescent beads measurement was 80–300 from devices by using novel on-chip lens systems and notched designs to reduce the background noise [68].

Table 3 shows the parameters of optofluidic microflow cytometers developed recently and their performance measured by the coefficient of variation (CV). The CV is defined as the ratio of the standard deviation to the mean of the light signal intensity expressed as a percentage. This effectively measures the dispersion of intensity of the detection events [82]. A smaller CV indicates that there is less error introduced by the actual device and that identical samples will have identical detected signals, meaning that the microflow cytometer has a higher ability to differentiate the slight differences of the type of particles or cells in the entire population.

The throughput of optofluidic microflow cytometer varies from 30 particles or cells/s to 2000 cells/s or even to 50,000 cells/s. Different levels of throughputs are achievable depending on the specific application. For *E. coli* or bacteria detection, where the concentrations of targeted cells are very low, a low throughput is used. For rare cell analysis or blood cell counting, high throughputs are required. As shown in Table 3, the CV values for cells are significantly higher than those of blank or fluorescent labeled beads. Since the refractive index contrast between cells and sample fluid (usually water or phosphate-buffered saline) is small, the intensity of scattered light is not as strong as that of beads. Fluorescent labeling is applied to provide an easily detectable parameter to help improve SSC detection by correlating the two parameters; if an FL is detected, then a SSC must be detected, as well. This can indirectly enhance the SNR of the SSC. The CV value of SSC intensity produced by *E. coli* cells was 37.5% [20], while the CV value of FL intensity produced by labeled human embryonic kidney (HEK) cells is 13.4% [38].

An optofluidic microflow cytometer with typical 2D hydrodynamic focusing, on-chip beam shaping and collection was studied by Watts *et al.* [55]. Scattered light signals of 1-, 2- and 5-μm blank beads were collected by on-chip waveguide, obtaining CV values of 16.4%, 11.0% and 12.5%, respectively. It also showed that the performance of optofluidic microflow cytometers is based on the combination of the beam geometry used and bead size. Barat *et al.* [2] demonstrated a 2D hydrodynamic focusing optofluidic microflow cytometer with an on-chip lens system for light guiding and grooves for inserted optical fibers for collection. The flow cytometer successfully differentiates 10–25-μm beads based on fluorescence and scattered light. The best CV value was 4.9% for the side scattered light intensity of 25-μm beads.

The performance of a 2D hydrodynamic focusing optofluidic microflow cytometer with free-space collection was determined to be very comparable to conventional cytometers. Watts *et al.* [54] focused the beam waist to 6 μm, and fluorescent signals from 2.5-μm beads showed a superior CV of 9.03%. Mu *et al.* [24] detected labeled *E. coli* cells, achieving a detection efficiency of 89.7% and 94.5% for fluorescence signals and scattered light signals, respectively. The detection accuracy was 84.3% and 88.8% for fluorescence and scattered light detection, respectively, as compared to the standard haemocytometer method.

Nawaz *et al.* [38] presented a novel microfluidic drifting-based 3D hydrodynamic focusing optofluidic microflow cytometer with free space light collection. The best CV of 2.37% for fluorescent beads was achieved, which is comparable to a commercial benchtop flow cytometer. Frankowski *et al.* [28,29] developed two microfluidic sensors based on optical and impedance analysis both operating simultaneously. They demonstrated a superior CV of 3.2% for 8.12-μm beads. A combination of multiple methods or techniques is a good way to improve the sensitivity of microfluidic devices.

Table 3. Performance of recently developed optofluidic microflow cytometers.

Flow Control	Beam Shaping	Light Collection	Sample	CV of SSC (%)	CV of FL (%)	Throughput (Cells or Particles/s)	Ref.
2D HF	Yes	Free-space	*E. coli*	37.5	–	~101	[20]
2D HF	Yes	On-chip	2 μm beads	11	–	~30	[55]
2D HF	Yes	On-chip	15 μm beads	12	17.1	~100	[2]
2D HF	No	Free-space	Labeled *E. coli*	36.2	30.7	~350	[24]
2D HF	No	Free-space	1 μm beads	14.95	24.73	~83	[24]
2D HF	Yes	Free-space	2.5 μm beads	–	9.0	~28	[54]
3D HF	No	On-chip	10 μm beads	12	8.3	-	[31]
3D HF (cascade focusing)	No	Free-space	8.12 μm beads	–	3.2	–	[29]
3D HF (microfluidic drifting)	No	Free-space	1.9 μm beads	–	2.4	~2163	[38]
3D HF (microfluidic drifting)	No	Free-space	HEK 293 cells	–	13.4	–	[38]
3D HF (cascade focusing)	No	Free-space	Beads	–	3.0	–	[28]
3D SSAW	No	Free-space	HL–60 cells	–	22.0	–	[41]
3D SSAW	No	Free-space	7 μm beads	–	19.4	~772	[41]
3D SSAW	No	Free-space	10 μm beads	–	10.9	~537	[41]

Typically, good 3D hydrodynamic focusing ability in both lateral and vertical directions can achieve a lower CV than 2D focusing. However, beam shaping can also improve the detection efficiency and obtain a lower CV value even with 2D hydrodynamic focusing. A CV of 15.9% for 2-μm beads was achieved by Watts *et al.* [55] using 2D hydrodynamic focusing, while a similar CV of 15.4% for 10-μm beads was obtained in a 3D hydrodynamic focusing made by Testa *et al.* [31]. This is because Watts *et al.* used an on-chip lens system to focus the beam waist to 1.5 μm and formed a superior uniform region of light intensity of the interrogation region [55]. Both devices provide free optical alignment, but the grooved structure in Testa's device is easier to fabricate.

Besides hydrodynamic focusing techniques, SSAW also provides a good focusing quality. A mixture of 7-μm beads and 10-μm beads was distinguished by an SSAW-based microfluidic cytometer studied by Chen *et al.* [41], with CVs of 19.4% and 10.9%, respectively. Fluorescently-labeled human promyelocytic leukemia cells (HL-60) were successfully detected with a CV of 22.0%.

The typical CV value achievable by the conventional benchtop flow cytometer is about 5%–15%. The performance of a optofluidic microflow cytometer has developed dramatically from 24.73% by Mu *et al.* [24] to 3% by Frankowski *et al.* [29] in the past few years. The performance of an optofluidic microflow cytometer now can be comparable to the conventional benchtop flow cytometer. The improvement of the device's performance is attributable to the development of microchip devices' enhanced flow control methods, the on-chip lens system that provides custom and robust beam shaping capabilities, the signal collection method and the rapidly-growing microfabrication techniques.

5. Conclusions and Future Perspective

Optofluidic microflow cytometers are attracting more and more research attention, combining multiple fields and disciplines in a microchip. Optofluidic microflow cytometers integrated with optics provide significant enhancements for flow cytometry. Low costs, higher sensitivity, free optical alignment and smooth interaction interfaces are the obvious advantages. Optofluidic microflow cytometers offer significantly lower costs and size reductions, as well as low reagent requirements and portability advantages over a benchtop flow cytometer.

Various attempts have been made to integrate on-chip waveguides or grooves for the guided insertion of optical fibers into the microchip. Besides on-chip lenses or waveguides fabricated by SU-8 or PDMS, novel types of liquid-core/liquid-cladding lenses, liquid-core/liquid-cladding waveguides and hybrid core waveguides have been used in optofluidic devices. The integrated lens system helps shape the beam emitted from the excitation source, providing an optimal geometry and uniform region for interaction with the specimen. By taking advantage of both optics and fluidics, the performance of optofluidic microflow cytometers has advanced to a point where devices are comparable to that of a conventional flow cytometer in the past few years. To the extent of our knowledge, the best CV value achieved for a microflow cytometer was less than 3% [29,38].

Currently, the optofluidic devices have successfully miniaturized the optical and fluidic components of the flow cytometer, while the miniaturization of the whole system is still challenging. System integration needs to have more attention paid to it. External syringe pumps, light collection detectors and other components still somewhat limit the portability of the optofluidic microflow cytometer. The miniaturization of these components needs to join the current stat of the optical and microfluidic control components for continuous development of future POC applications. For POC diagnostic and other field applications, a simple method for mass production should be invented in the future to further reduce the cost. For commercialization, optofluidic microflow cytometers need to provide significant operational advantage over conventional flow cytometers. A fully-portable, low cost, easy to operate and effective optofluidic microflow cytometer can be reasonably expected in both the research field and in the commercial market.

Acknowledgments: This research is partially supported by an Ontaio Research Fund (ORF) grant (Grant No. RE-WR-10) and an NSERC Discovery grant (Grant No. RGPIN/262023-2013).

Author Contributions: Changqing Xu and Zhiyi Zhang conceived of and designed the structure of this review article. Yushan Zhang collected the references and wrote this paper. Benjamin R. Watts, Tianyi Guo, and Qiyin Fang revised the manuscript.

Conflicts of Interest: The authors declare no conflict of interest.

References

1. Piyasena, M.E.; Graves, S.W. The intersection of flow cytometry with microfluidics and microfabrication. *Lab Chip* **2014**, *14*, 1044-1059.
2. Barat, D.; Spencer, D.; Benazzi, G.; Mowlem, M.C.; Morgan, H. Simultaneous high speed optical and impedance analysis of single particles with a microfluidic cytometer. *Lab Chip* **2012**, *12*, 118–126.
3. Volpatti, L.R.; Yetisen, A.K. Commercialization of microfluidic devices. *Trends Biotechnol.* **2014**, *32*, 347–350.
4. Psaltis, D.; Quake, S.R.; Yang, C. Developing optofluidic technology through the fusion of microfluidics and optics. *Nature* **2006**, *442*, 381–386.
5. Horowitz, V.R.; Awschalow, D.D.; Pennathur, S. Optofluidics: Field or technique? *Lab Chip* **2008**, *8*, 1856-1863.
6. Huang, N.T.; Zhang, H.L.; Chung, M.T.; Seo, J.H.; Kurabayashi, K. Recent advancements in optofluidics-based single-cell analysis: Optical on-chip cellular manipulation, treatment, and property detection. *Lab Chip* **2014**, *14*, 1230–1245.
7. Crosland-Taylor, P.J. A device for counting small particles suspended in a fluid through a tube. *Nature* **1953**, *171*, 37–38.
8. Justin, G.A.; Denisin, A.K.; Nasir, M.; Shriver-Lake, L.C.; Golden, J.P.; Ligler, F.S. Hydrodynamic focusing for impedance-based detection of specifically bound microparticles and cells: Implications of fluid dynamics on tunable sensitivity. *Sens. Actuators B Chem.* **2012**, *166-167*, 386–393.
9. Song, H.; Wang, Y.; Rosano, J.M.; Prabhakarpandian, B.; Garson, C.; Pant, K.; Lai, E. A microfluidic impedance flow cytometer for identification of differentiation state of stem cells. *Lab Chip* **2013**, *13*, 2300–2310.
10. Han, M.; Lee, W.; Lee, S.K.; Lee, S.S. 3D microfabrication with inclined/rotated UV lithography. *Sens. Actuators A Phys.* **2004**, *111*, 14–20.
11. Lee, C.Y.; Chang, C.L.; Wang, Y.N.; Fu, L.M. Microfluidic Mixing: A Review. *Int. J. Mol. Sci.* **2011**, *12*, 3263–3287.
12. Abgrall, P.; Gué, A.M. Lab-on-chip technologies: Making a microfluidic network and coupling it into a complete microsystem–A review. *J. Micromech. Microeng.* **2007**, *17*, R15–R49.
13. Whitesides, G.M. The origins and the future of microfluidics. *Nature* **2006**, *442*, 368–373.
14. Brennan, D.; Justice, J.; Corbett, B.; McCarthy, T.; Galvin, P. Emerging optofluidic technologies for point-of-care genetic analysis systems: A review. *Anal. Bioanal. Chem.* **2009**, *395*, 621–636.
15. Titmarsh, D.M.; Chen, H.; Glass, N.R.; Cooper-White, J.J. Concise review: Microfluidic technology platforms: Poised to accelerate development and translation of stem cell-derived therapies. *Stem Cells Transl. Med.* **2014**, *3*, 81–90.
16. Hashemi, N.; Erickson, J.S.; Golden, J.P.; Jackson, K.M.; Ligler, F.S. Microflow cytometer for optical analysis of phytoplankton. *Biosens. Bioelectron.* **2011**, *26*, 4263–4269.
17. Lei, K.F. Microfluidic Systems for Diagnostic Applications: A Review. *J. Lab. Autom.* **2012**, *17*, 330–347.
18. Tang, S.K.Y.; Stan, C.A.; Whitesides, G.M. Dynamically reconfigurable liquid-core liquid-cladding lens in a microfluidic channel. *Lab Chip* **2008**, *8*, 395–401.
19. Liang, L.; Zuo, Y.F.; Wu, W.; Zhu, X.Q.; Yang, Y. Optofluidic restricted imaging, spectroscopy and counting of nanoparticles by evanescent wave using immiscible liquids. *Lab Chip* **2016**, doi:10.1039/C6LC00078A.
20. Guo, T.; Wei, Y.; Xu, C.; Watts, B.R.; Zhang, Z.; Fang, Q.; Zhang, H.; Selvaganapathy, P.R.; Deen, M.J. Counting of *Escherichia coli* by a microflow cytometer based on a photonic-microfluidic integrated device. *Electrophoresis* **2015**, *36*, 298–304.
21. Huh, D.; Gu, W.; Kamotani, Y.; Grotberg, J.B.; Takayama, S. Microfluidics for flow cytometric analysis of cells and particles. *Physiol. Meas* **2005**, *26*, R73–R98.

22. Lau, A.T.H.; Yip, H.M.; Ng, K.C.C.; Cui, X.; Lam, R.H.W. Dynamics of microvalve operations in integrated microfluidics. *Micromachines* **2014**, *5*, 50–65.
23. Ainla, A.; Jeffries, G.; Jesorka, A. Hydrodynamic flow confinement technology in microfluidic perfusion devices. *Micromachines* **2012**, *3*, 442–461.
24. Mu, C.; Zhang, F.; Zhang, Z.; Lin, M.; Cao, X. Highly efficient dual-channel cytometric-detection of micron-sized particles in microfluidic device. *Sens. Actuators B Chem.* **2011**, *151*, 402–409.
25. McClain, M.A.; Culbertson, C.T.; Jacobson, S.C.; Ramsey, J.M. Flow cytometry of *Escherichia coli* on microfluidic devices. *Anal. Chem.* **2001**, *73*, 5334–5338.
26. Tung, Y.C.; Zhang, M.; Lin, C.T.; Kurabayashi, K.; Skerlos, S.J. PDMS-based opto-fluidic micro flow cytometer with two-color, multi-angle fluorescence detection capability using PIN photodiodes. *Sens. Actuators B Chem.* **2004**, *98*, 356–367.
27. Fu, L.M.; Tsai, C.H.; Lin, C.H. A high-discernment microflow cytometer with microweir structure. *Electrophoresis* **2008**, *29*, 1874–1880.
28. Frankowski, M.; Theisen, J.; Kummrow, A.; Simon, P.; Ragusch, H.; Bock, N.; Schmidt, M.; Neukammer, J. Microflow cytometers with integrated hydrodynamic focusing. *Sensors* **2013**, *13*, 4674–4693.
29. Frankowski, M.; Simon, P.; Bock, N.; El-Hasni, A.; Schnakenberg, U.; Neukammer, J. Simultaneous optical and impedance analysis of single cells: A comparison of two microfluidic sensors with sheath flow focusing. *Eng. Life Sci.* **2015**, *15*, 286–296.
30. Lee, G.B.; Hung, C.I.; Ke, B.J.; Huang, G.R.; Hwei, B.H.; Lai, H.F. Hydrodynamic Focusing for a Micromachined Flow Cytometer. *J. Fluids Eng.* **2001**, *123*, 672.
31. Testa, G.; Persichetti, G.; Bernini, R. Micro flow cytometer with self-aligned 3D hydrodynamic focusing. *Biomed. Opt. Express* **2014**, *6*, 54.
32. Kim, D.S.; Kim, D.S.D.; Han, K.; Yang, W. An efficient 3-dimensional hydrodynamic focusing microfluidic device by means of locally increased aspect ratio. *Microelectron. Eng.* **2009**, *86*, 1343–1346.
33. Sundararajan, N.; Pio, M.S.; Lee, L.P.; Berlin, A.A. Three-dimensional hydrodynamic focusing in polydimethylsiloxane (PDMS) microchannels. *J. Microelectromech. Syst.* **2004**, *13*, 559–567.
34. Hairer, G.; Pärr, G.S.; Svasek, P.; Jachimowicz, A.; Vellekoop, M.J. Investigations of micrometer sample stream profiles in a three-dimensional hydrodynamic focusing device. *Sens. Actuators B Chem.* **2008**, *132*, 518–524.
35. Golden, J.P.; Kim, J.S.; Erickson, J.S.; Hilliard, L.R.; Howell, P.B.; Anderson, G.P.; Nasir, M.; Ligler, F.S. Multi-wavelength microflow cytometer using groove-generated sheath flow. *Lab Chip* **2009**, *9*, 1942–1950.
36. Kim, J.S.; Anderson, G.P.; Erickson, J.S.; Golden, J.P.; Nasir, M.; Ligler, F.S. Multiplexed detection of bacteria and toxins using a microflow cytometer. *Anal. Chem.* **2009**, *81*, 5426–5432.
37. Sato, H.; Yagyu, D.; Ito, S.; Shoji, S. Improved inclined multi-lithography using water as exposure medium and its 3D mixing microchannel application. *Sens. Actuators A Phys.* **2006**, *128*, 183–190.
38. Nawaz, A.A.; Zhang, X.; Mao, X.; Rufo, J.; Lin, S.C.S.; Guo, F.; Zhao, Y.; Lapsley, M.; Li, P.; McCoy, J.P.; *et al.* Sub-micrometer-precision, three-dimensional (3D) hydrodynamic focusing via "microfluidic drifting". *Lab Chip* **2014**, *14*, 415–423.
39. Shi, J.; Mao, X.; Ahmed, D.; Colletti, A.; Huang, T.J. Focusing microparticles in a microfluidic channel with standing surface acoustic waves (SSAW). *Lab Chip* **2007**, *8*, 221–223.
40. Shi, J.; Yazdi, S.; Lin, S.C.S.; Ding, X.; Chiang, I.K.; Sharp, K.; Huang, T.J. Three-dimensional continuous particle focusing in a microfluidic channel via standing surface acoustic waves (SSAW). *Lab Chip* **2011**, *11*, 2319–2324.
41. Chen, Y.; Nawaz, A.A.; Zhao, Y.; Huang, P.H.; McCoy, J.P.; Levine, S.J.; Wang, L.; Huang, T.J. Standing surface acoustic wave (SSAW)-based microfluidic cytometer. *Lab Chip* **2014**, *14*, 916–923.
42. Schmid, L.; Weitz, D.A.; Franke, T. Sorting drops and cells with acoustics: acoustic microfluidic fluorescence-activated cell sorter. *Lab Chip* **2014**, *14*, 3710–3718.
43. Yu, C.; Qian, X.; Chen, Y.; Yu, Q.; Ni, K.; Wang, X. Three-dimensional electro-sonic flow focusing ionization microfluidic chip for mass spectrometry. *Micromachines* **2015**, *6*, 1890–1902.
44. Zhu, J.; Xuan, X. Dielectrophoretic focusing of particles in a microchannel constriction using DC-biased AC flectric fields. *Electrophoresis* **2009**, *30*, 2668–2675.

45. Chu, H.; Doh, I.; Cho, Y.H. A three-dimensional particle focusing channel using the positive dielectrophoresis (pDEP) guided by a dielectric structure between two planar electrodes. *Trans. Korean Soc. Mech. Eng. A* **2009**, *33*, 261–264.
46. Zhang, J.; Yan, S.; Alici, G.; Nguyen, N.T.; Di Carlo, D.; Li, W. Real-time control of inertial focusing in microfluidics using dielectrophoresis (DEP). *RSC Adv.* **2014**, *4*, 62076–62085.
47. Bender, B.F.; Garrell, R.L. Digital microfluidic system with vertical functionality. *Micromachines* **2015**, *6*, 1655–1674.
48. James, C.D.; McClain, J.; Pohl, K.R.; Reuel, N.; Achyuthan, K.E.; Bourdon, C.J.; Rahimian, K.; Galambos, P.C.; Ludwig, G.; Derzon, M.S. High-efficiency magnetic particle focusing using dielectrophoresis and magnetophoresis in a microfluidic device. *J. Micromech. Microeng.* **2010**, *20*, 045015.
49. Zeng, J.; Chen, C.; Vedantam, P.; Brown, V.; Tzeng, T.R.J.; Xuan, X. Three-dimensional magnetic focusing of particles and cells in ferrofluid flow through a straight microchannel. *J. Micromech. Microeng.* **2012**, *22*, 105018.
50. Fernandes, A.C.; Duarte, C.M.; Cardoso, F.A.; Bexiga, R.; Cardoso, S.; Freitas, P.P. Lab-on-chip cytometry based on magnetoresistive sensors for bacteria detection in milk. *Sensors* **2014**, *14*, 15496–15524.
51. Ateya, D.A.; Erickson, J.S.; Howell, P.B.; Hilliard, L.R.; Golden, J.P.; Ligler, F.S. The good, the bad, and the tiny: A review of microflow cytometry. *Anal. Bioanal. Chem.* **2008**, *391*, 1485–1498.
52. Lin, C.H.; Lee, G.B.; Fu, L.M.; Hwey, B.H. Vertical focusing device utilizing dielectrophoretic force and its application on microflow cytometer. *J. Microelectromech. Syst.* **2004**, *13*, 923 – 932.
53. Blue, R.; Dudus, A.; Uttamchandani, D. A Review of Single-Mode Fiber Optofluidics. *IEEE J. Sel. Top. Quantum Electron* **2015**, *22*, 1–12.
54. Watts, B.R.; Kowpak, T.; Zhang, Z.; Xu, C.Q.; Zhu, S.; Cao, X.; Lin, M. Fabrication and performance of a photonic-microfluidic integrated device. *Micromachines* **2012**, *3*, 62–77.
55. Watts, B.R.; Zhang, Z.; Xu, C.Q.; Cao, X.; Lin, M. Scattering detection using a photonic-microfluidic integrated device with on-chip collection capabilities. *Electrophoresis* **2013**, *35*, 271–281.
56. Matteucci, M.; Triches, M.; Nava, G.; Kristensen, A.; Pollard, M.R.; Berg-Sørensen, K.; Taboryski, R.J. Fiber-based, injection-molded optofluidic systems: Improvements in assembly and applications. *Micromachines* **2015**, *6*, 1971–1983.
57. Yalizay, B.; Morova, Y.; Dincer, K.; Ozbakir, Y.; Jonas, A.; Erkey, C.; Kiraz, A.; Akturk, S. Versatile liquid-core optofluidic waveguides fabricated in hydrophobic silica aerogels by femtosecond-laser ablation. *Opt. Mater.* **2015**, *47*, 478–483.
58. Fan, S.K.; Lee, H.P.; Chien, C.C.; Lu, Y.W.; Chiu, Y.; Lin, F.Y. Reconfigurable liquid-core/liquid-cladding optical waveguides with dielectrophoresis-driven virtual microchannels on an electromicrofluidic platform. *Lab Chip* **2016**, *6*, 847–854.
59. Chen, X.; Sakurazawa, A.; Sato, K.; Tsunoda, K.I.; Wang, J. A solid-cladding/liquid-core/liquid-cladding sandwich optical waveguide for the study of dynamic extraction of dye by ionic liquid BmimPF 6. *Appl. Spectrosc.* **2012**, *66*, 798–802.
60. Shi, Y.; Liang, L.; Zhu, X.; Zhang, X.; Yang, Y. Tunable self-imaging effect using hybrid optofluidic waveguides. *Lab Chip* **2015**, *15*, 4398–4403.
61. Choi, J.; Lee, K.S.; Jung, J.H.; Sung, H.J.; Kim, S.S. Integrated real-time optofluidic SERS via a liquid-core/liquid-cladding waveguide. *RSC Adv.* **2015**, *5*, 922–927.
62. Lim, J.M.; Kim, S.H.; Choi, J.H.; Yang, S.M. Fluorescent liquid-core/air-cladding waveguides towards integrated optofluidic light sources. *Lab Chip* **2008**, *8*, 1580–1585.
63. Yang, Y.; Liu, A.Q.; Lei, L.; Chin, L.K.; Ohl, C.D.; Wang, Q.J.; Yoon, H.S. A tunable 3D optofluidic waveguide dye laser via two centrifugal Dean flow streams. *Lab Chip* **2011**, *11*, 3182–3187.
64. Yang, Y.; Liu, A.Q.; Chin, L.K.; Zhang, X.M.; Tsai, D.P.; Lin, C.L.; Lu, C.; Wang, G.P.; Zheludev, N.I. Optofluidic waveguide as a transformation optics device for lightwave bending and manipulation. *Nat. Commun.* **2012**, *3*, 651.
65. Watts, B.R. Development of a Microchip-Based Flow Cytometer with Integrated Optics—Device Design, Fabrication , and Testing. Ph.D Thesis, McMaster University, Hamilton, ON, Canada, 2012.
66. Emile, O.; Emile, J. Soap films as 1D waveguides. *Optofluid. Microfluid Nanofluid.* **2014**, *1*, 27–33.
67. Watts, B.R.; Kowpak, T.; Zhang, Z.; Xu, C.Q.; Zhu, S. Formation and characterization of an ideal excitation beam geometry in an optofluidic device. *Biomed. Opt. Express* **2010**, *1*, 848–860.

68. Watts, B.R.; Zhang, Z.; Xu, C.Q.; Cao, X.; Lin, M. A photonic-microfluidic integrated device for reliable fluorescence detection and counting. *Electrophoresis* **2012**, *33*, 3236–3244.
69. Watts, B.R.; Zhang, Z.; Xu, C.Q.; Cao, X.; Lin, M. Integration of optical components on-chip for scattering and fluorescence detection in an optofluidic device. *Biomed. Opt. Express* **2012**, *3*, 2784–2793.
70. Watts, B.R.; Zhang, Z.; Xu, C.Q.; Cao, X.; Lin, M. A method for detecting forward scattering signals on-chip with a photonic-microfluidic integrated device. *Biomed. Opt. Express* **2013**, *4*, 1051–1060.
71. Ungerbock, B.; Charwat, V.; Ertl, P.; Mayr, T. Microfluidic oxygen imaging using integrated optical sensor layers and a color camera. *Lab Chip* **2013**, *13*, 1593–1601.
72. Yang, S.; Undar, A.; Zahn, J.D. A microfluidic device for continuous, real time blood plasma separation. *Lab Chip* **2006**, *6*, 871–880.
73. Eyer, K.; Root, K.; Robinson, T.; Dittrich, P.S. A simple low-cost method to enhance luminescence and fluorescence signals in PDMS-based microfluidic devices. *RSC Adv.* **2015**, *5*, 12511–12516.
74. Kettlitz, S.W.; Valouch, S.; Sittel, W.; Lemmer, U. Flexible planar microfluidic chip employing a light emitting diode and a PIN-photodiode for portable flow cytometers. *Lab Chip* **2012**, *12*, 197–203.
75. Hoera, C.; Ohla, S.; Shu, Z.; Beckert, E.; Nagl, S.; Belder, D. An integrated microfluidic chip enabling control and spatially resolved monitoring of temperature in micro flow reactors. *Anal. Bioanal. Chem.* **2014**, *407*, 387–396.
76. Nedbal, J.; Visitkul, V.; Ortiz-Zapater, E.; Weitsman, G.; Chana, P.; Matthews, D.R.; Ng, T.; Ameer-Beg, S.M. Time-domain microfluidic fluorescence lifetime flow cytometry for high-throughput Förster resonance energy transfer screening. *Cytom. A* **2015**, *87*, 104–118.
77. Liu, H.; Crooks, R.M. Three-dimensional paper microfluidic devices assembled using the principles of origami. *J. Am. Chem. Soc.* **2011**, *133*, 17564–17566.
78. Nge, P.N.; Rogers, C.I.; Woolley, A.T. Advances in microfluidic materials, functions, integration, and applications. *Chem. Rev.* **2013**, *113*, 2550–2583.
79. Zhang, Z.; Zhao, P.; Xiao, G.; Watts, B.R.; Xu, C. Sealing SU-8 microfluidic channels using PDMS. *Biomicrofluidics* **2011**, *5*, 1–8.
80. Ren, Y.; Huang, S.H.; Mosser, S.; Heuschkel, M.O.; Bertsch, A.; Fraering, P.C.; Chen, J.J.J.; Renaud, P. A Simple and Reliable PDMS and SU-8 Irreversible Bonding Method and Its Application on a Microfluidic-MEA Device for Neuroscience Research. *Micromachines* **2015**, *6*, 1923–1934.
81. Yang, C.C.; Wen, R.C.; Shen, C.R.; Yao, D.J. Using a microfluidic gradient generator to characterize BG-11 medium for the growth of cyanobacteria synechococcus elongatus PCC7942. *Micromachines* **2015**, *6*, 1755–1767.
82. Chen, H.T.; Wang, Y.N. Optical microflow cytometer for particle counting, sizing and fluorescence detection. *Microfluid. Nanofluid.* **2009**, *6*, 529–537.

Chapter 6

A Systematic Study on Transit Time and Its Impact on Accuracy of Concentration Measured by Microfluidic Devices

After the accomplishment of the pre-conditioning process and literature review, a microfluidic device based microflow cytometer platform was determined to solve the problem. In this chapter, a microflow cytometer has been built-up for particle/cell detection. The detailed fabrication process of the core microfluidic device can be found in Appendix A, and the design of the microfluidic devices was described in Appendix B. In a summary, a microflow cytometer was established in this chapter, and data analysis methods of the microflow cytometer was systematically studied

An optofluidic microflow cytometer with on-chip waveguide and focused laser beam was established as proposed. Before running with cyanobacterial samples, polystyrene microspheres were tested on the microflow cytometer, and post-acquisition data analysis were performed to figure out the setting of proper thresholds. The reliability, repeatability and accuracy needed to be verified before cyanobacterial experiments.

Meanwhile, a systematic study on transit time and amplitude threshold setting was performed to figure out the best data analysis for microflow cytometer. Based on empirical experiences and calculation, two gating thresholds were introduced to analyze the raw data obtained from photomultiplier tubes. Results have shown that amplitude threshold can filter out the weak background noises first and transit time threshold can further remove the false positive events. Therefore, the accuracy of the microflow cytometer can be improved significantly.

This chapter was reprinted from *Sensors* from MDPI and the author of this thesis is the first author and main contributor.

Zhang, Yushan, Tianyi Guo, and Changqing Xu. "A Systematic Study on Transit Time and Its Impact on Accuracy of Concentration Measured by Microfluidic

Devices." Sensors 20, no. 1 (2020): 14.

sensors

MDPI

Article

A Systematic Study on Transit Time and Its Impact on Accuracy of Concentration Measured by Microfluidic Devices

Yushan Zhang [1], Tianyi Guo [2] and Changqing Xu [3,*]

[1] School of Biomedical Engineering, McMaster University, Hamilton, ON L8S 4L7, Canada; zhang749@mcmaster.ca
[2] Forsee Instruments Ltd., Hamilton, ON L8P 0A1, Canada; guotianyi@gmail.com
[3] Department of Engineering Physics, McMaster University, Hamilton, ON L8S 4L7, Canada
* Correspondence: cqxu@mcmaster.ca; Tel.: +1-905-525-9140 (ext. 24314)

Received: 6 November 2019; Accepted: 14 December 2019; Published: 18 December 2019

Abstract: Gating or threshold selection is very important in analyzing data from a microflow cytometer, which is especially critical in analyzing weak signals from particles/cells with small sizes. It has been reported that using the amplitude gating alone may result in false positive events in analyzing data with a poor signal-to-noise ratio. Transit time (τ) can be set as a gating threshold along with side-scattered light or fluorescent light signals in the detection of particles/cells using a microflow cytometer. In this study, transit time of microspheres was studied systematically when the microspheres passed through a laser beam in a microflow cytometer and side-scattered light was detected. A clear linear relationship between the inverse of the average transit time and total flow rate was found. Transit time was used as another gate (other than the amplitude of side-scattering signals) to distinguish real scattering signals from noise. It was shown that the relative difference of the measured microsphere concentration can be reduced significantly from the range of 3.43%–8.77% to the range of 8.42%–111.76% by employing both amplitude and transit time as gates in analysis of collected scattering data. By using optimized transit time and amplitude gate thresholds, a good correlation with the traditional hemocytometer-based particle counting was achieved ($R^2 > 0.94$). The obtained results suggest that the transit time could be used as another gate together with the amplitude gate to improve measurement accuracy of particle/cell concentration for microfluidic devices.

Keywords: microfluidic; transit time; amplitude; particle/cell concentration counting; accuracy of measurement

1. Introduction

Microflow cytometers or microfluidic devices for particle/cell detection have been widely investigated and studied in recent years. A combination of electrical [1], mechanical [2], and optical properties such as side-scattered light [3] and laser induced fluorescence [4] have been measured to identify and differentiate the particles/cells. Recently, the physical property of transit time has also been introduced as an indicator for single cell identification using microfluidic devices [1,5]. Cells are squeezed through a constriction region with cell elongation, and the transit time can be recorded to differentiate cells of different sizes. Chen et al. [1] reported that a classification success rate of 93.7% for osteoblasts and osteocytes was achieved by using both transit time and impendence amplitude ratio as threshold gates in data analysis, while the classification success rate was 85.3% if impendence amplitude threshold was used alone.

The majority of the reported microflow cytometers have been used to measure the intensity of either forward scattered light (FSC) or side-scattered light (SSC), as well as the fluorescence light

intensity. In some studies, transit time of particles/cells passing through an interrogation region was also measured and used as a gate to filter noise in data processing for particle/cell counting based on a microflow cytometer. Kennedy et al. applied a time-domain filter of 5 μs to filter the raw data collected by a microflow cytometer and pulse duration was also studied [6]. Guo et al. used transit time to differentiate background noise and beads SSC signals from beads [7]. Transit time versus the magnitude of impendence in an impendence microflow cytometer was demonstrated by Bernabini et al. [8]. Transit time of blood cells passing through in capillary-like microchannels was studied for hematologic diseases [9]. Translocation profiles of cells passing through micropores were applied to identifying tutor cells and blood cells [10], and Ali et al. created a solid-state micropore device capable of distinguishing metastatic and non-metastatic tumor cells based on the translocation time and amplitude profiles [11]. Although transit time has been introduced in the data analysis of microflow cytometers, a systematic study on transit time and its impact on the performance of a microflow cytometer has not yet been reported. Questions such as how the transit time depends on measurement conditions remain unanswered.

The fundamental goal of microflow cytometers is to count and group cells/particles precisely [12]. Setting proper thresholds on the collected data is critically important to data analysis for microflow cytometers [13–18]. This paper presents a systematic study on transit time in processing data collected from a microflow cytometer under different measurement conditions. The effects of transit time on the accuracy of microsphere counting were investigated. An optimized transit time threshold setting method was provided to increase the accuracy of the microsphere counting. Moreover, the results of the microflow cytometer were compared to those based on the traditional hemocytometer counting.

2. Materials and Methods

2.1. Materials

The materials used in the measurements include polystyrene microspheres, SU-8 photoresist, and the Sylgard 184 Silicone Elastomer Kit. Polystyrene microspheres were purchased from Polysciences Inc. (Warrington, PA, USA), SU-8 photoresist from MicroChem Corp (Newton, MA, USA), and Sylgard 184 Silicone Elastomer Kit from Dow Corning (Midland, MI, USA).

2.2. Microflow Cytometer

The core element of the microflow cytometer is an optofluidic device fabricated by the standard photolithography and soft lithography techniques, as shown in Figure 1. The detailed fabrication process has been described in previous publications [3,7]. A 2D hydrodynamic focusing channel with two inlets and one outlet was fabricated by SU-8 (50 μm × 100 μm, SU-8 2075) and the channel was sealed by Polydimethylsiloxane (PDMS) using nitrogen plasma treatment [19]. An on-chip lens system was designed to guide and focus the excitation laser beam with a waist of 10 μm.

2.3. Sample Preparation

Polystyrene microspheres with a diameter of 2 μm were suspended in deionized water and a 3-fold serial dilution of the microspheres was performed, resulting in a serial of samples with microsphere concentration in a range between 1×10^6 and 6×10^3 microspheres/mL. The microsphere concentrations of the diluted samples were measured by both a hemocytometer under a microscope and the microflow cytometer more than three times.

In all microsphere experiments, surfactant (0.1% SDS) was added to reduce hydrophobicity. The samples in the test tubes were mixed on a vortex mixer and then underwent a sonication process to disrupt aggregates before use. The total flow rate was controlled under 16 mL/h to make sure the microspheres were distributed uniformly along the flow direction.

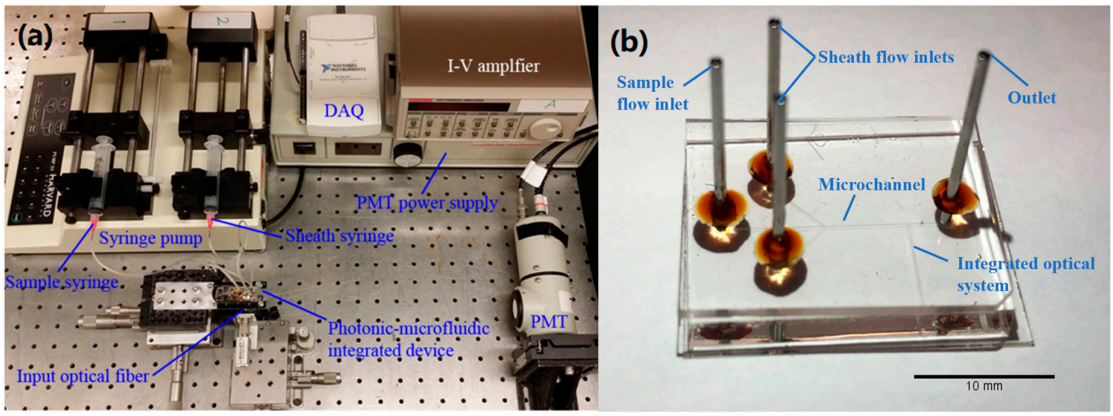

Figure 1. (**a**) A photo of the system setup of the microflow cytometer. (**b**) The microfluidic device.

2.4. Data Collection and Analysis

Side-scattered light signals of the microspheres were collected by a photomultiplier tube (PMT) connected to a data acquisition card (DAQ) with a sampling frequency of 250 kHz. An automatic data collection and analysis platform for the microflow cytometer was designed and implemented by a custom-made LabView (National Instruments) program on a computer.

3. Results and Discussion

3.1. Microflow Cytometer Data Analysis

Microspheres were injected into the microflow cytometer at a flow rate of 1500 µL/h and a total flow rate of 6000 µL/h. Figure 2a shows one second of raw data of SSC signal from a test with a duration of 60 s. Large spikes generated by microspheres and small spikes generated by background noise can be observed. Clearly, an amplitude threshold needs to be set to differentiate the positive events representing microspheres and false events representing the noise. Figure 2b shows an enlarged plot of raw signals in Figure 2a from 0.337911 to 0.338060 s. This pulse has a peak of 0.72 V, and thus can easily be picked up and counted as a positive event. In this case, an amplitude threshold of 0.18 V was applied, which was four times of the standard deviations above the baseline.

However, some pulses may not be created from microspheres even though amplitudes of these pulses are above the amplitude threshold, as shown in Figure 2c. The majority of the noise was under 0.18 V and was eliminated by the amplitude threshold, while a pulse of 0.21 V was considered as a positive event as it was 0.03 V greater than the threshold in Figure 2c. Based on empirical data, this pulse resulted from noise and it would cause a false positive event. A common characteristic of this noise is that their amplitudes were only a little bit larger than the amplitude threshold. Although this noise could be removed by setting a higher amplitude threshold, some weak pulses generated by microspheres not located in the center of the microchannel could be rejected as well. As a result, it is impossible to eliminate these false counts simply by applying an amplitude threshold.

As shown in Figure 2b, pulses resulted from positive events were tall and wide, i.e., high amplitude and long pulse duration. By contrast, the majority of pulses resulting from noise were weak and short (see Figure 2c). Therefore, it would be helpful to introduce a time-domain filter as an additional gate to the amplitude gate. Transit time is a natural choice for the time-domain filter. Transit time can be defined as the time period between the two cross-points of a pulse and the amplitude threshold, which can be read out from the raw data. Based on this definition, the transit time of the pulse in a positive event in Figure 2b was read as 29.4 µs, which matches well with the calculated time of 30 µs for the microspheres running through the optical beam in the experiments (average fluid velocity in the microchannel was 0.33 m/s, and the beam waist was 10 µm). By contrast, the transit time read from the false positive event in Figure 2c was about 8 µs, which is much shorter than the average transit

time. Therefore, the pulse with a transit time of 8 µs shown in Figure 2c can be rejected by employing a transit time gate.

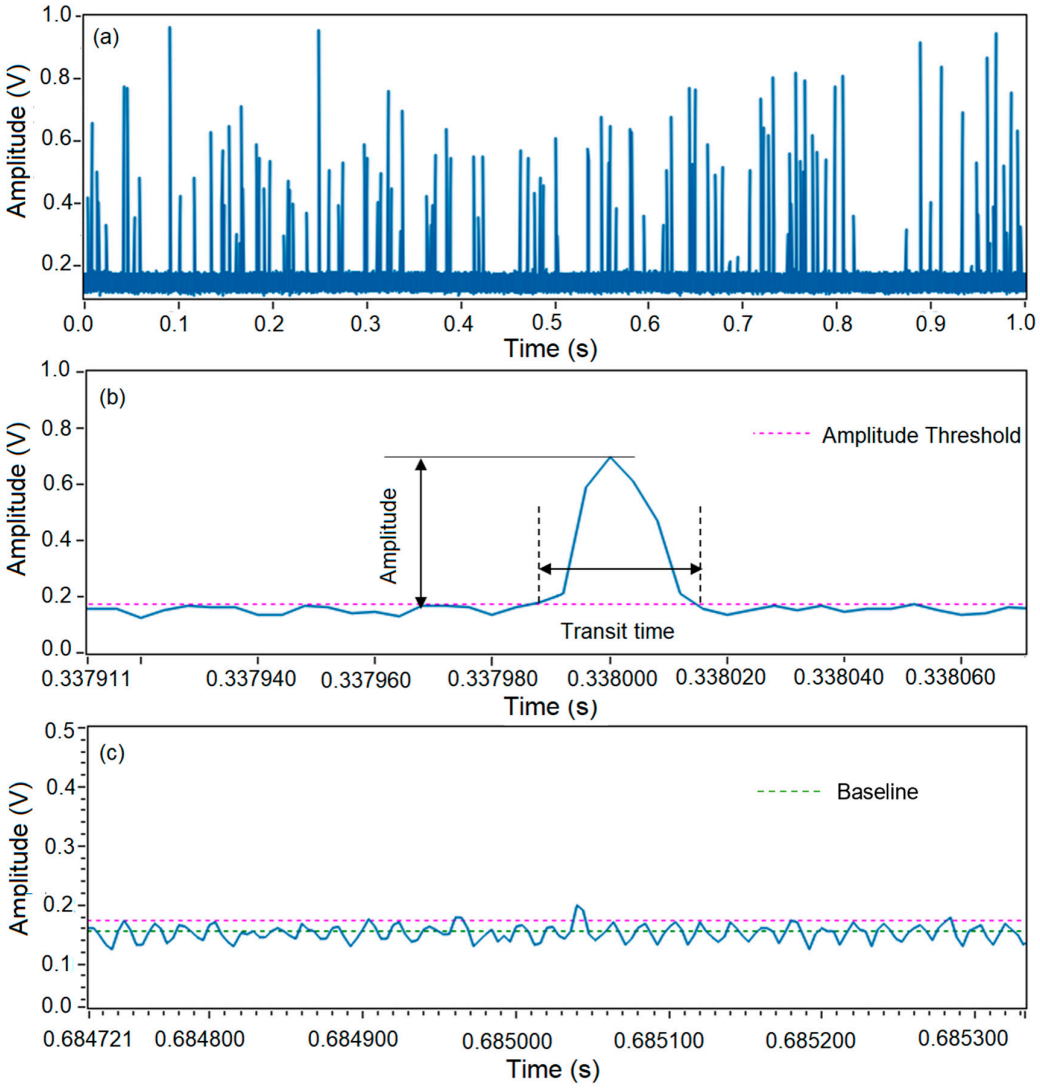

Figure 2. Data collection and analysis of a microsphere test using a microflow cytometer. (**a**) Raw data of 1 s from a test with a duration of 60 s. (**b**) Amplitude and transit time read out from a positive event. (**c**) Amplitude and transit time read out form a negative event.

As shown in Figure 3, the transit time and amplitude of every pulse can be read out from the raw data, and every pulse can be counted as an event. In this way, every event can be described by using both transit time and amplitude. Raw data of 60 s collected in Figure 2 is analyzed and plotted in Figure 3. In Figure 3a, the x-axis represents the number of events and the y-axis represents the transit time extracted from each event. Figure 3b shares the same y-axis with Figure 3a, and the x-axis represents the amplitude above the amplitude threshold. It is shown that the obtained profile of amplitude in Figure 3b is not apparently sharp enough to distinguish false events from positive events as discussed earlier in Section 3.1. If a higher amplitude threshold was applied in the data processing as amplitude threshold moved to the right of the y-axis in Figure 3b, some noise would be rejected, and some positive events generated by the microspheres would be rejected as well. If a lower amplitude threshold was set as the amplitude threshold moved to the left of the y-axis in Figure 3b,

more noise would be included. Due to the limitation of the amplitude gating, another gate is needed to solve the problem.

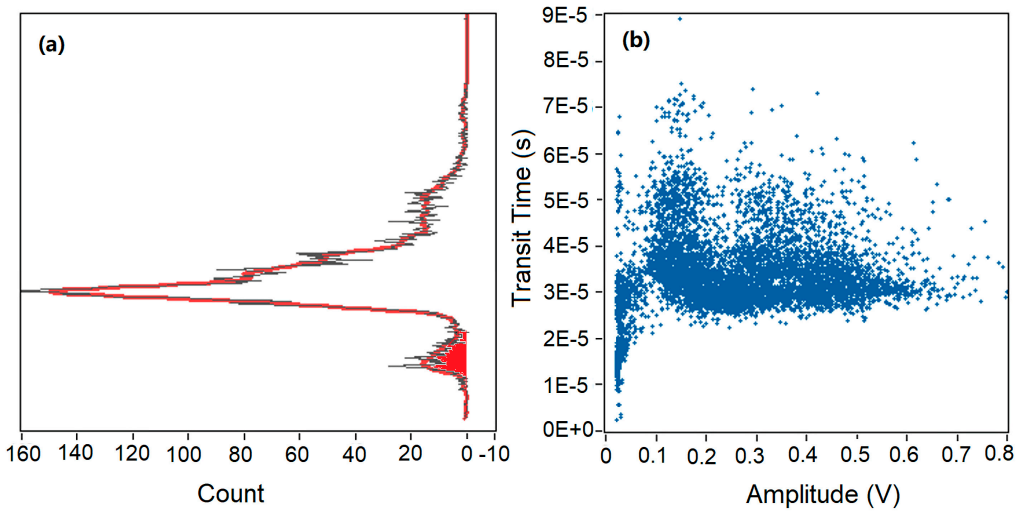

Figure 3. Data analysis of 60 s raw data. (**a**) Transit time distributions based on counts. (**b**) Scattering plot of all events based on transit time and relative amplitude above amplitude threshold.

In Figure 3a, a fitting curve (red) of counts versus transit time was achieved. One maximum peak of counts and a sub-peak were found in Figure 3a, corresponding to a transit time of 30 µs and 8 µs, respectively. Interestingly, similar peaks and sub-peaks were found in all experiments during the data analysis process. It can be observed that a majority of events had a transit time range of 25–40 µs, and a maximum count occurred at a transit time of 30 µs. As mentioned above, the estimated average transit time for the microspheres passing through the laser beam was also 30 µs. Thus, we can conclude that the maximum peak resulted from the microspheres and was corresponded to real events. In addition, a wide spread of transit time (0–75 µs) was found in Figure 3. Transit time varied from 10 to 22 µs in the red region in Figure 3a, and some events had a longer transit time (40–75 µs) above the average transit time. The wide spread of transit time was caused by the parabolic velocity profile in the 2D hydrodynamic focused microchannel. Microspheres were focused in the center of the microchannel along the flow direction, while they were distributed quadratically in the direction perpendicular to the flow.

Microspheres focused in the center of the channel passed through the interrogation region at a higher velocity and a shorter transit time, and microspheres distributed at the top and bottom of the microchannel had a lower velocity and a longer transit time. As we can see from Figure 3, a clear boundary between the maximum peak and the boundary peak was found based on the transit time. Thus, a transit time threshold was set at 22 µs to reject the background noise. Events in the red region of the sub-peak had a shorter transit time and a small amplitude above threshold. These events were considered as positive events by amplitude threshold alone, and they were rejected by applying the time-domain filter. Amplitude threshold alone was not able to eliminate the sub-peak caused by background noise, and transit time was a powerful tool for removing false counting. Therefore, it is necessary to use both amplitude and transit time thresholds to analyze the SSC data in microfluidic devices.

3.2. The Dependence of Inverse Transit Time on Total Flow Rate

To study dependence of the transit time on measurement conditions, a detailed study on transit time was performed and the raw data were analyzed using the methods explained in Section 3.1. Figure 4 shows the measured transit time under various total flow rates. In the experiments, the total

flow rate was increased from 4000 to 16,000 μL/h while the sheath flow rate to sample flow rate ratio was kept constant at three in order to maintain a good hydrodynamic focusing. As shown in Figure 4, the inverse transit time ($\tau_{avg}{}^{-1}$) had a very good linear relationship with the total flow rate (Q), which can be described well by the simplified equation below, where $\tau_{avg}{}^{-1}$ is the inverse of average transit time, L is the interrogation width and A is the cross-sectional area of the microchannel.

$$\tau_{avg}{}^{-1} = \frac{Q}{L * A}$$

The average velocity can be determined by the ratio of the total flow rate (Q) to the cross-sectional area (A), and it is also equal to the interrogation width over average transit time. Figure 4 indicates that the velocity depends on the flow rate and the linear relationship verified the performance of the microflow cytometer. The y-intercept of 0.0304 (μs^{-1}) was due to system error. As the scattered light can be produced wider than the beam waist in real experiments, the slope of the linear relationship was close to but not exactly equal to 1/(L*A).

It is worth noting that the average transit time at 6000 μL/h extracted from the raw data shown in Section 3.2 matches well with the calculated average transit time. With the increase of total flow rate, the velocity of the microspheres is increased, and the transit time is decreased. Therefore, the inverse transit time had a linear relationship with the total flow rate. Similar results were also found in experimental tests using microspheres of varying sizes (e.g., 6 μm). As the diameters of the microspheres increase, the average transit time will be longer, and the amplitude of the side-scattered light will be stronger.

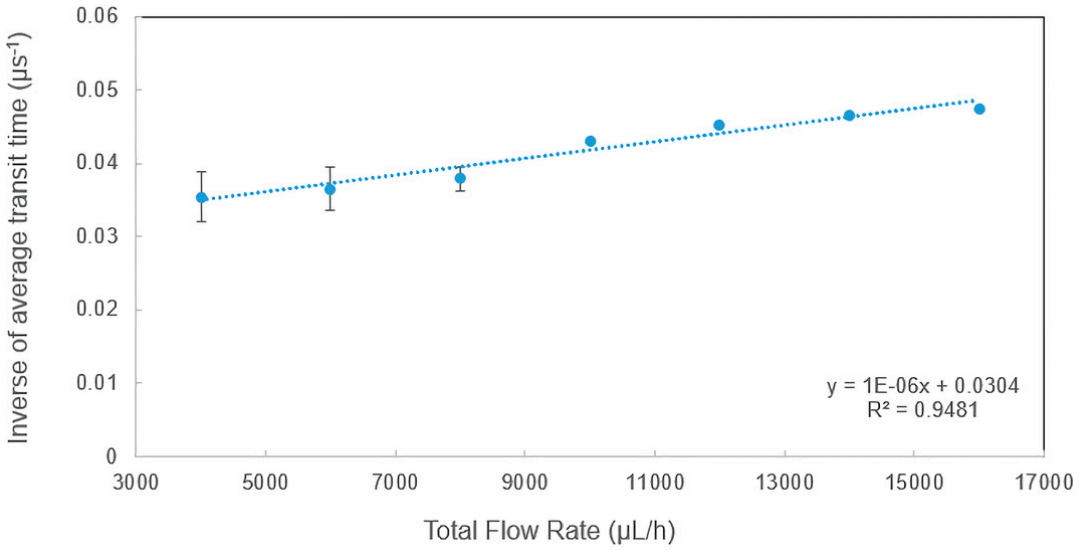

Figure 4. The dependence of inverse of average transit time on total flow rate.

3.3. Comparison between the Traditional Counting and the Microflow Cytometer

To verify the particle counting accuracy of the microflow cytometer, particle counting based on the traditional hemocytometer and the microflow cytometer was conducted, as shown in Figure 5. A 3-fold serial dilution based on an initial sample with a concentration of 1.14×10^6 microspheres/mL was performed to get six microsphere samples. The microsphere samples ran through the microflow cytometer for a 60 s test under the same experimental conditions described in Section 3.1, and the raw data were analyzed by applying both transit time and amplitude thresholds. At the same time, these samples were also counted under a microscope using a hemocytometer more than three times. The measured concentrations of these samples by the two methods were plotted on a logarithmic scale and fitted by a linear curve in Figure 5. A linear fitting with a R^2 value greater than 0.999

was achieved, and the relative standard deviation of the concentrations measured by the microflow cytometer was within a range of 0.99% to 4.73%, implying that the microflow cytometer has the capability of counting microspheres with a high accuracy over a wide concertation range of 6.13×10^3 to 1.14×10^6 microspheres/mL.

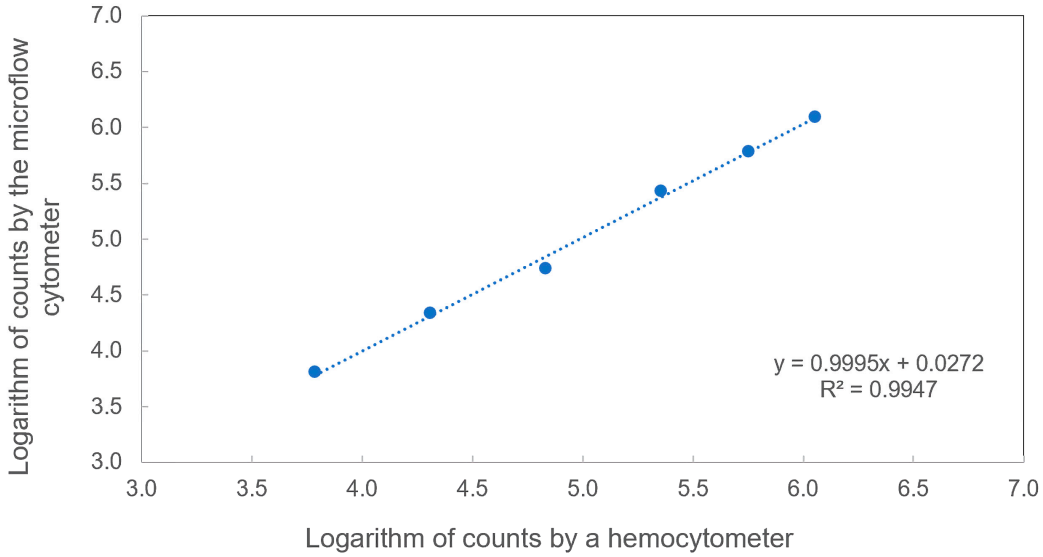

Figure 5. Comparison between two different methods. Microspheres were measured both by a hemocytometer and a microflow cytometer. The performance of the optofluidic microflow cytometer exhibited a linear response to hemocytometer counts on a logarithmic scale.

3.4. The Accuracy of Transit Time Threshold

Although Figure 5 demonstrated the results achieved from the microflow cytometer can be trusted, the impact of the transit time threshold on measurement accuracy of concentration still needs to be figured out. The raw data obtained in Section 3.3 were processed with and without setting of a transit time threshold and the logarithm of microspheres counting results for six samples were plotted in Figure 6. The standard deviations of tests without a transit time threshold ranged from 0.0072 to 0.043, while the values were in a range of 0.0058 to 0.018 in tests with a transit time threshold. Standard deviations can also be decreased by the transit time threshold, and these low standard deviations can also verify the good repeatability of the microflow cytometer. As shown in Figure 6, no significant differences between the two data analysis methods were shown when the concentration was high (samples 1 and 2). This result can be explained in that the false positive events caused by the background noise can be ignored due to the large number of positive events generated by microspheres at high sample concentrations, and it has validated our discussion in Section 3.1. As microsphere concentration was lower than 10^6 microspheres/mL, the measured results using amplitude threshold alone were greater than the results measured by employing both amplitude and transit time thresholds (samples 3–6 in Figure 6). This is because the pulses generated by background noise become comparable to the pulses created by microspheres as the microsphere concentration declines from 1.14×10^6 to 6.13×10^3 microspheres/mL. Therefore, eliminating false positive events by setting a transit time threshold is especially important to measurement accuracy at low concentration or at low microsphere throughput.

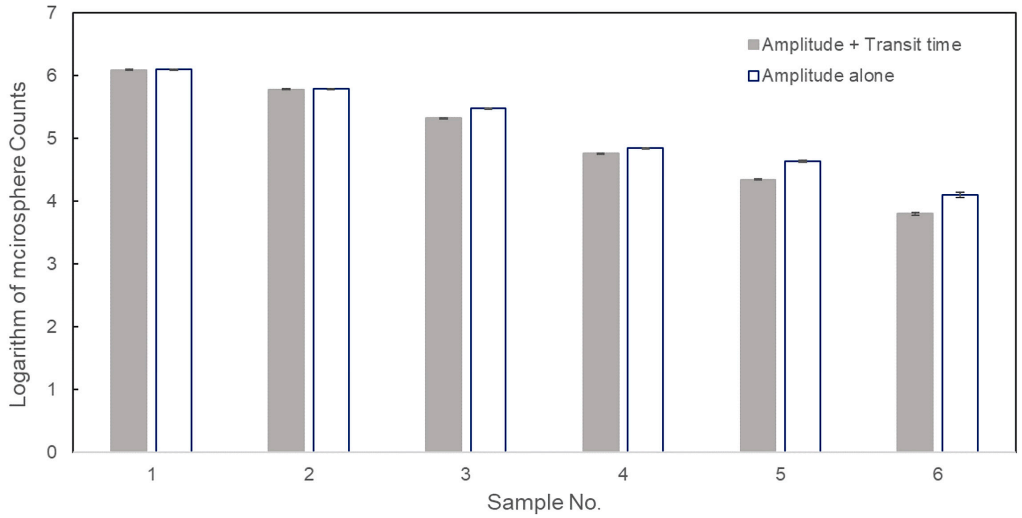

Figure 6. Logarithmic counting results of six microsphere samples using amplitude and transit time thresholds, and amplitude threshold alone.

Table 1 shows relative difference in percentage using amplitude threshold alone and using both transit time and amplitude thresholds. The relative difference in Table 1 is defined as the ratio of difference between the concentrations measured by the microflow cytometer and the values measured by a hemocytometer. When the concentration of the microspheres dropped to 10^3–10^4 microspheres/mL, the relative difference was as large as 108%–111% without setting a transit time filter. These results suggest that the transit time threshold can increase the accuracy of the measured microsphere concentration especially at low concentrations.

Table 1. Differences in accuracy of methods with and without transit time gating for counting microspheres.

Sample	Relative Difference with Transit Time Gating (%)	Relative Difference without Transit Time Gating (%)
1	8.77	9.65
2	6.67	8.42
3	−6.61	32.60
4	−6.96	12.46
5	7.84	111.76
6	3.43	108.81

4. Conclusions

This paper presented a systematic study on transit time and its impact on microsphere concentration detection. We have demonstrated how the transit time threshold can be set under various measurement conditions. Investigation of data analysis with or without setting a transit time threshold has been performed to evaluate its impact on the accuracy of the measurement. It has been found that the inverse of the average transit time depends on the total flow rate and the transit time can be used as a second gate to further differentiate real signals from background noise after filtering by the amplitude threshold. The measured accuracy has been improved significantly by applying both transit time and amplitude thresholds, which is especially important at low microsphere concentrations. The relative differences achieved without transit time gating ranged between 9.65%–111.76%, while these values dropped significantly to 3.43%–8.77% by employing both amplitude and transit time gating. The measured concentrations can be still reliable and accurate at lower concentrations (~10^3 microspheres/mL). At the same time, a linear fitting over a wide range of microsphere concentrations has been achieved between the microflow cytometer method and the traditional hemocytometer method. It has been shown that

transit time as a gate for microflow cytometers has the capability of enhancing the accuracy of the side-scattered light signal detection method, and it could be applied to other microfluidic devices for particle/cell detection as well.

Author Contributions: Conceptualization, Y.Z. and C.X.; methodology, Y.Z. and T.G.; writing—original draft preparation, Y.Z. and T.G.; software, T.G.; writing—review and editing, Y.Z. and C.X. All authors have read and agreed to the published version of the manuscript.

Funding: This research was funded by Global Water Futures (GWF).

Conflicts of Interest: The authors declare no conflict of interest.

References

1. Chen, J.; Zheng, Y.; Tan, Q.; Shojaei-baghini, E.; Zhang, Y.; Li, J.; Prasad, P.; You, L.; Wu, X.; Sun, Y. Classification of cell types using a microfluidic device for mechanical and electrical measurement on single cells. *Lab Chip* **2011**, *11*, 3174–3181. [CrossRef] [PubMed]
2. Hou, H.W.; Li, Q.S.; Lee, G.Y.H.; Kumar, A.P. Deformability study of breast cancer cells using microfluidics. *Biomed. Microdevices* **2009**, *11*, 557–564. [CrossRef] [PubMed]
3. Guo, T.; Wei, Y.; Xu, C.; Watts, B.R.; Zhang, Z.; Fang, Q.; Zhang, H.; Selvaganapathy, P.R.; Deen, M.J. Counting of Escherichia coli by a microflow cytometer based on a photonic-microfluidic integrated device. *Electrophoresis* **2015**, *36*, 298–304. [CrossRef] [PubMed]
4. Xun, W.; Feng, J.; Chang, H. A Microflow Cytometer Based on a Disposable Microfluidic Chip With Side Scatter and Fluorescence Detection Capability. *IEEE Trans. Nanobiosci.* **2015**, *14*, 850–856. [CrossRef] [PubMed]
5. Goddard, C.M.; Allard, M.F.; Hogg, J.C.; Herbertson, M.J.; Walley, K.R. Prolonged leukocyte transit time in coronary microcirculation of endotoxemic pigs. *Am. J. Physiol. Heart Circ. Physiol.* **1995**, *269*, H1389–H1397. [CrossRef] [PubMed]
6. Kennedy, M.J.; Stelick, S.J.; Sayam, L.; Yen, A.; Erickson, D.; Batt, C.A. Hydrodynamic optical alignment for microflow cytometry. *Lab Chip* **2011**, *11*, 1138–1143. [CrossRef] [PubMed]
7. Guo, T. An Optical System towards In-line Monitoring of Bacteria in Drinking Water. Ph.D Thesis, McMaster University, Hamilton, ON, Canada, 2016.
8. Bernabini, C.; Holmes, D.; Morgan, H. Micro-impedance cytometry for detection and analysis of micron-sized particles and bacteria. *Lab Chip* **2011**, *11*, 407–412. [CrossRef] [PubMed]
9. Rosenbluth, M.J.; Lam, A.; Fletcher, D.A. Analyzing cell mechanics in hematologic diseases with microfluidic biophysical flow cytometry. *Lab Chip* **2008**, *8*, 1062–1070. [CrossRef] [PubMed]
10. Asghar, W.; Wan, Y.; Ilyas, A.; Bachoo, R.; Kim, Y.T.; Iqbal, S.M. Electrical fingerprinting, 3D profiling and detection of tumor cells with solid-state micropores. *Lab Chip* **2012**, *12*, 2345–2352. [CrossRef]
11. Ali, W.; Ilyas, A.; Bui, L.; Sayles, B.; Hur, Y.; Kim, Y.T.; Iqbal, S.M. Differentiating Metastatic and Non-metastatic Tumor Cells from Their Translocation Profile through Solid-State Micropores. *Langmuir* **2016**, *32*, 4924–4934. [CrossRef]
12. Aghaeepour, N.; Finak, G.; Consortium, T.F.; Consortium, T.D.; Hoos, H.; Mosmann, T.R.; Brinkman, R.; Gottardo, R.; Scheuermann, R.H. Critical assessment of automated flow cytometry data analysis techniques. *Nat. Methods* **2013**, *10*, 228. [CrossRef] [PubMed]
13. Snow, C.K. Flow cytometer electronics. *Cytometry A* **2004**, *57*, 63–69. [CrossRef] [PubMed]
14. Herzenberg, L.A.; Tung, J.; Moore, W.A.; Herzenberg, L.A.; Parks, D.R. Interpreting flow cytometry data: A guide for the perplexed. *Nat. Immunol.* **2006**, *7*, 681–685. [CrossRef] [PubMed]
15. Jimenez-Carretero, D.; Ligos, J.M.; Martínez-López, M.; Sancho, D.; Montoya, M.C. Flow Cytometry Data Preparation Guidelines for Improved Automated Phenotypic Analysis. *J. Immunol.* **2018**, *200*, 3319–3331. [CrossRef] [PubMed]
16. Lugli, E.; Roederer, M.; Cossarizza, A. Data analysis in flow cytometry: The future just started. *Cytometry A* **2010**, *77*, 705–713. [CrossRef] [PubMed]
17. Pyne, S.; Hu, X.; Wang, K.; Rossin, E.; Lin, T.; Maier, L.M.; Baecher-allan, C.; Mclachlan, G.J.; Tamayo, P.; Hafler, D.A.; et al. Automated high-dimensional flow cytometric data analysis. *Proc. Natl. Acad. Sci. USA* **2009**, *106*, 8519–8524. [CrossRef] [PubMed]

18. Lo, K.; Brinkman, R.R.; Gottardo, R. Automated Gating of Flow Cytometry Data via Robust Model-Based Clustering. *Cytometry A* **2008**, *73*, 321–332. [CrossRef] [PubMed]
19. Zhang, Z.; Zhao, P.; Xiao, G.; Watts, B.R.; Xu, C. Sealing SU-8 microfluidic channels using PDMS. *Biomicrofluidics* **2011**, *5*, 1–8. [CrossRef] [PubMed]

Chapter 7

Quantification of Low-level Cyanobacteria Using a Microflow Cytometry Platform for Early Warning of Cyanobacteria Blooms

This chapter summarizes the overall work of method proposed to solve the harmful cyanobacterial blooms. In previous work, the pre-enrichment, and the detection platform were accomplished. This chapter shows the completion of the proposed methods.

The first aim of this work was to conduct the proof of principle study to explore the performance evaluations of the microflow cytometer on the measurements of cyanobacterial samples at a device level. Then, we aimed at exploring the performance evaluations based on the measurement of low-level cyanobacterial samples at a system level. In the first part of this chapter, cyanobacterial samples were measured to verify the labeling free detection of the optofluidic microflow cytometer with the optimized data analysis. Then, the verified automated bacterial concentration and recovery system was adjusted for cyanobacteria with reduced retentate volume and higher concentration ratio.

The overall objective of this project was accomplished by completion of each sub-objective addressed in previous chapters. An optofluidic microflow cytometer combined with a pre-concentration system platform was designed for labeling-free phycocyanin fluorescence detection to determine the biomass of cyanobacterial. To protect human health from the impairments caused by cyanobacteria and cyanotoxins, the microflow cytometer was capable of accurately measuring cyanobacterial cells above 15,000 cells/mL and it can provide safety alert for WHO Alert Level 2 (200,000 cells/mL).

Applied with the pre-concentrating process that contained an automated cyanobacterial concentration and recovery system, the quantification limit of the platform was significantly reduced to 5 cyanobacterial cells/mL. In other words, the platform can

provide WHO Alert Level 1 (2000 cells/mL) alerts as the cyanobacterial biomass exceeds the vigilance level. Moreover, this method can provide early warning alerts of a potentially harmful cyanobacterial bloom at least 15 days before it actually happens. Therefore, the authorities can have ample time to prevent or slow down the blooms and reduce the hazardous effects caused by the harmful blooms.

The author of this thesis is the first author and main contributor of this submitted manuscript. The experimental design and conduction, data analysis and manuscript writing were competed by the first author. Dr. Tianyi Guo and Prof. Chang-qing Xu contributed to experimental discussion and manuscript revision.

This chapter has been submitted to *Environmental Science and Technology* for their consideration of publication.

Quantification of Low-level Cyanobacteria Using a Microflow Cytometry Platform for Early Warning of Cyanobacteria Blooms

Yushan Zhang[1], Tianyi Guo[3], Chang-qing Xu[1,2]

[1]Department of Biomedical Engineering, McMaster University

[2]Department of Engineering Physics, McMaster University

[3]Forsee Instruments Ltd., Canada

Abstract:

This paper presents a microflow cytometry platform for labeling-free phycocyanin fluorescence detection, which can be used for the rapid quantification of low-level cyanobacteria and provide early warning alerts of potentially harmful cyanobacterial blooms. The microflow cytometry platform contains a pre-concentrating process and utilizes an on-chip interaction of a laser beam with an integrated microfluidic device to measure the *in vivo* fluorescence emitted from each individual cyanobacterial cell instead of measuring the overall fluorescence of the whole sample. By applying transit time and amplitude thresholds, the proposed cyanobacteria detection method was verified by the traditional cell counting technique using a hemocytometer with an R^2 value of 0.993. As a pre-concentrator, an automated cyanobacterial concentration and recovery system (ACCRS) was developed and optimized to reduce the assay volume from 1,000 mL to 1 mL to enhance the detection limit. It was shown that the limit of quantification of the microflow cytometry platform can be as low as 5 cells/mL for *Microcystis aeruginosa*, which is 400-fold lower than the Alert Level 1 (2,000 cells/mL) set by the World Health Organization (WHO). Furthermore, this method can provide early warning alerts at least 15 days before a potential cyanobacterial bloom, providing ample time for authorities to take actions.

Keywords: Phycocyanin; Cyanobacteria; Fluorescence; Microflow Cytometer; *Microcystis Aeruginosa*

1. Introduction

Increased human activities due to population explosion and modern societal development have caused the loading of nitrogen and phosphorus into rivers, lakes, and oceans. The resulting eutrophication has increased the reproductive rates of phytoplankton in aquatic ecosystems. The accumulation of buoyant microorganisms causes water discoloration, considered as a bloom. Within the phyla that can form a bloom or scum, cyanobacteria are the most notorious and problematic [1]–[4]. Data from the National Center for Environmental Health shows that from 2007 to 2011, 73% of samples collected from blooms were related to cyanobacteria and routine monitoring reports from 7 states in the United States were identified as cyanobacteria [5]. The top

three ranked cyanobacterial species were *Anabaena* spp., *Aphanizaomenon* spp., and *Microcystis* spp. [5]. Moreover, an overwhelming majority of the cyanotoxins (80%) were microcystins [5]. Microcystins are mainly produced by *Microcystis Aeruginosa* and can result in severe liver failure [6] and skin ailments [7] when consumed or exposed. According to a case study conducted in southern Quebec, Canada, *Microcystis aeruginosa* not only posed a threat to recreational water, but was also dominant within an untreated water source used by a drinking water treatment plant [8].

To prevent the production of cyanotoxins and harmful effects caused by cyanobacterial blooms, it is critically important to monitor cyanobacteria, even at low levels. An Alert Levels Framework has been established by the World Health Organization (WHO) for the monitoring and management of a potential cyanobacterial bloom in source water [9]. The cyanobacterial biomass threshold for Alert Level 1 is 2,000 cells/mL and 100,000 cells/ml for Alert Level 2 [9]. The WHO guideline value for cyanobacteria in recreational freshwater with a low possibility of harmful health effects is 20,000 cyanobacterial cells/mL [10]. It is worth noting that cyanobacterial cells can proliferate extremely fast in nutrient rich environments at a warm temperature. In a study on the growth rates of eight cyanobacteria species, the biomass of cyanobacteria doubled in 1.65 days at 20 °C and the doubling time decreased to 0.75 days at the optimum temperature (29.2 °C) [11]. The doubling time for cyanobacterial concentration varies from less than 20 hours for *Synechocystis* sp. to about 150 hours for *H. hongdechloris* [12]. The biomass of *Microcystis aeruginosa* can double in 1.23 days at 32 °C [13]. Other studies reported that the average doubling times for some bloom-forming species was approximately 2 days under optimal conditions [14]. To form a bloom, it may take days or months. The strategies to prevent and control cyanobacterial blooms include nutrient management, hydrodynamics such as water diversion, and chemical and biological control [1], [15]. Some strategies are effective but expensive, whereas others may only have temporary effects. It is costly and quite difficult to control and suppress cyanobacterial blooms. The best method is to stop potential blooms from growing as they begin to proliferate. Therefore, to ensure there is enough time to respond to potential cyanobacterial blooms, a low-cost, rapid, and accurate detection and monitoring method for cyanobacteria at a level far lower than 2,000 cells/mL is essential to provide early warning alerts.

More importantly, the conventional processes applied in drinking water treatment plants are not fully capable of removing cyanobacterial biomass and cyanotoxins. To reduce the potential health impairments from cyanobacteria or cyanotoxins, it is quite important to stop potential cyanobacterial blooms at a early stage [16]. Thus, a low-cost, rapid, and accurate detection and monitoring method for cyanobacteria at a level far lower than 2,000 cells/mL is also essential to monitor drinking water and recreational waters that humans may be exposed to.

Current methods for monitoring cyanobacteria in freshwater can be divided into three main categories including biological, biochemical, and physicochemical methods [17]. Biochemical and physicochemical methods include assays and chromatographic methods, such as enzyme-linked immunosorbent assays (ELISA) and high-performance liquid chromatography (HPLC) [17]. These methods are accurate, sensitive, and rapid. However, they are very expensive, and skilled personnel are required for their operation.

Microscopic counting, genomic methods, and indirect pigment measurement are the most common biological methods currently used [17]. Microscopic identification with a hemocytometer chamber is the conventional biological method for cell counting. Trained personnel are needed, and this method is time-consuming. Genomic methods (e.g., qPCR assay, DNA based chip) have been successfully applied in the detection of *Microcystis aeruginosa* in the laboratory. The biggest limitation of genomic assays is the complicated DNA extraction process [6]. Chlorophyll a (i.e., Chl-a) and phycocyanin are two typical photosynthetic pigments used for the determination of cyanobacteria using the indirect pigment measurement method. This method depends on the positive correlation between the value of the pigments and cyanobacterial biomass. Chl-a content in cells depends on the density of total phytoplankton. Phycocyanin, as the unique cyanobacterial pigment, can fluoresce and improve the selectivity of the method as compared to the Chl-a detection method. The reading of phycocyanin measured by *in vivo* phycocyanin fluorescence probes needs to be transformed into a cell concentration of cyanobacteria. Although *in vivo* fluorescence probes have been used in early detection of cyanobacteria, they ignore the effects of the metabolic state and size of individual cells on pigment contents. The post-calibration between the phycocyanin reading and the hypothesized cell counts may vary. The cyanobacterial threshold of a reported phycocyanin probe was 1 mm^3/L [8], which is higher than the WHO Alert Level 1 threshold (with a corresponding biovolume of 0.2 mm^3/L). Bastien et al. reported a phycocyanin probe with a limit of detection of 4,000 cells/mL for accurate detection of *Microcystis aeruginosa* [18]. Although these phycocyanin probes are capable of rapidly monitoring rich-cyanobacterial samples, they can hardly reach the WHO Alert Level 1 threshold. Moreover, some commercial probes can only provide qualitative results and a post-calibration correction is required for quantitative analysis [18]. Significant research effort has been made to reduce detection limit of cyanobacteria. For example, Lee et al. presented the quantitative detection of *Microcystis aeruginosa* by the NanoGene Assay in the laboratory and the limit of detection was determined to be 9 agal cells/mL in water [6]. This method has a complicated preparation process, and the low limit of detection can only be achieved in the laboratory.

A microflow cytometer is a powerful analysis tool for cell identification and can be used to combine the phycocyanin measurement with single-cell detection. Furthermore, a microflow cytometer can be fabricated on a chip with low cost and smaller size for the determination of cyanobacteria. Both side scatter and fluorescence properties can be employed for the characterization of cells of interest. Microflow cytometry has been applied for optical analysis of phytoplankton by Hashemi et al, however a minimum concentration of 50,000 cells/mL was used in their report [19]. In the previous publications, data analysis methods based on proper threshold setting and raw data filtering have been employed and optimized for particle/cell monitoring by using microfluidic devices [20].

In this paper, a detection and quantification method suitable for on-site monitoring of *Microcystis aeruginosa* was proposed and demonstrated based on side scatter and fluorescence of phycocyanin using a microflow cytometer, which has features including low cost, rapid, accurate and labeling-free, which are crucial to on-site monitoring of cyanobacteria. Performance of the microflow cytometer on *Microcystis aeruginosa* detection and quantification was investigated first. By employing both amplitude and transition threshold, very fast ($\leq$ 1 min) detection and quantification of *Microcystis aeruginosa* can be achieved with relatively low detection limit ($\sim$ 10,000 cells/mL)

by using the micro flow cytometer alone, which could be used for early warnings of cyanobacterial blooms for WHO Alert Level 2. By adding a pre-concentrating process, a detection limit as low as 5 cells/mL can be achieved, which is far below the threshold of WHO Alert Level 1. It is worth noting that reducing the detection limit is extremely important to the early warning since this gives decision-makers more time to take necessary actions allow to better protect public health in response to a potential cyanobacterial bloom.

2. Materials and Methods

2.1 A microfluidic device based microflow cytometer

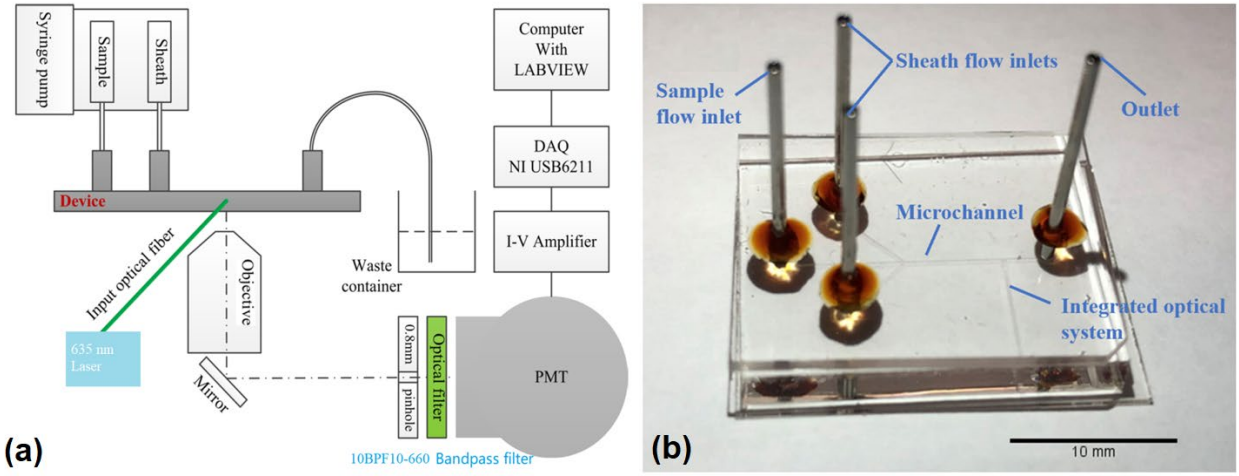

Figure 1. (a) A schematic diagram of a microflow cytometer. (b) A photo of a microfluidic device with integrated optics

Figure 1a shows a schematic diagram of the microflow cytometer. The core component of the microflow cytometer is a microfluidic device integrated with on-chip waveguides and microlenses fabricated by standard photolithography processes. Figure 1b shows the microfluidic device used in this study. It consists of three layers: a glass pad for protection on the top of the device, a polydimethylsiloxane (PDMS) layer for sealing in the middle, and a glass substrate coated with a functionalized SU-8 layer at the bottom. The microchannel was fabricated by SU-8, which was 100 µm wide and 50 µm in height. The fabrication process has been studied and optimized multiple times and can be found in previous publications [21]–[25].

Samples were injected at the sample flow inlet and hydrodynamically focused to the center of the microchannel by the sheath flow. As the samples passed through the region of interest, the interaction between light and cells was observed. Laser light (wavelength of 635 nm) was coupled into the on-chip waveguide to excite the cells of interest, and then the emitted light (through *in vivo* fluorescence from cyanobacteria cells) was reflected by a mirror and collected by a photomultiplier tube (PMT). A 0.8 mm pinhole and a 660 ± 10 nm bandpass filter were placed in front of the PMT to eliminate unwanted background noise and side scattered light. The raw data was amplified and converted into voltages and further processed by a data acquisition card (DAQ)

purchased from National Instruments (NI). Customized LabView programs were applied to determine the proper gating thresholds for the pulsed data and to quantify the presence of cyanobacterial samples. It is worth noting that no labeling process is involved in the proposed cyanobacteria detection method, which is essential to on-site monitoring of cyanobacteria for early warning alerts.

2.2 Microcystis aeruginosa preparation

Microcystis aeruginosa samples from the Canadian Phycological Culture Centre (CPCC) were used in the experiments. These cyanobacterial cells were grown and cultured in 3N BBM medium in glass tubes. A two-fold serial dilution was performed in 10 mL tubes to reduce the cell abundance of highly concentrated cyanobacterial samples (10^7~10^8 cyanobacterial cells/mL). The diluted samples were prepared in phosphate buffered saline (PBS) immediately before the measurements. Cell counts for cultured cyanobacterial samples were performed using a hemocytometer chamber under a microscope. Each sample was counted more than three times and the coefficient of variation was within 10%.

2.3 A pre-concentrating process by an automated cyanobacterial concentration and recovery system

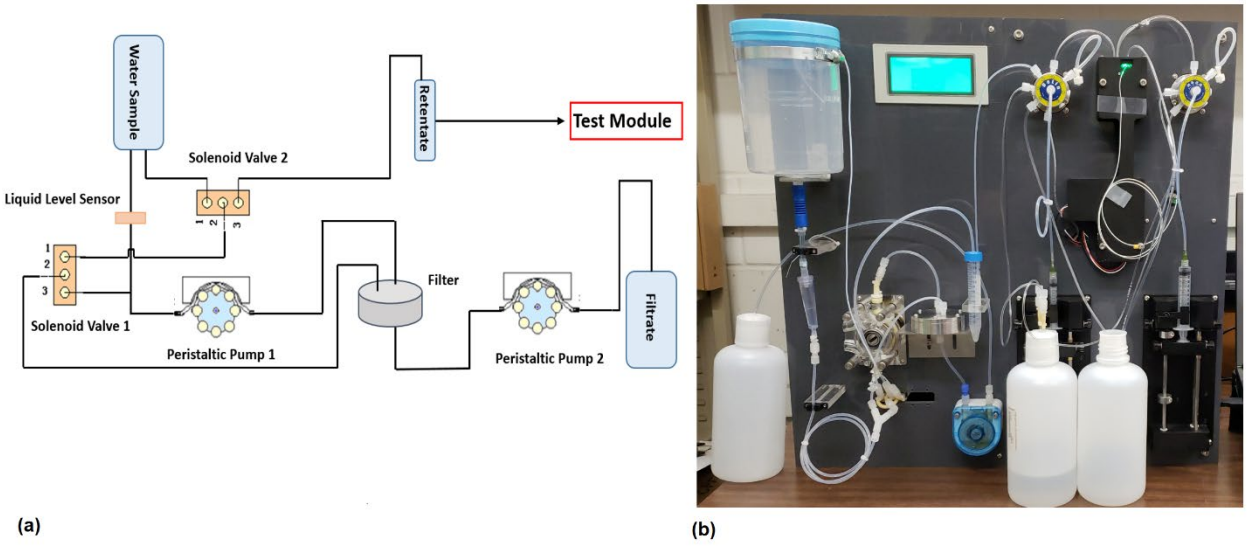

Figure 2. Automated cyanobacterial concentration and recovery system (ACCRS). (a) A schematic diagram of the ACCRS, (b) a picture of the physical setup.

In this study, the ability of a microfluidic device based microflow cytometer was investigated to determine the concentration of cyanobacterial samples at relatively high levels (>1000 cells/mL) without a pre-concentrating process. To extend the application of the microflow cytometer to practical on-site testing of low-level cyanobacteria, a pre-concentrating system was designed to

treat the samples and increase cyanobacteria concentration before the characteristic analysis. Thus, a sub-system was designed to process large amounts of environmental samples (more than 1 liter) in a short time. Moreover, the pre-concentrating process was able to capture the cells of interest from the original large volume samples and resuspend them in small volumes on a microliter scale by filtering out excess water.

Figure 2a shows the working principle of the proposed automated cyanobacterial concentration and recovery system (ACCRS) and the actual setup is shown in Figure 2b. The water sample was pumped into the system by a main peristaltic pump (Pump 1) and the flow proceeded through a ceramic filter with a pore size of 0.14 μm. As the cells of interest remained on the surface of the filter membrane, water molecules and particles smaller than 0.14 μm ran through the filter. Then the permeate flow was pumped into the filtrate reservoir by a less powerful peristaltic pump (Pump 2). The pre-concentration process did not end until the readouts from the liquid level sensor changed as the final retentate volume reached the desired level.

A similar setup has been created and applied for the pre-concentrating of *E. coli*, and the detailed working principle and detailed experimental data can be found in previous publications for concentrating and recovering *E. coli* [20], [26]. To meet the requirements of cyanobacterial pre-concentrating, a new setup was established based on previous experimental results and empirical analysis. A tangential flow technique and unique back-flushing techniques were the main methods used to improve the recovery efficiency of the system. As a result, the parameters of the pumping tube were recalculated, and the parameters of the back-flushing techniques were also optimized by changing the parameters of the two pumps. Most importantly, the final retentate volume was reduced significantly from ~5 mL to ~1 mL by a systematic study of controller parameter optimization and hardware enhancements.

In all experiments with the ACCRS, certain amounts of *M. aeruginosa* were spiked into 1000 mL PBS, and then samples were sent through the sub-system. The ACCRS, as shown in Figure 2, was optimized to increase the concentration level of the cells of interest and minimize the assay volume for bacterial detection. Then, the final retentate was transferred to the microflow cytometer for characteristic analysis. In the control group, the same cyanobacterial samples did not go through the ACCRS and were directly monitored by the microflow cytometer for characteristic analysis.

3. Results and Discussion

3.1 Fluorescent results of *Microcystis aeruginosa*

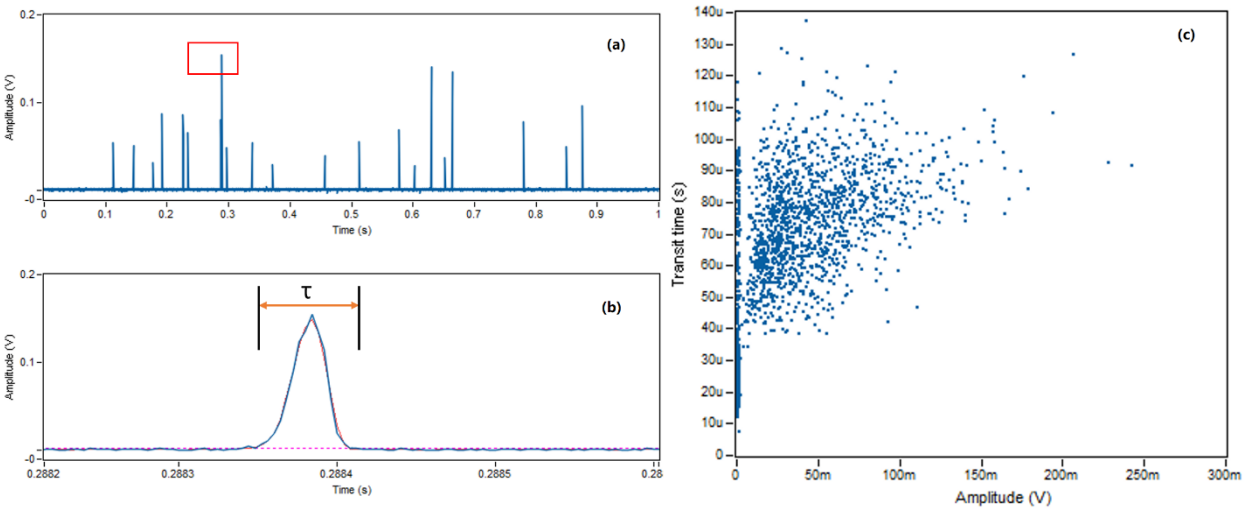

Figure 3. **Raw data from *Microcystis aeruginosa* fluorescent measurements. (a) Fluorescent signals of one second from one experimental measurement. (b) The enlarged view of one pulse in (a). (c) All events plotted with extracted transit time and amplitude in the same measurement.**

Figure 3a shows a one-second readout from a 60 s measurement of *M. aeruginosa* samples using the microflow cytometer, while Figure 3b shows the enlarged single pulse of the red area in Figure 3a. All of the events in the same 60-second experiment were plotted in Figure 3c. In Figure 3a, the x-axis represents time, and the y-axis shows the amplitude (voltage) of each pulse. As cells/particles pass through the interaction region formed by the focused laser beam and the hydrodynamically-focused sample flow in the center of the microchannel, fluorescent signals emitted by *Microcystis aeruginosa* samples were collected by the LabView programs. In Figure 3b, one pulsed signal in the red area in Figure 3a is enlarged and presented. As shown in Figure 3b, the collected signals can be simulated as half-sine pulses with specific amplitudes (y-axis) and durations (τ). Thus, the height of the pulse is defined as the amplitude, and the duration between the cross points of the pulse and the amplitude baseline is defined as the transit time (τ). The amplitude and transit time in Figure 3b were determined to be 0.16 V and 62 μs, respectively. As shown in Figure 3c, values of the transit time (y-axis) in the 60 s experiment were plotted according to the amplitude of each signal (x-axis).

As shown in Figure 3, transit time and amplitude can be used to present the pulsed signals as these values depend on the characterization of the particles/cells passing through the laser beam. It is clear that the thresholds of amplitude and transit time need to be properly established for microfluidic analysis. The amplitude threshold, defined as the mean plus 3 standard deviations, was used to eliminate outliers. It can be seen in Figure 3c that most dots are in the 35 µs to 110 µs range. A cut-off transit time threshold value of 30 µs was applied to distinguish positive signals from background noise.

In Figure 3, we can see that the transit time range from 35-110 µs and the transit time at 75.9 µs have the highest counts. When the diameter of *M. aeruginosa* was 4-8 µm, the average transit time for the cells passing through the 10 µm laser beam was calculated to be within the range of 63-81 µs. However, due to the 2D hydrodynamic focusing, the actual transit time has a wider range than the calculated average transit time. The shortest transit time for the cells in the centre of the microchannel flowing through the interrogation region is around 32 µs, which means that transit time values of positive signals are equal to or greater than this value. Considering the group characteristics of the plotted dots, a lower value of 30 µs was set to further eliminate background noise. A pulsed signal is necessary to satisfy both the transit time threshold and amplitude threshold to be considered as a positive signal produced by *M. aeruginosa.* Background noise that has a higher amplitude than the amplitude threshold while with a shorter transit time below 30 µs was considered as false-positive, and further filtered out. In conclusion, a transit time threshold can be applied to improve the accuracy of the measurement, especially in the side scatter detection of beads that can be found in a previous publication [20].

3.2 Linearity and Repeatability Experiments

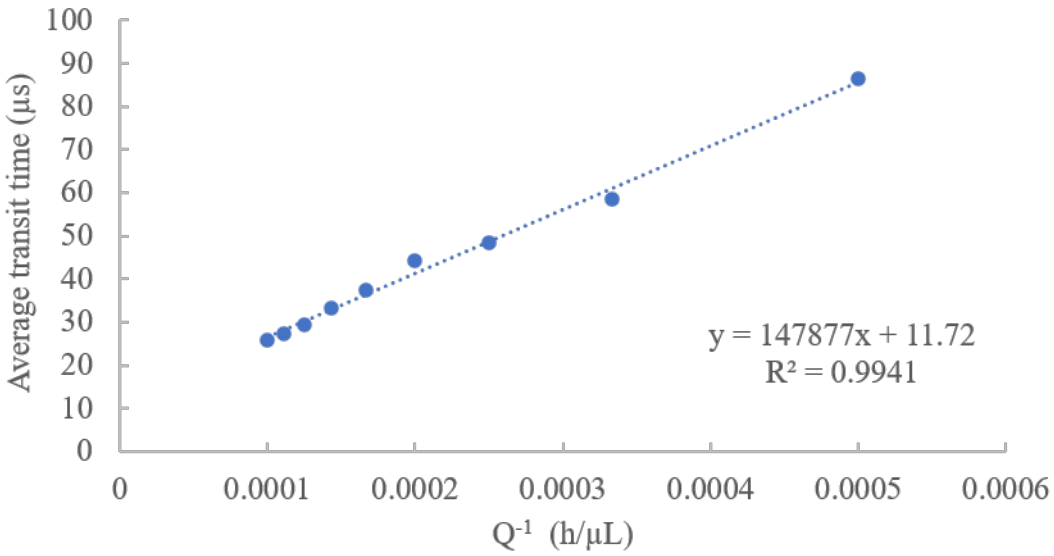

Figure 4. Relationship between the measured average transit time and the inverse of total flow rate.

Figure 4 presents the relationship between the transit time and the inverse of the total flow rate. *M. aeruginosa* samples were measured by the microflow cytometer under various total flow rate values with a fixed sample to sheath flow rate of 1:3. The observed average transit time linearly decreased from 86.34 µs to 25.93 µs when increasing total flow rate from 2000 µL/h to 10,000 µL/h. The analysis showed a good linearity (R^2 = 0.99) of the measured transit time with respect to the inverse of total flow rate. At the same time, the transit time threshold value was also affected by the total flow rate. The transit time value was set at 40 µs for a lower total flow rate of 2000 µL/h, while the value went down to 15 µs for a higher flow rate of 10,000 µL/h. These results confirm that transit time can be applied as a useful gating threshold in data analysis for microflow cytometers or time-domain microfluidic devices. The good linearity also indicates that the microflow cytometer is stable under various experimental conditions.

Each of the *M. aeruginosa* samples were measured multiple times under different conditions by the same microflow cytometer and the results are shown in Table 1. The cell concentrations of these samples ranged from 10^4 ~ 10^6 cells/mL and were prepared by a serial dilution. From Table 1, we can see that the lowest coefficient of variation (CV) was 3.82% at 590,000 cells/mL and the highest was 27.58% at 56,800 cells/mL. Although results show relatively large variation for lower cell concentrations of 56,800 and 28,400 cells/mL compared to samples of higher concentration, the coefficients of variation of the majority of the measurements (6 of 8 samples) were within 10%. The repeatability of the microflow cytometer measurements in higher cyanobacterial abundance samples was excellent (CV less than 10%), while larger variation of CVs at lower cell

concentrations were observed. The quantitative measurement of *M. aeruginosa* by the microflow cytometer is therefore repeatable in a wide concentration range.

Table 1 Repeatability of the microflow cytometer. N represents the number of replicates, SD means standard deviation, and CV is the coefficient of variation

Sample	Mean (cells/mL)	SD (cells/mL)	CV (%)	N
1	1,240,000	74,700	6.01	15
2	590,000	22,500	3.82	15
3	354,000	27,300	7.82	15
4	169,000	16,600	9.81	15
5	103,000	9,400	9.08	15
6	56,800	15,700	27.58	15
7	28,400	4,240	14.92	15
8	14,400	1,360	9.48	15

3.3 Quantitative Detection of *Microcystis aeruginosa* with the microflow cytometer

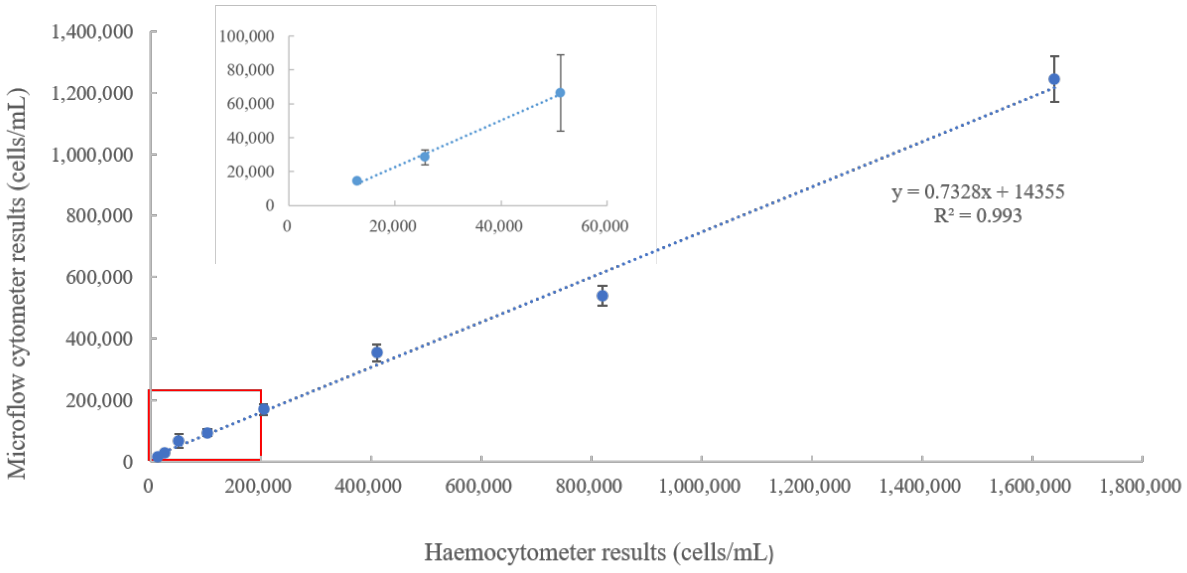

Figure 5. Quantitative detection of *M. aeruginosa* measured by a hemocytometer under a microscope and the microflow cytometer platform. The enlarged view shows the red area of the linear regression of cell concentrations lower than 200,000 cells/mL.

The quantitative detection results of *M. aeruginosa* samples were gathered and later compared with results quantified by traditional hemocytometer counting under a microscope. Figure 5 shows the comparison between these two methods, and the measured values of each sample by the microflow cytometer (y-axis) are plotted according to the results based on the hemocytometer (x-axis). A wide range of the *M. aeruginosa* samples ($10^4 \sim 10^6$ cells/mL) were measured at least three times by each method. As shown in Figure 5, a good linearity with an R^2 value of 0.993 was measured in a wide range from 15,000 cells/mL to more than 1,000,000 cells/mL. The linearity shows that the microflow cytometer results are consistent with traditional hemocytometer results within a wide concentration range of *M. aeruginosa*. As the lower limit required for a hemocytometer to make an accurate measurement is at least 10,000 cells/mL, the lowest cell concentration valid in this comparison is 15,000 cells/mL. The good linearity reveals that the quantification limit of the microflow cytometer is 15,000 cells/mL or potentially less. The quantification limit is lower than 100,000 cells/mL and therefore can provide alerts based on WHO Alert Level 2 in source water. Meanwhile, it can also be applied to monitor cyanobacteria in recreational water to protect the public from adverse health effects caused by cyanobacterial biomasses greater than 20,000 cells/mL [9], [10]. This microflow cytometer is capable of providing accurate results in response to a potential risk of cyanobacterial bloom in source water for WHO Alert Level 2 and protect the public from health impairments from cyanotoxins in recreational waters. In order to reach lower quantification limits of 2,000 cells/mL for WHO Alert Level 1 and provide early warning alerts, as will be described below, a pre-concentrating process can be added to meet these requirements.

3.4 **Quantification of low-level cyanobacterial samples for early warning alerts**

Table 2 Determination results of low-level cyanobacterial samples after pre-concentration

Sample	Concentration (cells/mL)	Retentate (cells/mL)	Retentate volume (mL)	Recovery efficiency (%)	Ratio
A	429 ± 5	394,000 ± 1,154	1.1	97.7 ± 5.8	909
B	39 ± 1	22,100 ± 153	1.5	85.3 ± 0.6	667
C	4.5 ± 0.5	3,050 ± 540	1.5	91.0 ± 6.8	667

To lower the limit of detection of the microflow cytometry platform, the ACCRS was built and optimized based on previous work as shown in Figure 2. The recovery system is capable of concentrating samples of 1 liter or more, and the cells of interest can be retained in a final retentate volume on the milliliter scale (1 ~ 1.5 mL). *M. aeruginosa* samples were first pre-concentrated by the sub-system and the resulting retentate was delivered to the microflow cytometer for quantification.

M. aeruginosa samples (4×10^7 cells/mL) were used in a 10-fold serial dilution to prepare the samples used in Table 2. The cell concentration was finally decreased by three orders of magnitude, and the diluted samples were counted by the microflow cytometer and hemocytometer for multiple times. The resulting cell concentrations were measured at 429,000 ± 5,131 cells/mL, 38,800± 1,257 cells/mL, and 4,470 ± 46 cells/mL, respectively. 1 mL of each sample was spiked into 1000 mL phosphate buffered saline, obtaining sample A, B and C. These three samples were spiked into the recovery system and the final retentate was monitored by the microflow cytometer. The pre-concentration results and the determination results are shown in Table 2. Due to the vibration of the peristaltic pump, the volume of the final retentate was within the range of 1.1-1.5 mL. All three samples were concentrated from 1000 mL, and the concentration ratios for sample A, B, and C were 909, 667, and 667, respectively. The high concentration ratios and milliliter scale retentate reveal that the sub-recovery system is capable of processing large amounts of water samples for microfluidic devices as a pre-concentrating process.

The recovery efficiency is defined as the ratio of the total cell abundance retained in the final retentate to the cell abundance in the initial sample, expressed as a percentage. The equation is as follows.

$$\text{Recovery efficiency (\%)} = \frac{\text{Concentration of the Retentate} * \text{Retentate Volume}}{Concentration * 1000}$$

The recovery efficiencies for sample A and C were 97.7% and 91.0%, respectively. The recovery efficiency for sample B, with a mean concentration of 39 cells/mL, was 85.3%. The high recovery efficiencies indicate that no significant loss of *M. aeruginosa* was caused due to the automated cyanobacterial concentration and recovery system. Results in Table 2 also prove that the microflow cytometer platform with the pre-concentrating process and detection process is capable of accurate quantification of cyanobacterial samples.

More importantly, the cyanobacterial cell concentrations for sample A, B, and C were in the range of 4.5 ~ 429 *M. aeruginosa* cells/mL. From Table 2, it can be observed that the limit of quantification of the microflow cytometry platform dropped to ~ 5 cells/mL and 91% of the cell abundance was retained and counted after the pre-concentration process with the combination of ACCRS. These results indicate that the microflow cytometer platform is capable of monitoring low concentration cyanobacterial samples with high accuracy and can treat large amounts of water samples. The limit of quantification of this platform can be considered as 5 cyanobacterial cells/mL which is 400-fold lower than the WHO Alert Level 1 (2,000 cells/mL), and it is safe to mention that the microflow cytometry platform can be used for early waring alerts for potential harmful cyanobacterial blooms.

To examine the impact of low cyanobacteria concentration detection on potential blooms, the time (in days) for cyanobacteria growth from 5 cells/mL to 2000 cells/mL was investigated. A.J. van der Westhuizen et al reported that the best doubling time (t_d) for *Microcystis aeruginosa* was 1.23 days at 32 °C, and the maximum time period increased to 6.79 days at 16°C [13]. The corresponding growth rates ($k = \ln 2/t_d$) were 0.56 day $^{-1}$ and 0.10 day $^{-1}$, respectively. Assuming

that every cyanobacterial cell doubles during every cell cycle and the degradation rate of the cells can be ignored, the proliferation of cells can be determined by the following equation:

$$N_t = N_0 * 2^{kt}$$

Where k (day $^{-1}$) is the growth rate, N_t (cells/mL) the cell concentration at time t (day), N_0 (cells/mL) the initial cyanobacterial cell concentration, and t (days) the time. Based on this growth model, it takes a minimum of 15.43 days for *Microcystis aeruginosa* to grow from 5 cells/mL to 2000 cells/mL at the maximum growth rate. Given that the calculation is based on maximum growth rate and the decay is ignored, the expected bloom time in real situation will be longer than the calculated time periods. In other words, the microflow cytometer platform can provide early warning alerts of at least 15 days to allow authorities to take actions to prevent a potential harmful cyanobacterial bloom.

Besides the low-level warning alert, large volumes (1 L) of low-level microbial samples have been effectively treated by the pre-concentrating process to make them suitable for microfluidic devices. Microfluidic devices manipulate samples on a micron or nano scale, making it difficult and time-consuming for them to capture the entire cell abundance on a liter scale. Moreover, the limit of detection of the microfluidic device can be significantly reduced with the pre-concentrating process.

4. Conclusions

In this study, a microflow cytometry platform was designed for the determination of cyanobacteria in water to provide alerts for cyanobacterial blooms that can produce harmful effects on health due to the production of cyanotoxins. First, the interaction of *in vivo* fluorescence of phycocyanin was studied for accurate detection of cyanobacteria. The fluorescent signal of every single cell was measured, and the transit time and threshold were extracted to distinguish positive signals from background noise. Thus, a time-domain filtering and an intensity threshold were applied to improve the accuracy of the detection. Meanwhile, the linear correlation between the fluorescence and cyanobacterial cell concentration also guaranteed the accuracy of the results. Results from the microflow cytometer showed good consistency with the traditional hemocytometer method ($R^2 >$ 0.99), and the repeatability experiments have also been conducted to confirm the performance of the microflow cytometer. The measured quantification limit of the microflow cytometer was 15, 000 cells/mL and is capable of accurately monitoring cyanobacterial cells for WHO Alert Level 2. Currently, it can provide health impairment alerts to protect the public from cyanotoxins in recreational waters.

Second, an ACCRS was designed for the determination of low-level cyanobacterial samples. The limit of quantification of this platform was further lowered to ~5 cyanobacterial cells/mL, which meets the requirements for WHO Alert Level 1. Furthermore, this platform can be used to provide early warning alerts that give authorities at least 15 days to respond to potentially harmful cyanobacterial blooms before they reach the limit for WHO Alert Level 1. Moreover, the microbial sample can be reduced from a liter scale to a 1 mL scale by the pre-concentrating system and is

suitable for other microfluidic devices. Thus, this platform can also be applied to microfluidics that measure large volume environmental samples of low-level microbial targets.

Acknowledgments

The authors would like to thank Tyler Kashak and Mathieu Chenier for their careful proof reading of the manuscript and the Global Water Futures (GWF) and NSERC Discovery grants for the support of the project.

References

[1] J. Huisman, G. A. Codd, H. W. Paerl, B. W. Ibelings, J. M. H. Verspagen, and P. M. Visser, "Cyanobacterial blooms," *Nature Reviews Microbiology*, vol. 16, no. 8, pp. 471–483, 2018.

[2] J. M. O'Neil, T. W. Davis, M. A. Burford, and C. J. Gobler, "The rise of harmful cyanobacteria blooms: The potential roles of eutrophication and climate change," *Harmful Algae*, vol. 14, pp. 313–334, 2012.

[3] H. W. Paerl and T. G. Otten, "Harmful Cyanobacterial Blooms : Causes , Consequences , and Controls," *Microb Ecol*, vol. 65, pp. 995–1010, 2013.

[4] M. T. Dokulil and K. Teubner, "Cyanobacterial dominance in lakes," *Hydrobiologia*, vol. 438, pp. 1–12, 2000.

[5] L. C. Backer, D. Manassaram-Baptiste, R. LePrell, and B. Bolton, "Cyanobacteria and algae blooms: Review of health and environmental data from the harmful algal bloom-related illness surveillance system (HABISS) 2007–2011," *Toxins*, vol. 7, no. 4, pp. 1048–1064, 2015.

[6] E. H. Lee, K. S. Cho, and A. Son, "Detection and quantification of toxin-producing microcystis aeruginosa strain in water by nanogene assay," *Journal of Microbiology and Biotechnology*, vol. 27, no. 4, pp. 808–815, 2017.

[7] L. W. Sun *et al.*, "Identification and detection sensitivity of Microcystis aeruginosa from mixed and field samples using MALDI-TOF MS," *Environmental Monitoring and Assessment*, vol. 190, no. 12, 2018.

[8] N. McQuaid, A. Zamyadi, M. Prévost, and F. Bird, "Use of in vivo phycocyanin fluorescence to monitor potential microcystinproducing cyanobacterial biovolume in a drinking water source.," *Journal of environmental monitoring : JEM*, vol. 13, pp. 455–463, 2011.

[9] J. Bartram, W. W. Carmichael, I. Chorus, G. Jones, and O. M. Skulberg, *Toxic Cyanobacteria in Water: a guide to their public health consequences, monitoring and management*. Londan and New York: CRC Press, 1999.

[10] WHO, *Guidelines for safe recreational water environments*, vol. 1. World Health Organization, 2013.

[11] M. Lürling, F. Eshetu, E. J. Faassen, S. Kosten, and V. L. M. Huszar, "Comparison of cyanobacterial and green algal growth rates at different temperatures," *Freshwater Biology*, vol. 58, no. 3, pp. 552–559, 2013.

[12] Y. Li, Y. Lin, P. C. Loughlin, and M. Chen, "Optimization and effects of different culture conditions on growth of Halomicronema hongdechloris – a filamentous cyanobacterium containing chlorophyll f," vol. 5, no. February, pp. 1–12, 2014.

[13] A. J. Van Der Westhuizen and J. N. Eloff, "Effect of temperature and light on the toxicity and growth of the blue-green alga Microcystis aeruginosa (UV-006)," *Planta*, vol. 163, pp. 55–59, 1985.

[14] C. Svrcek and D. W. Smith, "Cyanobacteria toxins and the current state of knowledge on water treatment options: a review," *Journal of Environmental Engineering and Science*, vol. 3, no. 3, pp. 155–185, 2004.

[15] J. Zhu, X. Lei, J. Quan, and X. Yue, "Algae Growth Distribution and Key Prevention and Control Positions for the Middle Route of the," *water*, vol. 11, no. 1851, pp. 1–18, 2019.

[16] K. Izydorczyk, M. Tarczynska, T. Jurczak, J. Mrowczynski, and M. Zalewski, "Measurement of phycocyanin fluorescence as an online early warning system for cyanobacteria in reservoir intake water," *Environmental Toxicology*, vol. 20, no. 4, pp. 425–430, 2005.

[17] A. Srivastava, S. Singh, C. Y. Ahn, H. M. Oh, and R. K. Asthana, "Monitoring approaches for a toxic cyanobacterial bloom," *Environmental Science and Technology*, vol. 47, no. 16, pp. 8999–9013, 2013.

[18] C. Bastien, R. Cardin, É. Veilleux, C. Deblois, A. Warren, and I. Laurion, "Performance evaluation of phycocyanin probes for the monitoring of cyanobacteria," *Journal of Environmental Monitoring*, vol. 13, no. 1, pp. 110–118, 2011.

[19] N. Hashemi, J. S. Erickson, J. P. Golden, K. M. Jackson, and F. S. Ligler, "Microflow Cytometer for optical analysis of phytoplankton," *Biosensors and Bioelectronics*, vol. 26, no. 11. pp. 4263–4269, 2011.

[20] Y. Zhang, T. Guo, and C. Xu, "A systematic study on transit time and its impact on accuracy of concentration measured by microfluidic devices," *Sensors (Switzerland)*, vol. 20, no. 1, 2020.

[21] T. Guo, "An Optical System towards In-line Monitoring of Bacteria in Drinking Water," McMaster University, Hamilton, ON, Canada, 2016.

[22] B. R. Watts, "Development of a Microchip-Based Flow Cytometer with Integrated Optics – Device Design , Fabrication , and Testing," McMaster University, 2012.

[23] B. R. Watts, T. M. Kowpak, Z. Zhang, C.-Q. Xu, and S. Zhu, "Optical simulation, design, and optimization of a microchip-based flow cytometer," vol. 7099, pp. 70990K-70990K–10, 2008.

[24] B. R. Watts, Z. Zhang, C.-Q. Xu, X. Cao, and M. Lin, "Integration of optical components on-chip for scattering and fluorescence detection in an optofluidic device," *Biomed.Opt.Express*, vol. 3, no.

Chapter 8

Conclusions and Future Work

In this chapter, the results of this thesis work are summarized and the limitations of current work are described. Meanwhile, future work that can establish on our work and this thesis is proposed.

8.1 Conclusions and achievements

Cyanobacteria, as the origin of plants, are the most ancient autotrophic phytoplankton on the planet. Cyanobacteria have a unique position in aquatic ecosystem. However, the cyanobacteria have been considered as a nuisance due to the harmful cyanobacterial blooms. These blooms can produce toxic compounds and pose risks to the pubic. Meanwhile, the control methods for cyanobacterial blooms are expensive and time-consuming. It is better to prevent these harmful blooms before they already form. Thus, the objective of this work is to provide early warning alerts for potential harmful cyanobacterial blooms and prevent the blooms at the very early beginning.

A microflow cytometry platform including a microfluidic device and an automated cyanobacterial concentration and recovery system was applied for quantification of cyanobacteria, and providing early warning alerts for potential harmful cyanobacterial blooms. The achieved goals of this project contain a pre-conditioning step for sample preparation, the optimized data analysis methods for particle/cell detection, quantification of labeling free of cyanobacteria and early warning alerts of potential blooms.

8.1.1 An automated cyanobacterial concentration and recovery system

An automated cyanobacterial concentration and recovery system was designed and built up as a pre-conditioning process for practical environmental samples. Two main purposes of this system were achieved. First, the assay volume can be reduced from

large amounts (at the liter scale) to a few milliliter scale (e.g. 1 mL). Second, the concentration of the cells of interest can be increased significantly (e.g. 1000 times). Thus, the processed sample can be suitable to be transferred to microfluidic devices for further analysis. The core structure of the developed system was a ceramic membrane with a pore size of 0.14 μm. Tangential flow filtration technique and optimized back-flushing techniques were applied to increase the recovery efficiency and reduce the final retentate volume. The system achieved a good performance on the average recovery efficiency (above 90%). The pre-enrichment limit of the system was as low as 0.005 CFU/mL, and the concentration ratio can be up to 1000.

8.1.2 Optimized data analysis methods microflow cytometer platform for particle/cell detection

A microfluidic device with on-chip optical system was designed and fabricated as a core device for a microflow cytometer. Beads test was first performed to evaluate and verify the performance of the microflow cytometer. Preliminary results showed that transit time can be used for data filtering along with amplitude threshold. Relative difference of the measured concentration ranged from 3.43% to 8.77% by employing both the transit time and amplitude thresholds, while the valves were in the range of 8.42% to 111.76%. Meanwhile, a linear correlation ($R^2 > 0.94$) between the traditional hemocytometer counting method and the improved data analyzing method with two thresholds was observed. Furthermore, the inverse of measured transit time depends on the total flow rate. In conclusion, the transit time can be functioned as a time-domain filter to improve the accuracy for particle measurement in microflow cytometry.

8.1.3 Quantification of cyanobacteria using a microflow cytometer

A labeling-free phycocyanin fluorescence detection platform based on microflow cytometry for cyanobacteria was built up. Experiments on *Microcystis aeruginosa* were conducted to test the feasibility and effectiveness of the optimized data filtering methods. A threshold of three times the standard deviation above the baseline was utilized to detect the fluorescent signals of the pulsed events. Meanwhile, a time-domain transit time filter was applied to further remove the false positive events.

The performance of the microflow cytometer was evaluated under various experimental conditions. A wide range (14,400 $\sim$ 1,240,000 cyanobacterial cells/mL) of samples were tested, and results have shown that the coefficients of variation of the measurements on cyanobacteria were within 10% for most samples. A good linearity ($R^2 > 0.99$) was found between the traditional hemocytometer counting results and the values measured by the microflow cytometer. The quantification limit on cyanobacterial detection was determined at 15,000 cells/mL, which was more than six times lower than the WHO Alert Level 2 (100,000 cells/mL). Results have verified that the microflow cytometer can be used for monitoring cyanobacteria in source water and in recreational water to protect the public from hazardous effects caused by potential cyanobacterial blooms.

8.1.4 Early warning alerts of potential cyanobacterial blooms

Quantification of low-level cyanobacterial samples was achieved for early warning alerts of potential harmful cyanobacterial blooms. Preliminary results showed a quantification limit of ~ 5 cyanobacterial cells/mL using the microflow cytometer platform.

Results have approved that it is capable of providing ample time for authorities to take actions in response to a potential bloom.

An automated cyanobacterial concentration and recovery system was established for pre-concentration of low-level cyanobacterial samples. This subsystem can concentrate original sample solutions with large volumes (e.g. 1 liter or more) to a final retentate on a small scale (1 $\sim$ 1.5 mL). The concentrations of the sample dropped to 4.5 $\sim$ 229 *M. aeruginosa* cells/mL, and the recovery efficiencies for the cells in original sample solutions ranged from 85.3% to 97.7%. In summary, the platform is capable of capture a few cells (e.g. $\sim$ 5 cells) from a large water solution (e.g. 1 liter or more) and transfer them into the retentate on milliliter scale (e.g. 1 mL) for detection. Moreover, it may take at least 15.43 days for the cells to proliferate from 5 cells/mL to 2000 cells/mL (WHO Alert Level 1) based on a maximum growth rate. The established platform can be utilized to provide early warning alerts to prevent the growth of cyanobacteria and stop the potential blooms.

The sub-system can also work with other emerging microfluidic devices as a pre-concentration process to extend their applications in many other fields. It is helpful to reduce the assay volume of the original sample solution, and increase the detection range of these devices. It is helpful to extend the applications of other microfluidic devices.

8.2 Future work

Some recommendations are made on how to improve the performance of the work and make it more suitable for end-users for practical environmental tests. In addition, possible future directions based on this work are addressed in this section.

8.2.1 In-line real time detection of cyanobacteria

As the demand of rapid in-line real time monitoring cells of interest, potential future work can focus on practical environmental applications. The sub-system (ACCRS) for sample preparation can work automatically, and it could potentially be used for real-time sample preparation. The core device of the microflow cytometry was a microfluidic device with on-chip optical system. The dimension of the core device is on milliliter scale, while the dimension of the overall platform should be further scaled down to meet the requirements of in-line real time or in-situ monitoring. Furthermore, current liquid transfer from the ACCRS to detection and analysis module (microflow cytometer) was manually performed. An automated highly integrated functional system is recommended for in-line real time monitoring of cyanobacteria in the future.

8.2.2 The extended application of the ABCRS

The assay volume for most microfluidic devices are on milliliter scale, and it may takes a few hours or longer for them to process large amounts of water samples. Meanwhile, unwanted suspended solids in some environmental samples need to be removed first. The automated bacterial concentration and recovery system contain a ceramic membrane with a pore size of 0.14 μm. Initial validation and feasibility testing of the ABCRS was first verified with *E.coli*, and the adjusted system also showed success of concentrating and recovering *Microcystis aeruginosa*. Thus, it is safe to expect that we can expand the use of the ABCRS for concentrating other bacteria or virus with a pore size larger than 0.14 μm.

This ABCRS can not only work for the microflow cytometer setup used in this thesis, it can also work with similar microfluidic devices. Emerging biosensors have been

developed significantly in recent decades. Latest microbial biosensors are now capable of detecting single cell. However, the remaining challenge for practical application is how to capture the cells of interest in water samples on litter scale. Apparently, the ABCRS can be modified by adjusting the control parameters of the system in order to expand the application of more biosensors.

8.2.3 Size differentiation of cyanobacteria

The scope of cyanobacteria monitoring was huge. In this work, the feasibility was validated by *Microcystis aeruginosa*. However, cyanobacteria contain a group of Gram-negative bacteria that use sunlight as the energy source to produce oxygen and organic compounds. In the future work, more species of cyanobacteria can be tested using this microflow cytometer platform.

The abundance and diversity of cyanobacteria vary in different water bodies due to many parameters such as temperature, nutrients, salinity, pH. It is important to identify the localized bloom-forming species and regularly monitor the common cyanobacteria present in local water bodies. Other than the fluorescent signals, forward scatter can be measured for the discrimination of cells by size. Based on flow cytometry, various cyanobacterial species may be differentiated by cell size.

8.2.4 Cyanobacterial imaging

In recent years, the need to build up a local on-line database of cyanobacteria and algae is increasing. Other than the cell concentration and size, the morphology of the cyanobacteria is also important for database. Imaging of cyanobacterial cells can be introduced into the monitoring platform as well.

Microflow cytometer is a powerful and reliable tool for cell quantification and analysis. It can be combined with other techniques (i.e. CCD cameras) to provide more information of cells of interest. As the fast development of high-speed camera in recent decades, the cost of high-speed camera has been reduced while the performance (e.g. frames per second) has been increased significantly.

The output of the unique fluorescent signals emitted by the cyanobacterial cells can be used as a signal to trigger the high-speed camera to take pictures of the cyanobacterial cells flowing in the microchannel. The morphology can be combined with microflow cytometry for identification of various cyanobacterial species.

8.2.5 Other potential applications

This microflow cytometry platform can be also used for other medical or biological fields. Agglutination can be combined with the microflow cytometer for the determination of the presence and concentration of analyte. Soluble antibodies can be coated to the surface of particles (e.g. magnetic beads). When antigens are present in the solution, strong affinity between the antigen and antibody can result in the formation of clumps. Apparently, the agglutination reaction indicates the presence of antigens. The conjugated particles can be tested by the microflow cytometer based on the side scatter light intensities and the transit time for the particles to pass through the laser beam.

Based on the principle of agglutination, some diagnostics may also be performed with the microflow cytometer. For example, agglutination found in blood analysis may indicate diagnostic of immune-mediated hemolytic anemia (IMHA). Red blood cells (RBC) clump together, owing to the affinity between antibodies on one RBC and

antigens on other RBCs. Immunoglobulin G and M (IgG or IgM) are most observed as the anti-RBC antibodies in the cases of IMHA. Microflow cytometer is capable of perform cell analysis by sizing, it is safe to claim that it may be helpful for the diagnostics.

Appendix A

Fabrication Process of the Microfluidic Device

The microfluidic device involves three main layers made by glass cover, PDMS, and SU-8 photoresist. Photolithography, soft photolithography, plasma bonding and device assembly are the main steps for the fabrication of the microfluidic device.

A.1 Photolithography

The core microfluidic device is made of SU-8 2075 and 3005 photoresist by photolithography. The details are as follows.

1. Fabrication of the intermediate layer.

A thin SU-8 2035 film is used as an adhesive layer to bond the glass substrate and the functional SU-8 2075 layer. Glass substrates should be clean and dry before use.

Coat. The SU-8 2035 photoresist is diluted by the SU-8 thinner at a volume ratio of 1:1 to get a solution of lower density for spin-coating. Dispense 3mL of diluted

resist on a 3-inch Pyrex glass substrate, and spin at 500 rpm for 30 seconds with acceleration of 100 $\sim$ 200 rpm/second. Spin at 3000 rpm for 60 seconds to get a film of 500 nm.

Soft bake. A hotplate providing accurate temperature control and good uniformity is used for soft bake. Preheat the hotplate to 95°C and put the coated wafer onto it for 5 minutes. Remove the wafer to a flat place and cool it down to room temperature.

UV Exposure. Exposure energy of 150 mJ/cm^2 is enough for a 500 nm resist. Use the mask aligner to expose the SU-8 2035 for 50 mJ/cm^2 and repeat this three times.

Post Exposure Bake (PEB). Preheat the hotplate to 95°C and put the wafer onto it for 5 minutes right after UV exposure.

2. Fabrication of the functional layer.

A SU-8 2075 layer of 50 *um* is made as the microchannel layer with on-chip optical system.

Coat. Dispense 3 5mL of SU-8 2075 on the substrate and avoid any air bubbles inside the resist. Make sure SU-8 2075 cover most area of the substrate. Spin at 1000 rpm for 1 $\sim$ 3 minutes with acceleration of 100 rpm/second to remove the unnecessary resist. Then spin at 2000 rpm for 120 seconds, and finally decelerates with acceleration of 300 rpm/second.

Edge bead removal (EBR). Excessive SU-8 2075 may accumulate on the edge of the substrate after the spin coat step. The build up needs to be removed for close contact with the photomask and reducing the contamination of the hotplate or oven. 1 $\sim$ 3mL SU-8 developer is used at the edge of the wafer at 1000 rpm to remove the

edge bead.

Soft bake. The SU-8 2075 coated wafer is placed into an oven with programmable temperature controller and good uniformity. The program is set to ramp up from room temperature to 95°C in one hour and cool down to room temperature in 3 hours. This 4 hour soft bake process ensures the release of stress by the difference of thermal expansion coefficients of SU-8 photoresist and the glass substrate.

UV Exposure. Exposure energy of 120 mJ/cm^2 is recommend to obtain vertical sidewalls in SU-8 2075. The total exposure energy can be divided into 5 equal parts of 24 mJ/cm^2 with an interval of $15 \sim 30$ seconds.

PEB. Put the resist into the same programmable oven immediately after exposure. The ramping up temperature is 90°C in one hour, and cool it down to room temperature in 3 hours.

Development. Submerge the wafer into SU-8 developer for 5 minutes. Agitation speeds may facilitate the development.

Rinse and dry. A small stream of Isopropyl Alcohol (IPA) is applied to rinse the wafer. Then rinse with DI water and air dry with filtered nitrogen.

Inspection. Put the special features under a microscope to inspect the aspect ratio and special features.

Encapsulation. Spin coat Shipley S1818 or S1808 photoresist at 1000 rpm for 60 seconds on the wafer for insulation and protection. Put it on a hotplate for 3 minutes and cool it down to room temperature.

3. Device Dicing.

MicroAce Dicing Saw is used to cut the wafer into 6 pieces. A $10 \sim 20$ um gap between the edge of the waveguide and the edge of glass substrate is obtained when

dicing the wafers. Remove S1818 layer by a small stream of IPA or ethanol after dicing, and rinse with DI water. Inspect the wafers before use.

A.2 Soft Lithography

Soft lithography is utilized to provide microstructures which acts as inlets and outlets for cells/particles to flow in and out of the microchannel. Soft lithography-fabricated transparent PDMS is used as the cover to seal the microchannels.

Mould design. A aluminum fabricated mold is designed for fabrication of the PDMS cover sheet. The mold consists of two aluminum plates of 8 X 6 cm^2, and the distance between the two plates is 3 mm. One of the plate have 3 mm metal cylinders which have the same diameter of the inlets and outlets. The design of the metal cylinders are consistent with the all inlets and outlets of the SU-8 device. Two plates are coated with a thin SU-8 3005 layer to achieve a flat and smooth surface.

Fabrication of PDMS sleet. A Sylgard 184 silicone elastomer kit (including PDMS monomer and curing agent) purchased from Dow Corning is used to prepare the flat PDMS sheet. Silicone elastomer base and curing agent are mixed together at a mass ratio of 1:1 in a small beaker. Pour the mixture into the aluminum mold and put the mould onto a flat surface at room temperature for 24 hours. After 24 hours, put the mould into an oven at 150°C to enhance the cross-linking of monomers. Cool down the mould to room temperature and carefully pull the PDMS slip out of the mould and cut the PDMS into 3 pieces.

A.3 Nitrogen Plasma Bonding

Nitrogen plasma is used to bond the PDMS sheet and SU-8 device and oxygen plasma can be applied for bonding between the glass cover and PDMS top surface. Plasma treated surface can enhance the bonding efficiency and make the bonding durable. Amino groups can be generated on the PDMS surface using nitrogen plasma and react with the residual epoxy groups of SU-8D device. The amine-expoxide chemical reaction occurs at the interface and a strong and durable chemical bonding is established between the PDMS sheet and SU-8 device.

Nitrogen plasma treatment of PDMS sheet. The flat PDMS sheets are put into a Plasma Asher from Center for Emerging Device Technology (CEDT) at McMaster University. The PDMS sheets are treated under a vacuum at $3 \sim 5$ Pa and purged with nitrogen of 99.99% purity. Repeat the vacuuming and purging cycles for more than 10 times, and then adjust the chamber pressure to $30 \sim 50$ Pa for plasma generation. Set the power at 100W with reflection of less than 10W for 4 minutes. After 4 minutes, the device is ready to bond to prepared SU-8 device.

Nitrogen modification of SU-8 device. SU-8 devices are placed into a nitrogen/vacuum oven. The oven is first vacuumed to less than 1000 Pa and then purged with nitrogen to 50 kPa. The devices must remain in this nitrogen environment for more than 21 hours.

Device Pre-bake. Set the temperature of the oven to 65°C for another 5 hours. The devices are ready for bonding after 5 hours and stable for a couple of hours after removal from the nitrogen environment before bonding to the PDMS sleets.

PDMS sleet/SU-8 device bonding. Nitrogen plasma treated PDMS sheets are immediately placed onto the SU-8 devices under the microscope. Carefully align

the inlets/outlets on PDMS with the reservoirs on the SU-8 devices. This process must be done within 2 minutes of the PDMS removal from the plasma asher otherwise the bonding is no longer strong and durable due to the passivation of the activated amine groups.

Device heating. SU-8 devices bonded with PDMS are placed into the oven at 100°C to active the bond. Pressure needs to be applied to the device to ensure a close contact between the two materials.

Inspection. The sealing performance needs to be inspected under a microscope to ensure the entire area of the device is bonded.

A.4 Device Assembly

The device assembly procedure steps are performed as follows:

1. PDMS/Glass Pad bonding.

The bonding between the top surface of the PDMS and the glass pads is simpler using air or oxygen plasma. Before the bonding, glass pads need to be diced and drilled with holes.

Glass pads preparation. Glass is cut into small pieces using MicroAce Dicing Saw. Diced glass pads are drilled with holes using a drill bit with a diameter of 1.1 mm. The holes must align with the inlets and outlets in the PDMS sleets and the reservoirs on the Su-8 devices.

PDMS sheet/Glass pad bonding. BD-20A high frequency generator bought from Electro Technic Products Inc is used to generate the oxygen plasma. Glass pads and PDMS sheets are exposed to the oxygen plasma for one minute. Insert the metal pins into the PDMS prior to the plasma treatment to guide the placement of

the glass pads to ensure the exact vertical alignment. Inspect the alignment under a microscope and apply some pressure to force a close contact. Remove the metal pins after the alignment and put the device into the oven at 100°C for 1 hour to active the bonding.

2. Pin Insertion and epoxy application.

Hollow metal 22 guage pins are inserted into the PDMS holes. Make sure that no dirts or PDMS debris moves into the SU-8 microchannel during the process. Epoxy is applied to stabilize the pins and fill the void between the PDMS, glass holes and the pins.

3. Device Bake.

Devices are put into an oven at 120°C for 30 minutes to react the epoxy.

Appendix B

Photolithographic mask

The mask for photolithographic procedure to fabricate SU-8 devices are designed as follows. There are 6 designs with different on-chip lens systems on a 3-inch wafer. Key features are curved on the edge of the mask for optimization of photolithographic procedure.

The reservoirs have a diameter of 1 mm and the microchannel is 20 mm long. After photolithography process, the microchannel is 100 μm in width and 50 μm in height. Curved waveguide is designed on Device 1 (Figure B.2) in which the incident angle of the laser beam is 20°C relative to the normal of the flow direction. Reflectors are also added to enhance the signal-to-noise ratio. Device 2 (Figure B.3) contains all straight waveguides and the laser beams are normally incident to the flow direction in the microchannel. Forward scatter notched lenses are designed on Device 3 as shown in Figure B.4. Straight waveguides for incident laser beam and angled waveguide for collection are design on Device 4 (Figure B.5). Device 5, as shown in Figure (B.6) includes angled waveguide for incident laser beam and angled waveguide for on-chip fluorescent light collection. Notched lens with angled waveguide is shown on Device

6 (Figure B.7) for on-chip detection of forward scattered light.

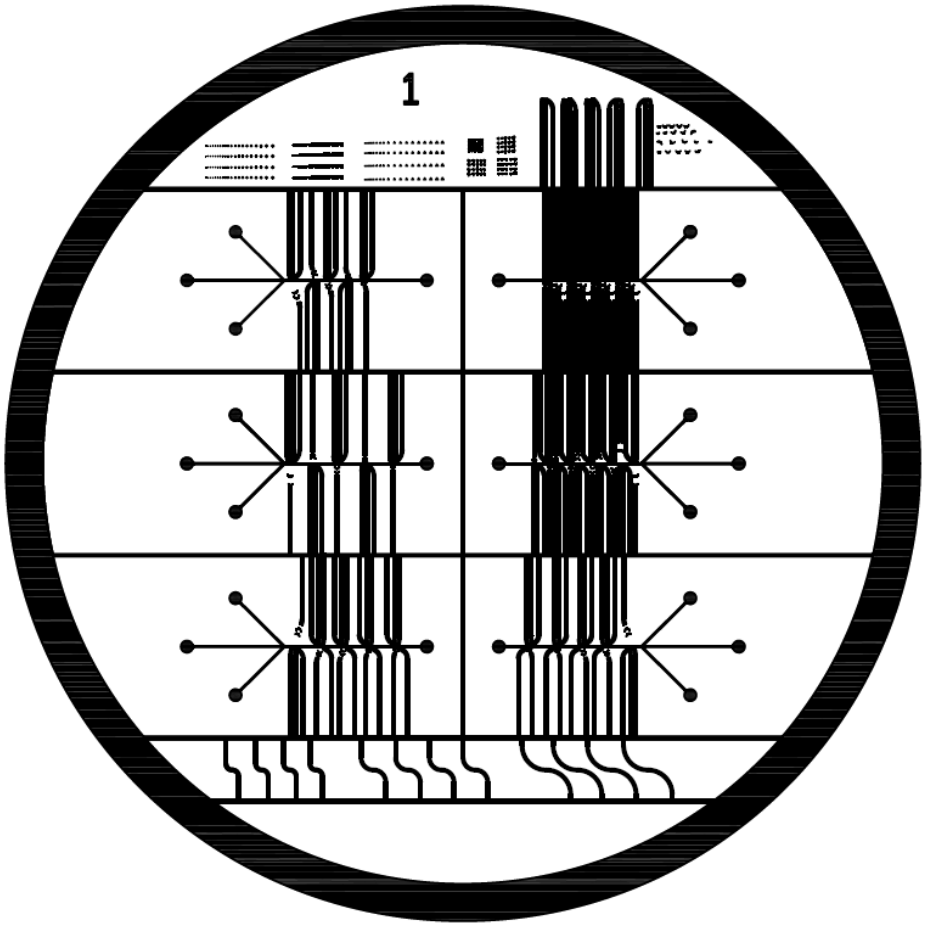

Figure B.1: PL mask of 6 devices

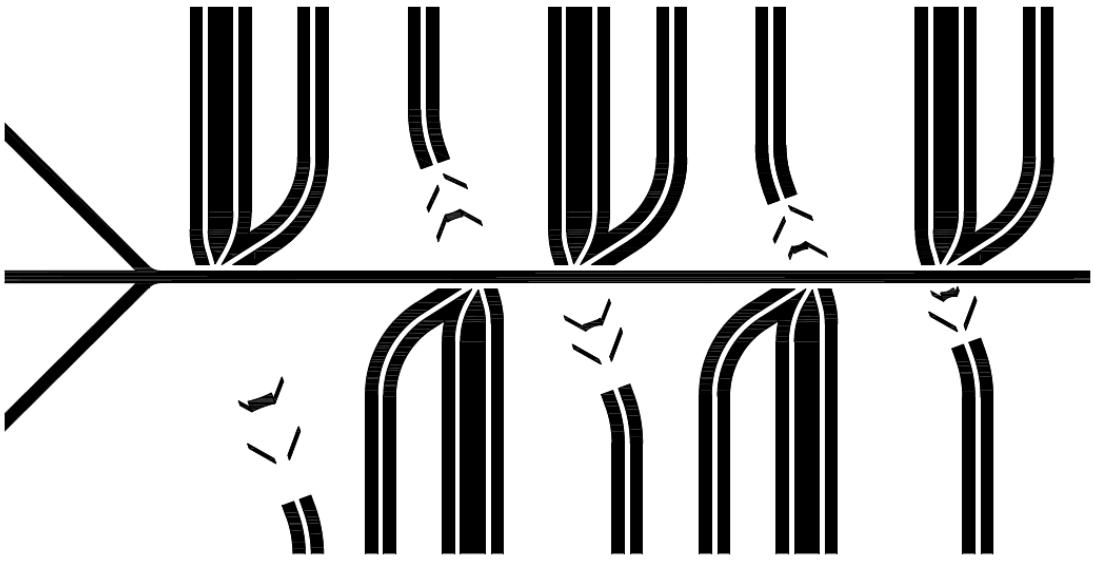

Figure B.2: Structure of Device 1 based on the PL mask

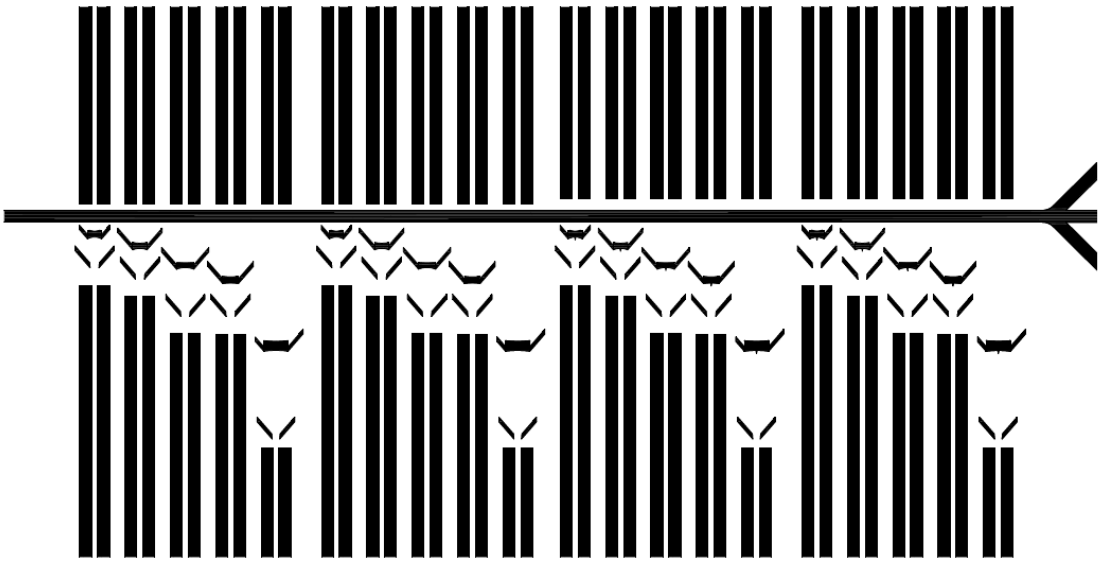

Figure B.3: Structure of Device 2 based on the PL mask

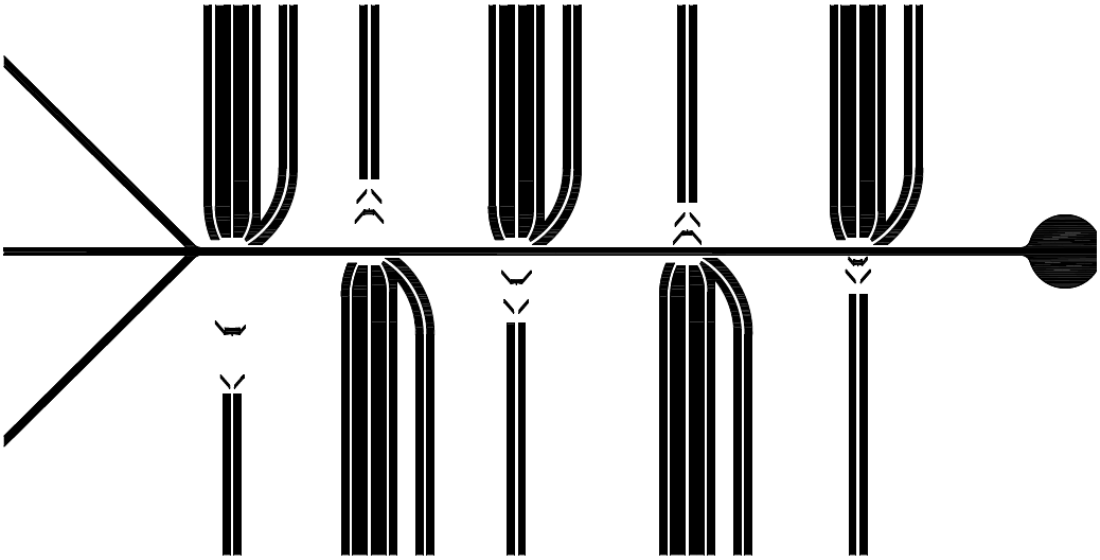

Figure B.4: Structure of Device 3 based on the PL mask

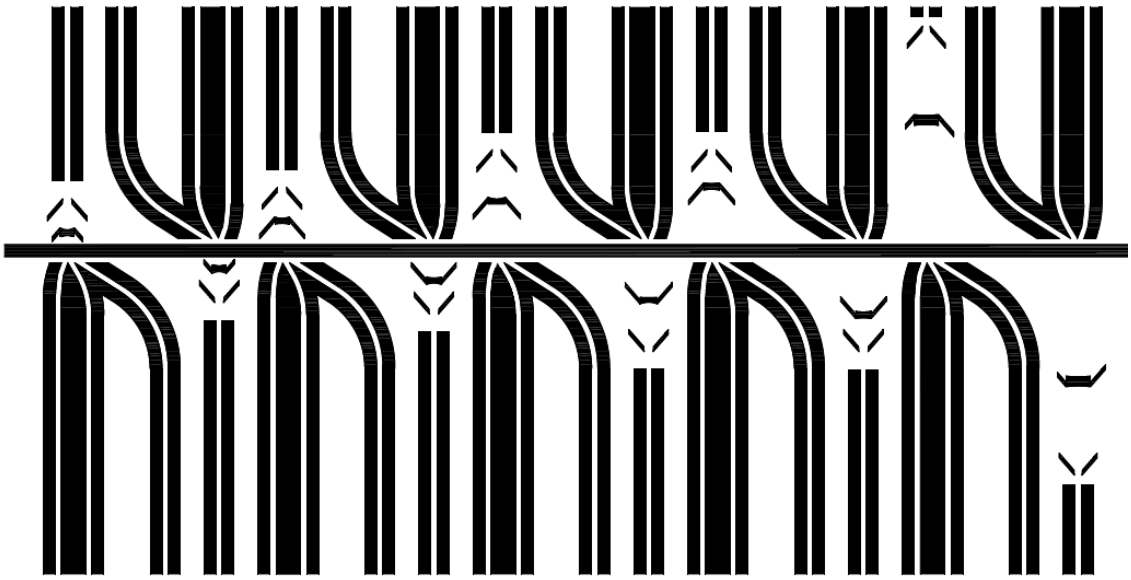

Figure B.5: Structure of Device 4 based on the PL mask

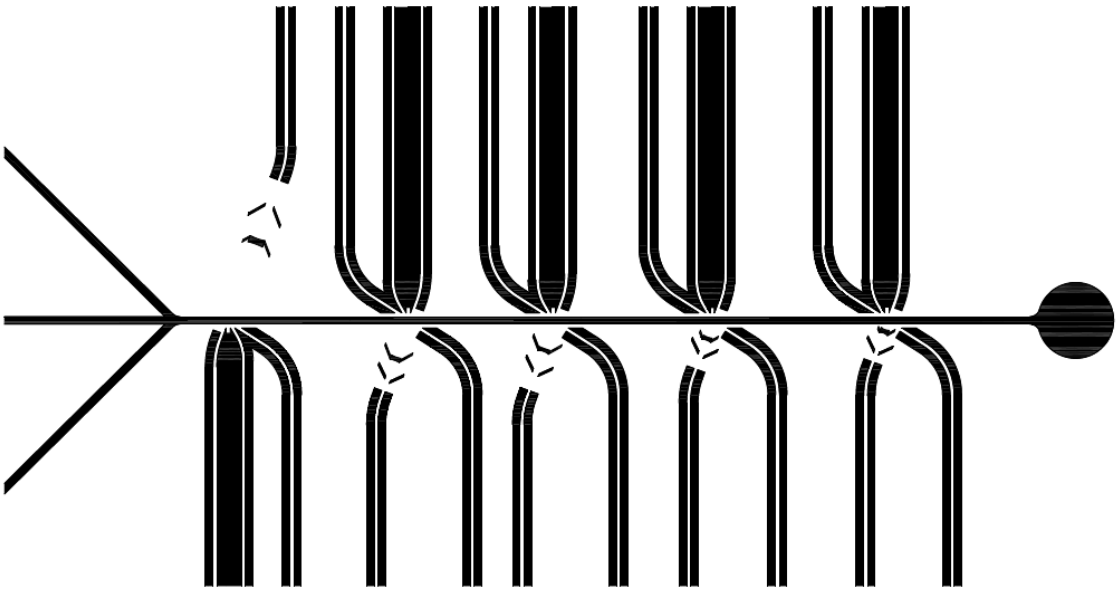

Figure B.6: Structure of Device 5 based on the PL mask

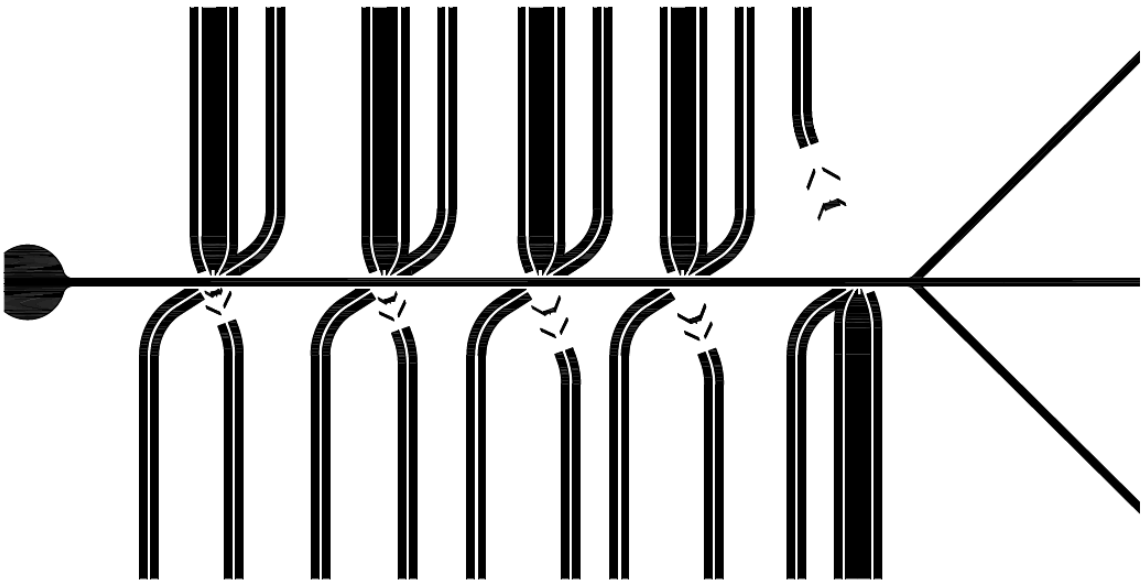

Figure B.7: Structure of Device 6 based on the PL mask